



**Trinity College Dublin**  
Coláiste na Tríonóide, Baile Átha Cliath  
[The University of Dublin](#)

School of Engineering

# **Synthesis of Li-ion Battery Degradation Data for AI-Driven Battery Health Prognostics**

Maria Isabella Corcoran

Supervisor: Assistant Prof. Hossein Javidnia

April 22, 2025

A dissertation submitted in partial fulfilment  
of the requirements for the degree of  
MAI Electronic and Computer Engineering

# Declaration

I hereby declare that this dissertation is entirely my own work and that it has not been submitted as an exercise for a degree at this or any other university.

I have read and I understand the plagiarism provisions in the General Regulations of the University Calendar for the current year, found at <http://www.tcd.ie/calendar>.

I have completed the Online Tutorial on avoiding plagiarism 'Ready Steady Write', located at <http://tcd-ie.libguides.com/plagiarism/ready-steady-write>.

I consent to the examiner retaining a copy of the thesis beyond the examining period, should they so wish (EU GDPR May 2018).

I agree that this thesis will not be publicly available, but will be available to TCD staff and students in the University's open access institutional repository on the Trinity domain only, subject to Irish Copyright Legislation and Trinity College Library conditions of use and acknowledgement.

Signed: \_\_\_\_\_

Date: \_\_\_\_\_

# Abstract

Physics-based models, such as electrochemical models provide a high accuracy in simulating battery behaviour, but they are computationally expensive to integrate in battery management systems (BMS), and unsuited to real-time application. Conversely, data-driven models are efficient but lack physical interpretability. A hybrid approach, focused on the synthesis of lithium-ion battery degradation data, is investigated in this study. Data-driven battery health prognostics are hindered by dataset scarcity, as collecting long-term degradation data under varied conditions is time-consuming and costly. This project addresses the data gap by generating high-fidelity synthetic battery data using an electrochemical model. The validity of the synthetic data is evaluated firstly against a ground-truth dataset, for which it achieves low RMSE error. A support vector regression (SVR) model is then trained on the synthetic dataset and achieves a high predictive accuracy of 94.1%, within  $\pm 1\%$  error of the true SoH, indicating that the synthetic curves captured key real-world degradation patterns. Despite being trained on exclusively simulated examples, the SVR model generalised well to real measurements, further validating the synthetic dataset. Despite these promising results, some limitations were noted. The simulation model fit was less accurate at high SoH, the reasons behind which are speculated. Future work could extrapolate the P2D model to more diverse conditions. Overall, the project demonstrates how the simulation model can alleviate dataset scarcity in AI-based battery health prognostics, with applications for low-power devices which integrate BMS.

# Acknowledgements

I would like to sincerely thank my supervisor, Prof. Hossein Javidnia, for his mentorship. His support, guidance and patience were what made the project possible. I would also like to thank my friends and family for their support and encouragement this year, and over the past 5 years at Trinity as a whole.

# Contents

<b>1</b>	<b>Introduction</b>	<b>1</b>
1.1	Context and Research Motivation . . . . .	1
1.2	Problem Statement . . . . .	2
1.3	Project Goals . . . . .	2
<b>2</b>	<b>Literature Review</b>	<b>5</b>
2.1	State-of-Health Estimation . . . . .	5
2.1.1	Direct Methods . . . . .	5
2.1.2	Indirect Methods . . . . .	6
2.1.3	Model-Based Methods . . . . .	7
2.1.4	Data-driven Methods . . . . .	10
2.2	Datasets . . . . .	11
2.3	An Exploration of Synthetically-Created Data . . . . .	14
2.4	Mathematical Foundations of Degradation Mechanisms . . . . .	16
<b>3</b>	<b>Methodology and Findings</b>	<b>19</b>
3.1	Synthetic Data Generation . . . . .	19
3.1.1	P2D Model . . . . .	19
3.1.2	Experimental Data . . . . .	22
3.1.3	Generating the Synthetic Dataset . . . . .	27
3.2	Validation of the Generated Data . . . . .	41
3.2.1	Data Pre-processing . . . . .	41
3.2.2	Modelling the Data . . . . .	45
<b>4</b>	<b>Results and Evaluation</b>	<b>55</b>
<b>5</b>	<b>Conclusions and Future Work</b>	<b>56</b>
<b>A1</b>	<b>Appendix</b>	<b>67</b>
A1.1	P2D Model MATLAB Implementation . . . . .	67
A1.2	Experimental Data . . . . .	71

A1.2.1 Cell Capacity . . . . .	71
A1.2.2 Comparative Analysis of the M50 vs. M50T . . . . .	72
A1.2.3 Additional Diagnostic Data . . . . .	73
A1.2.4 UDDS Cycling Protocol . . . . .	74
A1.3 Establishing Mathematical Relationships Between the 8 Key Electrochemical Parameters and Common Degradation Mechanisms . . . . .	74
A1.3.1 Equations of Degradation Mechanisms . . . . .	75
A1.3.2 Feature Analysis - More Plots . . . . .	76
A1.3.3 Baseline Experiment Results . . . . .	78

# List of Figures

2.1	Commonly-Used Direct Methods and their Pros & Cons . . . . .	6
2.2	Commonly-used Indirect Methods . . . . .	7
2.3	Categorisation of SoH Estimation Techniques . . . . .	11
2.4	Degradation Mechanisms, Modes and Effects . . . . .	17
3.1	Parametrisation Requirements of the Physical, Chemical, and Electrochemical Aspects of Electrodes and Separator/Electrolyte [1] . . . . .	20
3.2	UDDS Cycling Protocol: CC and CV charging is alternated, then in Step 5 a CC discharge to 80% SOC is carried out. UDDS discharge begins in Step 6 [2].	23
3.3	Step 6 of Cycling Protocol (UDDS), from the US Environmental Protection Agency [3] . . . . .	23
3.4	Timeline of the Cycling Protocol, Including Periodic Diagnostic Tests (RPTs) [2]	24
3.5	Experimental Dataset Structure for [2] . . . . .	24
3.6	Cell W9's voltage-time curves as it degrades over 341 Cycles . . . . .	26
3.7	Relationship between Battery Cycling and Capacity Fade of Each Cell . . . . .	27
3.8	Average Loss Across All Cells During Degradation: X-axis represents bound width ( $0.10 = \pm 10\%$ , $5 = \pm 500\%$ ), Y-axis represents RMSE Loss Between Simulated and Experimental Data . . . . .	31
3.9	Average D1 Value For Bounds of $\pm 30\%$ Initial Value - No Apparent Trend .	31
3.10	Average D1 Value Across Bounds of $\pm 10\%$ to $\pm 150\%$ - Shows Decreasing Trend	32
3.11	Average D1 Value Across Bounds of $\pm 80\%$ to $\pm 100\%$ - Shows Decreasing Trend	32
3.12	Average D1 Value Across Bounds of $250\%$ to $500\%$ - No Apparent Trend .	32
3.13	Average D1 Value Across Bounds of $500\%$ to $1000\%$ - No Apparent Trend .	33
3.14	Mean RMSE (V) Across All Diagnostic Tests . . . . .	35
3.15	Occurrence of Different RMSE Values Across All Diagnostic Tests . . . . .	36
3.16	Occurrence of Different RMSE Values Across Diagnostic Tests 4-15 . . . . .	36
3.17	Average SoH per Diagnostic Test . . . . .	37
3.18	Differing Initial Capacities of the M50T Cells . . . . .	37
3.19	Synthetic Voltage-Time curves based on Cell W9's data, as it degrades over 341 Cycles . . . . .	38

3.20 Very High RMSE Synthetic Sample for V4 Diagnostic #1 . . . . .	38
3.21 High RMSE Synthetic Sample for W4 Diagnostic #1 . . . . .	39
3.22 Average RMSE Synthetic Sample for W5 Diagnostic #12 . . . . .	39
3.23 Very Low RMSE Synthetic Sample for W5 Diagnostic #4 . . . . .	40
3.24 Statistical Comparison of Voltage-Time Curves . . . . .	42
3.25 Random Data Sample . . . . .	43
3.26 Random Data Sample - Zoomed . . . . .	43
3.27 Random Data Sample - Further Zoomed on Experimental Curve to show noise . . . . .	43
3.28 Hyperparameter Tuning Results for Different I/P Features and Sequence Prep. Methods . . . . .	49
3.29 Example of Experiment 1 Best Model Predicting on Synthetic Data . . . . .	49
3.30 Example of Experiment 1 Best Model Predicting on Synthetic Data . . . . .	50
3.31 Hyperparameter Tuning Results for Different I/P Features and Sequence Prep. Methods . . . . .	50
3.32 Example of Experiment 2 Best Model Predicting on All Experimental Data . . . . .	51
3.33 Example of Experiment 2 Best Model Predicting on All Experimental Data . . . . .	51
3.34 Scatter of predicted vs. actual labels with $\pm 1\%$ error bounds; 95 of 101 predictions (94.1%) lie within tolerance. . . . .	53
3.35 Scatter of predicted vs. actual labels with $\pm 0.8\%$ error bounds; 82 of 101 predictions (81.2%) lie within tolerance. . . . .	53
3.36 Scatter of predicted vs. actual labels with $\pm 0.5\%$ error bounds; 82 of 101 predictions (52.5%) lie within tolerance. . . . .	54
3.37 Scatter of predicted vs. actual labels with $\pm 0.1\%$ error bounds; 17 of 101 predictions (16.8%) lie within tolerance. . . . .	54
A1.1 Define Baseline Parameters . . . . .	68
A1.2 Define Initial Guesses and Bounds for PSO . . . . .	68
A1.3 Objective Function Definition . . . . .	69
A1.4 Solver . . . . .	70
A1.5 Particle Swarm Optimisation . . . . .	70
A1.6 Establishment of Initial Conditions . . . . .	71
A1.7 Differing Initial Capacities of the M50T Cells . . . . .	72
A1.8 Average $\sigma_n$ Value Across Bounds of 10% to 150% - Slightly Decreasing Trend	76
A1.9 Average $\sigma_n$ Value Across Bounds of 100% to 1000% - No Apparent Trend .	76
A1.10 Average $\sigma_p$ Value Across Bounds of 10% to 150% - Slightly Decreasing Trend	77
A1.11 Average $\sigma_p$ Value Across Bounds of 100% to 1000% - No Apparent Trend .	77
A1.12 Average RMSE Error Value Across Bounds of 10% to 1000% . . . . .	78
A1.13 Average $D$ Value Across Bounds of 10% to 1000% . . . . .	78
A1.14 Average $\kappa$ Value Across Bounds of 10% to 1000% . . . . .	79

A1.15	Average $\sigma_p$ Value Across Bounds of 10% to 1000% . . . . .	79
A1.16	Average $\sigma_n$ Value Across Bounds of 10% to 1000% . . . . .	79
A1.17	Average $k_p$ Value Across Bounds of 10% to 1000% . . . . .	80
A1.18	Average $D_{s,p}$ Value Across Bounds of 10% to 1000% . . . . .	80
A1.19	Average $D_{s,n}$ Value Across Bounds of 10% to 1000% . . . . .	80
A1.20	Experiment 1 Best Model Predicting on Experimental Data . . . . .	82
A1.21	Experiment 1 Best Model Predicting on Synthetic Data . . . . .	82

# List of Tables

2.1	Summary of Battery Degradation Datasets . . . . .	13
3.1	Kinetic and Transport Parameters . . . . .	20
3.2	Number of Cycles Undergone for Each Cell . . . . .	25
3.3	Voltage Average Statistics . . . . .	42
3.4	Optimal SVR hyperparameters for each experiment and input-preparation method. . . . .	48
3.5	Prediction accuracies within various absolute error bounds. . . . .	52
A1.1	Cell specifications for M50 vs. M50T . . . . .	83
A1.2	UDDS Cycling Protocol Steps and Exit Conditions . . . . .	84
A1.3	UDDS Protocol Charge C-rates Defined at 23 °C for Each Cell, with Corresponding Number of RPT cycles . . . . .	84
A1.4	Upper and lower bounds used for the eight identified parameters in the P2D model [4]. Bounds were set to $\pm 30\%$ of the initial guess values for each parameter at each temperature. . . . .	85
A1.5	Top-ranked SVR hyperparameters ( $C$ , $\epsilon$ , $\gamma$ ) and corresponding average MSE for each experiment and method. . . . .	86

# 1 Introduction

Lithium-ion batteries (LIBs) have a wide range of applications in consumer, industrial and military applications due to their high energy density, light weight, and long cycle life. However, they inevitably degrade over time, which impacts their performance and lifespan. The battery State-of-Health (SoH) is a metric which can be used to quantify this degradation, by reflecting how well a battery is performing compared to when it was new. It is important to be able to assess the current SoH of a lithium-ion battery for a variety of reasons. For example, SoH can be used to determine if a degraded battery can be repurposed for second-life usage, which maximises its usable life and minimises waste. It can also enable predictive maintenance, which minimises the downtime of equipment and facilitate the early detection of potential safety hazards. Overall, reliable SoH estimation can be used to maximise return on investment of battery assets, reduce waste, and improve overall system resilience.

## 1.1 Context and Research Motivation

Lithium-ion batteries have revolutionised modern life. It is forecasted that the global market share for the Li-Ion battery supply chain will grow by 22-30% per year until 2030, when it will reach a value of up to \$400 billion USD [5] [6] [7]. This is expected to be driven primarily by the increasing demand for electric cars and vehicles. Worldwide, governments are adopting policies and providing incentives to achieve net-zero targets, which is driving the increased consumer adoption of green technologies like electric vehicles (EVs). All EU member states offer some form of tax benefit for EVs [8], and in 2023 the EU adopted a law to make all new cars and vans sold in Europe zero-emission from 2035 [9]. By 2027, EVs are expected to make up around 41% of all new car sales across Europe [10], and similarly in the USA it is projected that EVs will make up 50% of new car sales by 2030 [11].

Most EV companies set 80% of the battery's initial capacity as the end of life (EOL) criteria [12], because the cell's capacity tends to decline more quickly beyond that point. This threshold under which the cell can operate safely and reliability is quite narrow, and a method of health estimation of the battery is required to maintain it. This is particularly

true for EVs, which have a high capacity and large serial-parallel numbers of cells, making accurate health assessments crucial for ensuring the vehicles remain efficient and safe and supporting the long-term sustainability of EV infrastructure. SoH is a parameter which can reflect the performance of a battery compared to when it was new. Real-time SoH assessment can be used to recognise continuous or abrupt degradation of the battery, avoiding potential failure in the electrical system and, consequently, the vehicle itself.

## 1.2 Problem Statement

There are multiple recurring challenges in real-time SoH estimation. One key challenge is the lack of high-quality, publicly accessible datasets that cover a diverse range of battery types and real-world ageing under a variety of operating conditions. More comprehensive dataset are needed to improve SoH estimation systems but it requires a lot of time and resources to run large samples of battery units through extended sequences of charge/discharge cycles there is a lack of such datasets. Having more dataset would allow us to build models to better interpret data from an individual battery under dynamic operationg conditions. However, as the generation of such data is a time-consuming and exceedingly expensive process this study will explore the potential of generating synthetic battery data, or augmenting available battery datasets in new ways that can improve SoH estimation on real batteries.

## 1.3 Project Goals

The project involved a number of key work packages with associated goals and outputs. Initially a review of the available research literature was undertaken to (i) determine what suitable datasets were available in the public domain, and (ii) from a review and evaluation of the research literature on battery models, determine if some of the available models might provide a method to simulate internal ageing of the battery physical-chemistry to provide a means to generate new battery data.

After completing this review phase two additional work packages were developed. The first involved the investigation of the most promising electrochemical model of a Li-Ion battery, and the adaptation of this model to provide a source of battery degradation data. This adapted model was then used to create an extended dataset incorporating combinations of both real and synthetic data. This approach provides a time and cost-efficient method of generating data, but the quality of the synthesised data needs to be evaluated to determine the value of the data in the context of developing an improved SoH evaluation method.

This leads to the next work package for this project which involved using the newly generated data to train a machine learning (ML) model for SoH prediction. The

performance of the ML model serves as a means to assess the utility of the synthetic data, as a higher accuracy in the SoH prediction would indicate that the generated data is representative of the underlying degradation behavior of Li-Ion batteries.

## 1. Literature Review and Dataset Evaluation

- A comprehensive review of recent literature on battery degradation modelling and machine learning applications for SoH prediction will be conducted.
- Multiple publicly available battery datasets will be evaluated based on criteria such as completeness, diversity of data, measured parameters in the dataset, operating conditions, and relevance to target degradation mechanisms. Additionally, parallel research must be conducted to find a suitable simulation model for the experimental dataset.
- The most suitable dataset and simulation model will be selected and used as the benchmark for validating model performance. A summary table of all considered datasets will be provided.

## 2. Generation of synthetic data

Any necessary calibration for the simulation model will be done. The synthetic dataset will be generated and pre-processed. Investigation into the chosen simulation model will be carried out, in parallel to the analysis of the chosen experimental ground-truth dataset which will serve as one primary method of validation for the synthetically-generated data. An investigation into the degradation mechanisms that occur in battery ageing is carried out. Any necessary calibration for the simulation model will be done. For example, electrochemical models (EM) may simulate the battery's degradation processes - SEI layer growth or lithium plating are common capacity fade phenomena [13]. An understanding of these degradation modes can be applied to calibrating the model parameters or their bounds. The EM will then be used to generate synthetic data of the battery's degradation processes.

## 3. Validation of Synthetic Data through Machine Learning-based SoH Estimation

- A machine learning model will be trained on the synthetic dataset, to predict the SoH of a LIB based on certain input parameters. A number of different approaches will be compared.
- Congruence between the model's predictions and real experimental data will be used as second method of validating the data generation process, or more specifically to assess whether the model can capture the battery degradation with

high fidelity.

The primary goal is to investigate this hybrid approach and provide insights into how EMs can be paired with data-driven methods for the improvement of SoH estimation of LIBs. This should provide a significant contribution to the field of battery health management and predictive maintenance.

Chapter 2 presents a literature review; foundational techniques and publicly available battery degradation datasets are researched. A comparative evaluation was conducted based on criteria such as data completeness, operational conditions, and relevance to SoH modelling. The dataset ultimately selected is identified as the most suitable for the goal of this work, in addition to its compatibility with the selected P2D model.

Chapter 3 outlines the methodologies employed.

Chapter 4 details the experimental design and execution. Multiple experimental sequences are described, followed by a critical analysis and discussion of their results.

Chapter 5 summarises the key findings, draws conclusions, and offers ideas for expansion on the work.

## 2 Literature Review

This chapter provides the results of a review of the latest literature on battery technology with a focus on Lithium-Ion batteries as these are the predominant form of battery chemistry in widespread use today. This section provides some background information needed to understand the underpinnings of the later project work. It also formed the basis of selecting the battery chemistry model used later in this study and also led to determining the core dataset for battery degradation used in the study. This section will cover the current State-of-the-Art, as reflected in contemporary literature in the field, while also explaining background concepts and techniques that are relevant for understanding the process, workflow, and results of this project.

### 2.1 State-of-Health Estimation

Significant recent research has focused on developing and refining State-of-Health (SoH) estimation techniques for lithium-ion batteries. These techniques are typically divided into two major categories - direct and indirect measurement techniques. An overview is first given of the most commonly used techniques within these categories.

Figure 2.3, at the end of this section, presents an overview of these techniques.

#### 2.1.1 Direct Methods

The direct methods of SoH estimation involve the direct measurement of the battery's operational parameters, for example voltage, current and temperature [14]. These methods are considered to be simple and effective, but in most cases involve the interruption of normal battery operation, and sometimes the physical dismantling of the battery [15] [16]. These invasive techniques are thus not suitable for real-time SoH estimation.

Some of the most commonly used methods include Electrochemical Impedance Spectroscopy (EIS) [17]; Hybrid Pulse Power Characterisation (HPPC) [18]; Open Circuit Voltage (OCV)-based Methods [19]; and Destructive Testing (in which the battery must be dismantled for analysis at the microscopic level) [20].

Ampere hour counting and Coulomb counting are two established direct methods which can be carried out during the real-time operation of LiB. There are also some emerging methods like ultrasonic testing or dynamic EIS, used for the same purpose [21], however, each has its flaws.

Figure 2.1 presents a summary of the most common direct methods and also some promising emergent techniques. It can be concluded that, deriving the battery's SoH in real-time operation, using its directly-measurable parameters, is challenging. Direct methods are susceptible to error as they require expensive, high-accuracy measurement technology. They generally rely on the battery being either outside of its normal operational context, or within a very stable environment. EVs for example, operate within a very dynamic environment; there is constantly changing ambient temperature, vibrational noise, and electrical noise, which all interfere with the accurate real-time SoH estimation.

Direct Methods				
	Description	Pros	Cons	
Coulomb-Counting		Tracks the charge input/output during operation to assess capacity degradation.	Can be used for real-time measurement; high accuracy and simple implementation.	Prone to error accumulation; lack of chemical insight and accuracy heavily depends on correct initial SoC being known.
EIS		Impedance measured by applying AC voltage across range of freqs., to analyse IR & identify degradation mechanisms.	Sensitive to small changes in battery impedance & internal processes. Insight into electrochemical & aging mechanisms	Expensive, specialised equipment needed. Sensitive to noise.
HPPC		A series of charge/discharge pulses are applied to determine IR and power capability at different states of charge.	Simple, widely used for evaluating power capability and IR.	Expensive, specialised equipment needed. Time-consuming.
OCV-Based Methods		Tracks changes in voltage after rest periods to infer capacity and degradation.	Low cost compared to alternative methods, simple and high accuracy	Requires rest period of several hours of battery disconnected from load/charging source. Imprecise in highly-aged batteries.
DST		Battery physically disassembled to analyse its internal structure and aging mechanisms microscopically.	Often serves as a benchmark to validate other non-destructive or indirect methods due to its high-accuracy.	Expensive, specialised equipment needed. Battery cannot be used again after testing.
Ultrasonic Testing		Uses sound wave reflections to detect internal structural changes and degradation.	Can be used for real-time measurement; is fast and can detect internal changes before they manifest in external performance metrics.	Measures mechanical/structural changes, not chemical changes. Not universally applicable to all battery types (best for pouch/prismatic cells)

Figure 2.1: Commonly-Used Direct Methods and their Pros & Cons

## 2.1.2 Indirect Methods

The indirect methods of SoH estimation can be divided into three categories: model-based methods, data-driven methods, and hybrid methods [14].

Model-based approaches are generally divided into three categories including mathematical, electrochemical (EM), and equivalent circuit models (ECM) [22].

Data-driven methods use machine learning algorithms and artificial intelligence to predict SoH from large datasets gathered under various operating conditions.

Hybrid methods essentially integrate two or more of these methods.

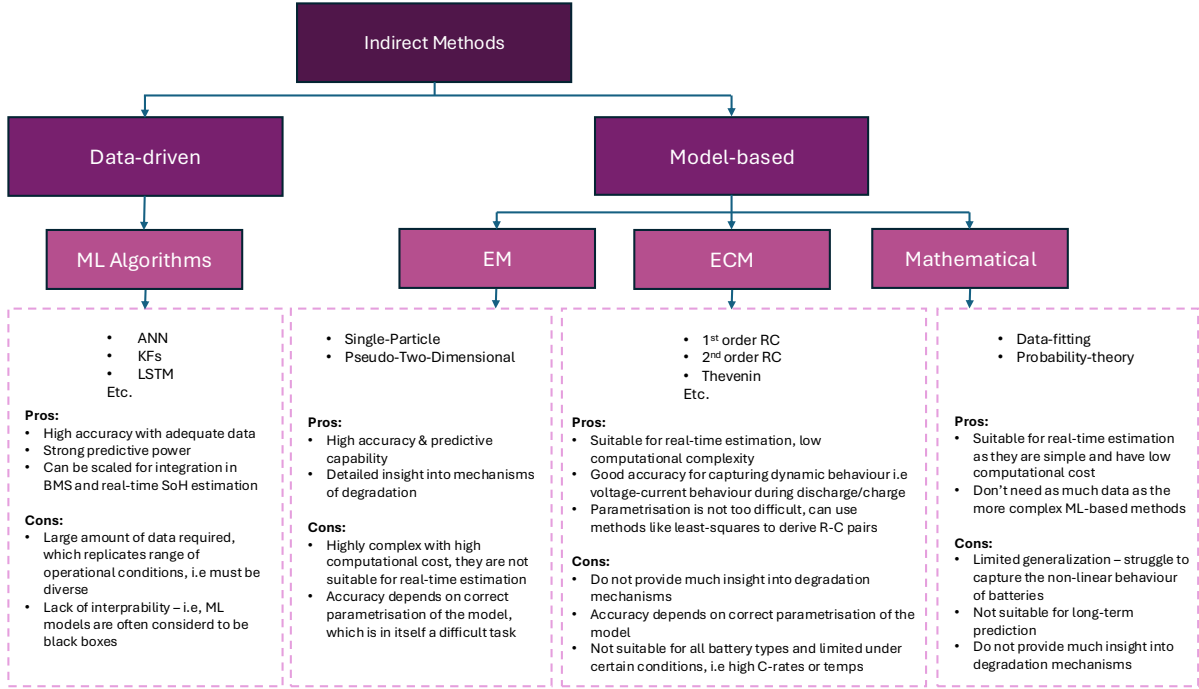


Figure 2.2: Commonly-used Indirect Methods

### 2.1.3 Model-Based Methods

#### Mathematical Models

Empirical degradation-based methods and probability-based methods are included in this category. The SoH of a LIB can be inferred from the parameters of the LIB and their relationships within the corresponding mathematical model.

Empirical methods refer to analytical models which incorporate empirical data fitting. The battery's health is thus extrapolated from experimental data [23]. This is supported by the establishment of a capacity fade model that relates discharge behaviour to battery degradation [24]. Factors that contribute to the battery's degradation are determined by establishing a relationship between the battery's capacity, charge cycles and its lifespan [25]. The main drawback of empirical methods is the requirement to tailor or parameterise the model for the specific battery cell, and they do not capture non-linearities as effectively as more complex data-driven models, which is an important consideration in modelling battery behaviour due to the large number of factors which can affect the degradation.

Methods based on probability theory are also commonly used, e.g. a recently proposed probability density function (PDF)-based method [26] - through analysis of the battery's charge and discharge cycle data, the SoH can be estimated.

Bayesian models are also used, for example in [27] they are combined with ECMS and state transition models for the SoH estimation.

There are limitations to these methods, however, such as a phenomenon known as ‘voltage plateaus’, which can skew the results of the PDF method due to differential voltage values that are very small or even equal to zero [26]. In the case of Bayesian models, as well, they can be computationally complex to implement, and are also prone to skewed results if unrepresentative or inaccurate ‘prior’ data is fed to the Bayesian model [26].

## Electrochemical Models

There are various electrochemical mechanisms that underlie the aging of a LIB. They are highly dynamic and inherently nonlinear [14], and thus quite complex to model. These mechanisms can be incorporated into the EM of a battery to model the degradation behaviour, and provide accurate predictions of the SoH. There are two main types of EM used in literature; the pseudo-two-dimensional model (P2D) and single-particle (SP) models.

The P2D model can accurately predict both the internal dynamics of the battery (for example its solid and electrolyte concentrations) and its terminal voltage [28]. It is based on various theories, such as the concentrated solution theory, the porous electrode theory and the Butler-Volmer equations. These are used to model various types of activity that take place within the battery, e.g. ion transport through the electrolyte, reactions at the electrodes, and changes in concentration and potential across the battery structure. The P2D model is considered to provide the most accuracy in predicting SoH [29] amongst EM models due to thorough representation of the physical processes that underlie the LIB aging. It is described by various partial differential equations (PDEs) that implement the aforementioned theories. These equations are needed to model the nonlinear interactions that occur, and the variations in both time and spatial dimensions.

The P2D model has been extensively validated and thus remains a popular tool for studying Li-ion battery behavior; however, its main disadvantage is its computational complexity, due to the numerous nonlinear PDEs used to represent the model [30].

The SP is a simplified version of the P2D model and another commonly used EM. It is however a poor choice for accurately modelling the degradation behaviour and thus estimating the SoH, as it disregards many aging behaviours and reactions that occur during the degradation process [29] [31] [14]. The main benefit of SP is its much lower computational complexity and thus it can be used for real-time SoH estimation, albeit providing much lower fidelity compared to the P2D model.

## Equivalent-Circuit Models

The ECM is a widely used method for studying the dynamic behavior of LIBs. It models the battery using simple electrical components like voltage sources and resistors but generally

does not account for the LIB's electrochemical composition.

To use an ECM for predicting the SoH of a LIB, the process consists of roughly three steps:

1. **Selection of the ECM:** There exist various types of ECM. Research has been done to understand which type of ECM is best-suited to which battery chemistries, e.g. it is suggested that the best-suited model for the LFP and NCA battery chemistries was the 1st-order RC model with hysteresis ECM, while the most suited model for the NMC and LMO chemistries was the 1st-order RC ECM [32]. Another study came to the same conclusion, that 1st-order RC model was best suited to NMC batteries and the 1st-order RC model with hysteresis was best suited to LFP batteries [33].
2. **Parameter Identification:** Parameters of the ECM can be determined using various methods, with some of the most common being least squares, meta-heuristic algorithms (e.g. multi-swarm particle swarm optimization), and filtering methods (e.g. Kalman or Particle filters) [14]. Generally, the parameters are identified by processing experimental data, like the battery's charge and discharge cycles, using one of the suitable methods.
3. **Solving for SoH:** To infer the SoH, various methods can be used. It is possible to combine data-driven methods or mathematical-models with the ECM for SoH prediction; For a practical example, it is possible to observe the R-C pairs in a 1st-order model and train a data-driven model to predict the SoH based on observed changes in R and C over time.

The ECM thus provides an accurate representation of the battery's voltage-current characteristics and its transient responses.

There have been some innovative approaches for the parameterisation of the ECM, for example fractional variable-order ECMs have been developed to allow for the dynamic adjustment of parameters based on the battery's charge and discharge cycles [34]. This, in turn, captures the non-linear behaviour more effectively.

ECMs are suitable for real-time SoH estimation due to their simplicity and low computational complexity, with much fewer parameters than the P2D model for example, but they also have some drawbacks. In specific operational contexts, the ECM cannot fully capture the complex dynamics of battery behaviour; for example, in electric vehicles very large currents are used, which stimulates complex dynamics within the battery [33]. The accuracy of the SoH estimation will be lower under high current loads. The accuracy also depends on the correct parametrisation of the ECM.

## 2.1.4 Data-driven Methods

Data-driven methods do not rely on the relationship between the internal electrochemical or electrical properties of the battery and the SoH. Instead, a rough model is built and then refined with data to establish the relationships between measured data (e.g. the voltage, current and temperature) and the SoH. Thus the analysis is only based on operational data, and direct measurements or physical modelling are not involved (unless a hybrid-approach is used).

The data-driven methods have some parallels to the mathematical modelling techniques in a few ways, for example there is a large reliance on historical data; thus data-driven methods require large quantities of data, usually significantly more than mathematical models. This is because they are less simplistic and aim to capture more of the non-linear patterns in the degradation behavior of the battery, compared to purely mathematical models (e.g. regression-based models, or probability-theory-based models).

Data-driven methods usually involve machine learning algorithms. One popular technique is the Kalman Filter (KF) and its variations. Many studies have demonstrated the efficacy of the KF in SoH estimation [35] [36], but some challenges have appeared as well in that the KF is typically more suited for the state-estimation of linear systems. Thus its variations have been explored, for example the Extended Kalman Filter (EKF) [37] [38] [35] [39], Dual Extended Kalman Filter (DEKF), or Unscented Kalman Filter (UKF). KFs can be implemented in real-time and have high accuracy, but require complex matrix operations and a lot of data storage.

Artificial Neural Networks (ANNs) have also been explored extensively. Typical input parameters such as current, voltage, resistance, capacity, etc. are given as input to the model and used to develop a correlation between the physical input characteristics and the SoH. The major drawback is the extensive training required, which in turn requires a large amount of data and high computational costs. This can complicate their integration into a Battery Management System (BMS) [40]. However, advancements in hardware accelerators for AI and ML are continuing to evolve rapidly, which is making integration of ANNs as well as other data-driven methods into BMS a more practical and resource-efficient solution.

Time-series based methods are also commonly used for the SoH estimation of LIBs. They are designed to utilise the sequential nature of data, which is highly applicable to the SoH estimation problem due to the dependence of battery degradation on previous states. One study [41] applied a Recurrent Neural Network (RNN) to simulate the ageing process of LIBs and thus estimate and monitor the SoH. However, Long Short-Term Memory (LSTM) networks, a specialised type of RNN, are a much more popular method than RNNs in recent years. They are better suited to tasks involving sequences with complex and lengthy temporal dependencies; the battery's SoH is very much related to its historical usage

patterns and degradation over time, so this is an understandable development.

In [42], an LSTM-based prediction model for the SoH of batteries was developed and compared to RNN and Relevance Vector Machine (RVM) models. The LSTM approach achieved the highest predictive accuracy amongst the models and was also capable of adapting dynamically to new data. It has been established that LSTM networks can maintain short-term memory more effectively for SoH estimation and deliver superior predictive performance [43]. However LSTMs suffer from a shared problem among most of the data-driven methods, in that they are generally resource intensive and computationally complex, and thus make integration into BMS a difficult task.

The methods covered thus far represent just a small selection from a much broader array of techniques - there are many more popular data-driven methods including Particle Filters; Gaussian Process Regression; Support Vector Machines; Relevance Vector Machines and so on. In the area of LIB SoH estimation, new improvements are constantly being made by expanding on and combining different methods. Approaches that involve combining methods are usually referred to as a 'hybrid' approach, or fall under the broad categorisation of 'hybrid' methods [14]. I will be discussing some previously-explored hybrid methods further in Section 2.3, in which I refine further the focal point of this project.

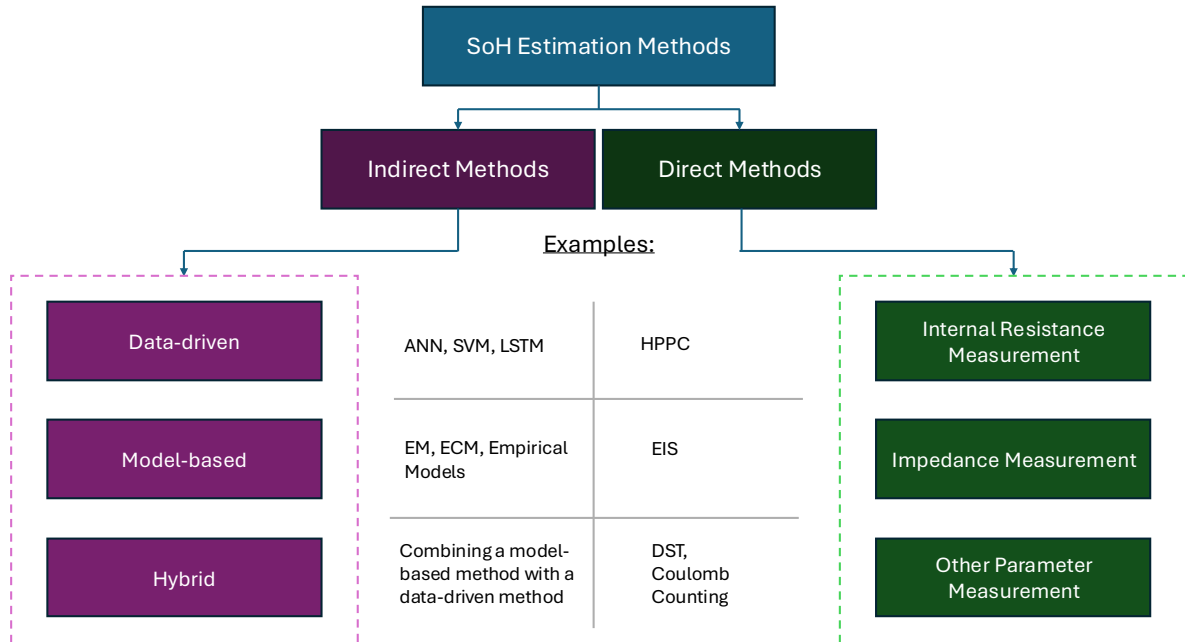


Figure 2.3: Categorisation of SoH Estimation Techniques

## 2.2 Datasets

I have compiled Table 2.1, a table of public datasets that can be used for a study involving the SoH estimation of LIBs.

As part of this literature review and preparation work for this study I downloaded each dataset, explored its methods, features and noted any significant flaws in the data or data annotations. \*(Notably, 3 of the datasets incorporate real-driving charge profiles)\*.

In some cases, there was no paper which described how the dataset was created - in place of this, I cited the primary publication that the dataset was created for. In the case of missing information, 'N/A' is used as a placeholder.

Table 2.1 presents an abundance of publicly available data for the purpose of SoH estimation studies.

However, before getting into a detailed consideration of these datasets it is important to discuss a key deficit. During their operation, LIBs are exposed to a broad range of conditions that are not typical of the ideal conditions present in a lab. For example, a battery which is used in an EV would face cycles of intense and fluctuating demands, followed by long stretches of disuse. The same type of battery could also be used in power tools, laptops, smartphones, medical devices, satellites, and so on. In each of these applications, it would undergo different charge and discharge profiles, and operational conditions. Accordingly, it is important to have access to experimental data that is tailored to the specific application at hand - that replicates the same conditions that a battery would undergo in the relevant context. This is critical for the development of reliable models that are intended to be integrated into BMS.

In Table 2.1, there are 3 datasets that replicate 'real' operating scenarios.

For example, the datasets from Stanford and McMaster University, replicate the aging of a battery which undergoes the typical electric vehicle charge/discharge profiles. Different driving schedules that can be used, including the commonly used Urban Dynamometer Driving Schedule (UDDS), Highway Fuel Economy Testing (HWFET), Los Angeles Driving Cycle (LA92), and Supplemental Federal Test Procedure (US06). Each is designed to simulate different driving conditions. UDDS for example is designed to simulate city driving conditions with frequent stops and starts. LA92 is designed to simulate driving conditions in Los Angeles specifically, so it is more aggressive than UDDS, with more accelerations and higher speeds.

In the Stanford dataset for example, the cells were tested according to UDDS over a period of 23 months, in a temperature-controlled environment. The 'real-driving' scenarios in this case were thus simulated and not exactly 'real', as the tests are conducted in lab conditions. This is typical of the 'real-driving' datasets - even the cycling tests which simulate 'real' scenarios are prone to bias in that they do not fully simulate the operational conditions the LIB would be subjected to - physical stress, temperature variations, irregular charging patterns, and so on.

Table 2.1: Summary of Battery Degradation Datasets

Source of Data	Reference	Battery Tested	Form Factor	Year	Battery Chemistry	# Cells Tested	Dataset Link	Additional Notes
Beijing Institute of Technology	Battery Degradation Datasets (Two Types of Lithium-ion Batteries) [44]	Panasonic NCR18650BD, Go-Prismatic 18650	2023 NCA and LFP	6	[44]			
Huazhong University of Science and Technology	The Dataset for: Real-time personalized health status prediction of lithium-ion batteries using deep transfer learning [45]	Panasonic IFP2010014A, A123 APR18650M1A	2022 LFP	77	[46]			
Stanford University	Lithium-ion battery aging dataset based on electric vehicle real-driving profiles [2]	LG Chem INR21700-M50T	2022 NMC	10	[47]	Real-driving		
University of Science and Technology of China Severson et al	Experimental data of lithium-ion battery and ultracapacitor under DST and UDDS profiles at room temperature [48]	IFP-1665130	2017 LFP	4	[48]	Real-driving; DST		
University of Warwick	Data-driven prediction of battery cycle life before capacity degradation [49]	A123 APR18650M1A	2019 LFP	124	[50]			
University of Oxford University of Oxford Part 1 [53]	Experimental data for "Development of Experimental Techniques for Parameterization of Multi-scale Lithium-ion Battery Models" [1]	LG 21700 M50	2020 NMC	25	[51]			
University of Oxford Oxford energy trading	Oxford Battery Degradation Dataset 1 [52]	Kokam SLPB533459H4	2017 NMC	8	[52]			
University of Oxford	Path Dependent Battery Degradation Dataset Part 1 [53]	Panasonic NCR18650BD	2020 NCA	12	[54]			
NASA Ames Prognostics Center of Excellence	Battery Data Set 1 [57]	Kokam SLPB78205130H	2020 NMC	6	[56]			
NASA Ames Prognostics Center of Excellence Center for Advanced Life Cycle Engineering	Randomized Battery Usage [59]	"Commercially available Li-ion 18650 sized rechargeable batteries"	2007 N/A	34	[58]	Not enough information about batteries tested		
Sandia National Laboratories	Battery Data [60]	"Four 18650 Li-ion batteries" as part of each experiment	2014 N/A	28	[58]	Not enough information about batteries tested		
University of Wisconsin-Madison McMaster University	Degradation of Commercial Lithium-Ion Cells as a Function of Chemistry and Cycling Conditions [61]	INR 18650-20R Battery, A123 cell, unspecified, CS2, CX, PL	N/A NMC, LFP, LCO, LCO, Prismatic, Pouch	144	[60]	Several datasets published by Calce		
EVERLASTING	Panasonic 18650PF Li-ion Battery Data [63]	A123 Systems APR18650M1A, Panasonic NCR18650B, LG Chem 18650HG2	2020 LFP, NCA, NMC	86	[62] - filter for 'snl'			
Hawaii Natural Energy Institute	LG 18650HG2 Li-ion Battery Data [64]	Panasonic 18650PF	2018 NMC	1	[65]	Real-driving: UDDS, HWVFET, LA92, US06		
	Cyclic ageing with driving profile of a LIB module [66] [67]	LG 18650HG2	2020 NMC	1	[68]	Two cells per condition - four temperatures and various discharge rates tested		
		LG Chem INR18650 MJ1	2021 NMC	N/A	[68]	Not enough information about batteries tested		
		"Commercial 18650 cells with a graphite negative electrode and a blended positive electrode composed of NMC and LCO"	2018 NMC-LCO	14	[70] - filter for HNEI			

It is also typical for the duration of the experiment to take a long time, in the range of months to years. This is generally due to the fact that the time it takes to complete these cycles is significant, because each cycle involves charging the battery fully and then discharging it to a predetermined level, which must be repeated hundreds of times to simulate extended usage. For instance, in the Stanford dataset, the M50T battery takes approximately 25 hours to complete one diagnostic test, which consists of a full charge and discharge cycle, based on the charge rate of 0.3C and discharge rate of 0.05C. 15 of these are completed for each cell (there are 10 cells). The cycling tests are faster, but still take quite a while for the battery to exceed the safe usage limit of 300 cycles; e.g. cell W9 takes approximately 110 days to achieve 350 cycles.

It is also a very expensive process collecting this type of data. The equipment needed to carry out such experiments often costs > €100K. For example, the dataset developed by Stanford was generated using a variety of specialised equipment. A machine from the Arbin LBT series was used to perform the controlled charging and discharging cycles. I could not find a public listing for the specific machine used (LBT21024) but similar machines in the series are listed online as costing in the range of €130K euros [71] [72]. An Amerex IC500R thermal chamber is also used; a similar model is listed online for 6k euros [73]. The EIS system is listed for 10k euros [74]. Needless to say, the operating costs incurred by this specialised equipment are substantial, and can pose a significant financial barrier for institutions or individuals that want to conduct battery testing and generate valuable data.

These challenges in data-collection restrict further progress into battery research. Despite the seemingly large amount of publicly-accessible data, there remains a need for more diverse and comprehensive data. The generation process is very time-consuming and costly. Most of the existing datasets are limited in the range of conditions they emulate, in terms of both charge/discharge profiles and also environmental stressors; they do not fully represent the diverse operational realities faced by batteries in actual use. It is thus valuable to consider alternative methods of generating data, or augmenting existing data. One possible solution is the creation of synthetic battery-degradation data, which will be discussed next.

## 2.3 An Exploration of Synthetically-Created Data

As discussed in Section 2.1.3, different models can represent different forms of battery degradation. EMs provide a detailed representation of the internal physicochemical processes that occur during the battery degradation process, such as solid electrolyte interphase (SEI) growth or lithium plating. ECMs can simulate the electrical behaviour of a battery, and thus link the degradation to factors like an increase of internal resistance. However, they do not represent the chemical processes and thus offer less insight into the degradation

mechanisms. Mathematical models can use data-fitting to understand the connection between external parameters and the battery's degradation, but they do not account for the underlying chemical and physical processes, which limits their ability to explain why certain behaviors occur.

Overall, the different modelling approaches vary in their accuracy regarding the representation of the underlying physical phenomena of battery degradation. EMs are considered the most precise, followed by ECMs, and finally, mathematical models, in descending order of their ability to depict the actual processes leading to battery wear.

Another important consideration is that their practicality for on-system implementation also varies. EMs are more complex and computationally intensive, making them less practical for real-time applications. ECMs are more commonly integrated in BMS because they are less computationally complex and thus can be used for real-time SoH estimation (with the exception of using a very higher order ECM). Mathematical models are most suited for on-system implementation, and real-time SoH estimation, but they do not adapt well to changes in operating conditions without recalibration. Data-driven models offer a solution to both problems, but they require a substantial amount of computational resources for training, as well as a large amount of data. However, once trained, the model can be optimised for real-time applications e.g. BMS.

My project considers the following,

1. EMs provide the highest fidelity among the discussed battery modelling approaches, but they are not feasible for real-time applications.
2. Data-driven models are suitable to implement on-system, and provide real-time SoH prediction, given certain conditions are met; they must be optimised for efficient real-time execution in BMS. But they must be trained on a diverse range of scenarios to be effective.

It would seem to be a reasonable approach to attempt to integrate these two methods - i.e, it is possible to simulate battery degradation using an EM, and use these results to generate an extensive synthetic SoH degradation dataset. This method could then enable the creation of an extended dataset, which contains both 'real' experimental data and synthetically-generated data. It should be possible to expand the diversity of the data by adding controlled but physically valid changes to the synthetic data.

The actual mechanisms underlying the battery's degradation will be examined more in Appendix A1.3.1.

After the generation of the synthetic dataset, a data-driven model could be trained on 1) solely the 'real' experimental data; 2) the extended dataset, and 3) solely the synthetic degradation data. Each model could be evaluated using a 'real' data testset, and the validity

of the approach could be assessed.

Some previous works have investigated a similar approach. For instance, a ‘physics-informed neural network’ was developed for a similar purpose, using synthetic data which was generated using a P2D model at various SoH levels [75]. The neural network was also trained on experimental lab data and real-driving data, for comparison. These datasets were integrated to train the neural network, allowing it to utilise correlations between modelled internal states and the measurable SoH. The physics-informed neural network demonstrated excellent performance using the synthetically-generated data, achieving a RMSE of below 2% in SoH estimation. For laboratory data, the RMSE remained under 3%.

This physics-informed approach not only outperformed several purely data-driven methods but also highlighted its benefits through increased accuracy and wider applicability due to the integration of physico-chemical insights.

Another study [76] uses a P2D model to generate synthetic responses of the LIB at high C-rates (C-rate refers to the charging/discharging rate), for various aged states. The model is then fine-tuned with ‘real’ experimental data. The deep-learning model is trained on the synthetic high-rate responses, which enables it to estimate the battery SoH from rapid charging/discharging voltage responses. Overall, the model had less than 2.5% absolute error in predicting loss-of-lithium inventory and less than 3% error in predicting loss-of-active material, compared to the Reference Performance Test (RPT)-based predictions. (RPT integrates various methods, e.g. coulomb counting, EIS, HPPC, etc). And, unlike RPT that requires extended periods to collect data, this method can assess battery condition in real-time during regular use without interruptive testing.

## 2.4 Mathematical Foundations of Degradation Mechanisms

Stanford has made the LG Chem INR21700-M50 electrochemical battery model publicly available [4]. It would be possible to use this model for the purpose of synthetic-data generation, and then to validate the data using the experimental ‘real-driving’ data that Stanford has published, which is for the same battery type (more in Appendices A1.2.2 where any discrepancies between the M50 and M50T will be discussed). However, this model does not incorporate any degradation mechanisms. In this section, I will explore the degradation mechanisms that could potentially be integrated into this model.

LG Chem INR21700-M50 has an NMC 811 formulation for the cathode and a Graphite-SiO<sub>x</sub> anode [77]. The degradation mechanisms [78] were found to be suitable for this specific battery. There are 3 main mechanisms described: SEI layer growth, Lithium plating, and Particle Fracture. These mechanisms contribute to 5 main modes of degradation: loss of

lithium inventory (LLI), loss of active material (LAM) in both the negative and positive electrodes, stoichiometric drift and impedance change [78]. I have illustrated this in Figure 2.4.

Additionally, positive and negative feedback loops can happen as the modes of degradation begin to affect the mechanisms of degradation. For example, LLI provides negative feedback by reducing cyclable lithium, which prevents the negative electrode from reaching a highly lithiated state prone to lithium plating. Conversely, LAM triggers a positive feedback loop as it promotes particle fracture by decreasing the interface between the active material and the electrolyte.

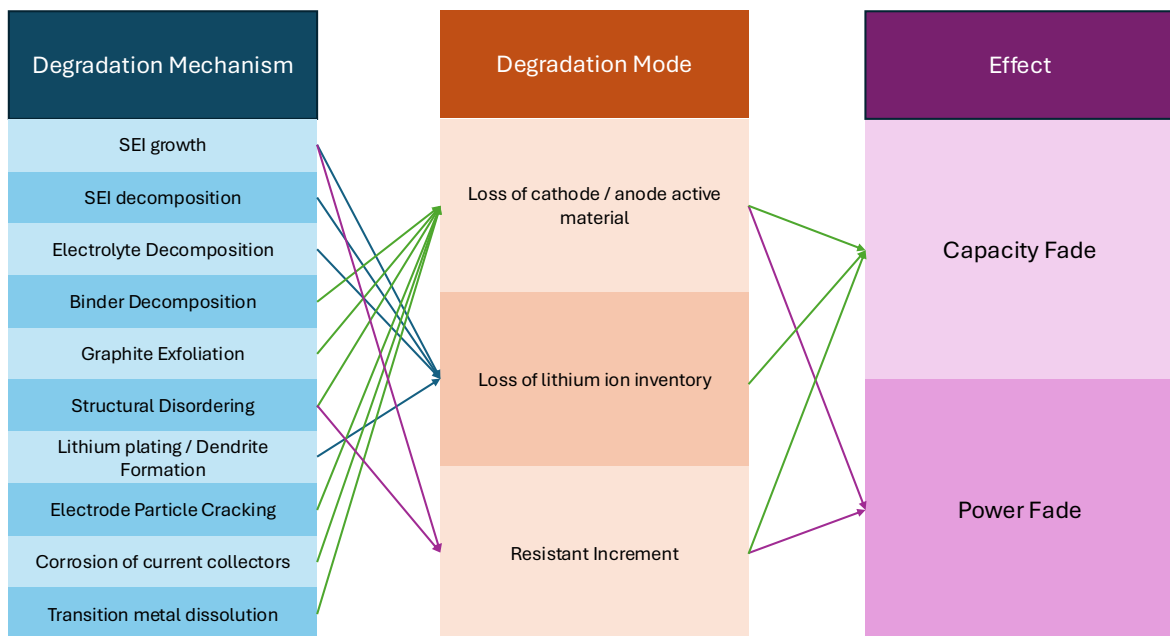


Figure 2.4: Degradation Mechanisms, Modes and Effects

The governing equations for the degradation mechanisms [78] are investigated in Appendix A1.3. Noticeably, LAM is included. LAM was considered an outcome or degradation mode of the degradation mechanisms (like particle cracking or SEI growth), but it can also be treated as a standalone variable in a model because it quantifies the effect of these mechanisms on the battery's usable capacity.

Various studies have explored the integration of degradation mechanisms into P2D models for the understanding of LIB ageing. For example, a few studies were able to incorporate SEI layer growth and Li-Plating into the P2D model to simulate capacity-fade phenomena [79] [80]. Other studies implemented physical effects like mechanical stress and thermal effects were also implemented into the P2D model to investigate their effects on safety issues [81] [4].

One study explored the model parameters that change most significantly with ageing, for

NMC cells used in EVs. The parameters most indicative of ageing were the particle surface area of the cathode, the stoichiometry limits, and the porosities [82]. A review on the NMC-battery degradation mechanisms has been done [83], also considering the anode materials. The 4 main mechanisms of degradation included lithium plating, SEI formation, particle cracking and the loss of active material. This aligns with the main mechanisms of degradation laid out by [78] which will be explained in Appendix A1.3 and incorporated into the P2D model as part of the project's methodology.

Another review determined the graphite-silica anode to be most prone to loss of lithium inventory due to the formation and thickening of the SEI, and the cathode to be most prone to loss of active material resulting from structural changes and stress from lithium intercalation/deintercalation [84]. The M50 battery used by Stanford consists of the NMC Chemistry with graphite-silica anode, so these studies are all relevant to the proposed methodology.

# 3 Methodology and Findings

## 3.1 Synthetic Data Generation

### 3.1.1 P2D Model

To create synthetic battery degradation data, it is important to choose a suitable simulation model - ideally, one which can reproduce the battery's behaviour with high fidelity. As discussed in section 2.1.3, the P2D model is the preferred choice for this purpose. One of the most suitable options is the LG Chem INR21700-M50 model published by Stanford [4].

#### Initial Parametrisation of the Model

The parameterisation of the model is one of the most important factors in its ability to accurately simulate the battery's behaviour. The P2D model requires over 30 parameters to fully describe the physical, chemical, and electrochemical properties of the cell and enable accurate simulation of its behaviour, the exact number depending on the way the model is defined [1].

The Stanford model's parameters were informed by this paper [1]. These parameters were obtained using various methods, depending on the nature of the parameter at hand. Many of the physical parameters were obtained from direct measurement, i.e via destructive methods like teardown or cell opening. This is a straightforward way of obtaining the dimensions of the electrodes, separators, current collectors. After teardown, other physical parameters i.e the porosities, particle shape, and densities were determined using focused ion beam milling together with an imaging method called electron microscopy.

Some parameters were estimated using empirical formulae instead of direct measurement, i.e the Bruggeman coefficients. Certain electrochemical parameters were obtained through specialised experiments (i.e via EIS or 'GITT') or external data (i.e electrolyte transport property values were taken from the literature).

However, a few of the key electrochemical parameters are not as easily estimated. These include kinetic and transport parameters like the diffusion coefficients, conductivities, and

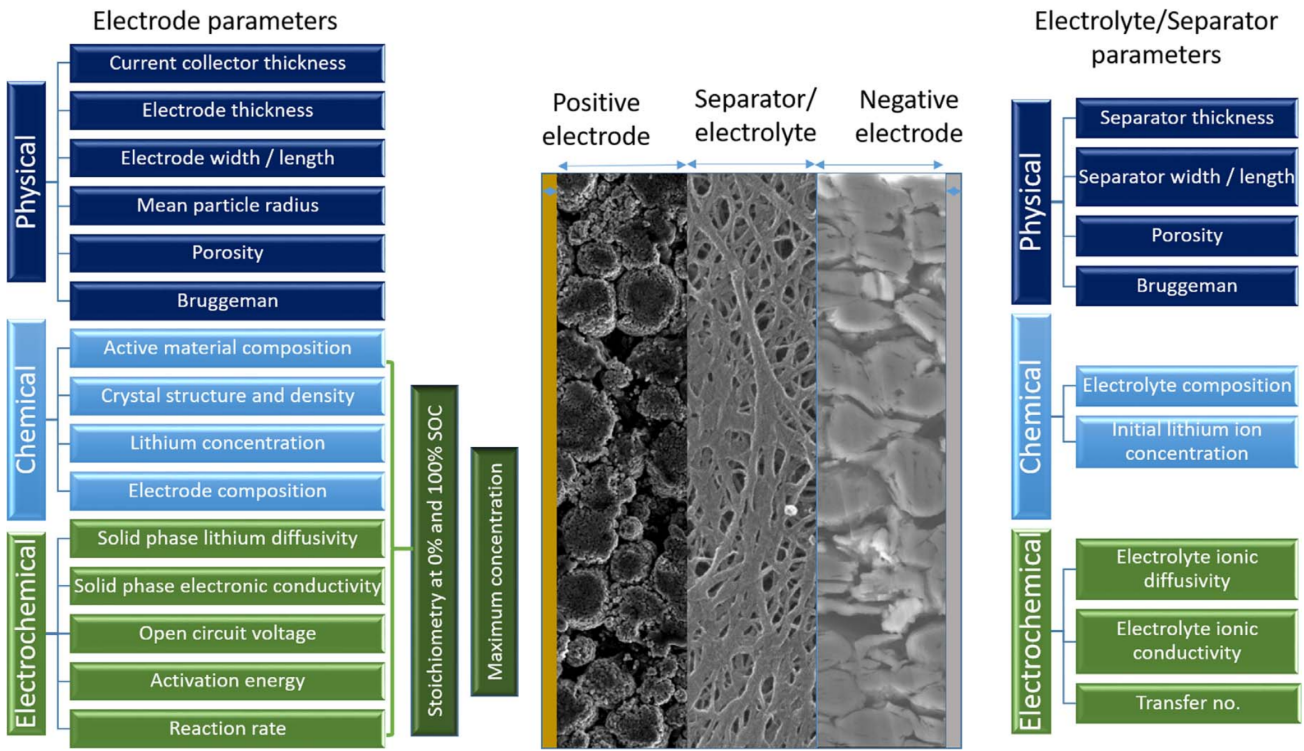


Figure 3.1: Parametrisation Requirements of the Physical, Chemical, and Electrochemical Aspects of Electrodes and Separator/Electrolyte [1]

reaction rate constants, as presented in Table 3.1. These parameters change in a short time span during battery operation, and as such they must be continually updated during operation to accurately model the battery's behaviour [4].

Table 3.1: Kinetic and Transport Parameters

Symbol	Parameter Name
$D$	Electrolyte diffusion coefficient
$\kappa$	Electrolyte conductivity
$\sigma_p$	Solid phase conductivity at positive
$\sigma_n$	Solid phase conductivity at negative
$D_{s,p}$	Solid phase diffusivity at positive
$D_{s,n}$	Solid phase diffusivity at negative
$k_p$	Reaction rate constant at positive
$k_n$	Reaction rate constant at negative

Thus, the Stanford model treats these 8 key kinetic and transport parameters as unknowns to be identified during the process of fitting the P2D model to experimental data. The algorithm used to find the optimal parameter values is called "Particle Swarm Optimisation" (PSO).

## Particle Swarm Optimisation

Particle Swarm Optimisation (PSO) is a population-based optimisation algorithm, which was inspired by the social behaviour of flocks of birds and schools of fish. In PSO you have a set of "particles" or candidate solutions which explore a parameter search space in parallel. Each particle's position represents a potential solution – in this case, it would be an 8-dimensional vector of the P2D model parameters. The 8 parameters are optimised simultaneously, as a vector rather than one-at-a-time, thus PSO can also capture interactions between parameters. PSO is well-suited for this kind of multi-parameter, non-linear optimisation [85].

Good initial guesses of the parameters are required for PSO - these are again taken from [1]. The bounds of the parameters are also an important factor, which in this case are defined as a fixed percentage deviation around the initial guess ( $\pm 30\%$ ). These bounds constrain the swarm's search space so that identified values should remain physically plausible, and also serve to improve convergence stability. See further discussion about the bounds in Section 3.1.3.

The first step of the PSO algorithm involves initialising each of the particles with a random set of parameter values within the specified bounds - this randomness helps in exploring various regions of the solution space initially. The position of each particle is evaluated using some error metric, and its velocity and position is adjusted according to this, until after several iterations the specified convergence criteria are met and an optimal solution is found.

The error metric used in this case is the RMSE between the simulated voltage and the experimental voltage, over the duration of a battery discharge test. The experimental data was sampled at 1 Hz, meaning each second of the discharge test corresponds to one data point. Thus PSO seeks to minimise:

$$obj = \min \left( \frac{1}{N} \sum_{j=1}^N (V_{\text{exp},j} - V_{\text{model},j}(\mathbf{p}))^2 \right)$$

$$\text{s.t. } p^L < \mathbf{p} < p^U$$

Where  $N$  is the total number of experimental data points and  $V_{\text{exp},j}$  and  $V_{\text{model},j}(\mathbf{p})$  are the experimental and model-predicted voltage values for the  $j$ -th data point, respectively.  $\mathbf{p}$  is the vector of estimating parameters, and  $p^L$  and  $p^U$  represent the lower and upper bounds for the vector of estimating parameters.

The convergence criteria can be changed depending on what is required. For example, in the

original implementation of DEARLIBs the stopping criterion is defined using the 'MaxIterations', which is basically a bound on the number of solver iterations [86]. This was changed to use the 'FunctionTolerance' criterion instead, which sets "a lower bound on the change in the value of the objective function during a step". This change meant the algorithm would terminate only when the objective function was no longer improving, generally meaning that the optimal solution was found (with the exception of getting stuck in local minima, though PSO is good at avoiding this with its global 'best' solution strategy. In this implementation a swarm size of 10 particles was adequate to avoid this.)

The simulated output was much more consistent and achieved lower average RMSE using 'FunctionTolerance' compared to simply stopping the computation when the specified number of iterations was reached via 'MaxIterations', at the expense of longer computation time.

To summarise, the P2D model can generate synthetic data based on some reference experimental data which represents a degraded battery's voltage response. This experimental voltage profile serves as the target that the PSO will try to match by tuning parameters. The relationships established in AppendixA1.3 infer that degradation should impact these parameters, i.e degradation often causes lower diffusion coefficients (due to loss of active material or particle cracking), lower reaction rate constants (due to surface film buildup like SEI increasing resistance), or reduced electrolyte conductivity (due to solvent decomposition or Li inventory loss). It might thus be expected that the values of  $D_{s,n}$ ,  $D_{s,p}$ ,  $k_n$ ,  $k_p$ , etc. will reduce by some percentage based on the amount of degradation present in the experimental data. This will be examined in Section 3.1.3.

An explanation about how the Particle Swarm Optimisation process is implemented in the MATLAB code is given in Appendices A1.1.

### 3.1.2 Experimental Data

For this project, data from [2] is used as the experimental reference. In this data, LG Chem INR21700-M50T cells are cycled under conditions that are meant to simulate real-world urban driving conditions, according to the Urban Dynamometer Driving Schedule (UDDS).

#### Cycling Protocol

To create this dataset, 10 LG Chem INR21700-M50T cells underwent the real-driving cycling protocol defined by UDDS. UDDS is one of many driving schedules which can be used to assess the performance of EVs in various situations, in this case 'urban driving conditions' means there are acceleration, deceleration, and idle periods (like when stuck in traffic). So, the UDDS-based cycling of the battery represents a real usage scenario, and the

battery degradation occurs under realistic conditions. More information about the UDDS cycling protocol is given in Appendices A1.2.4.

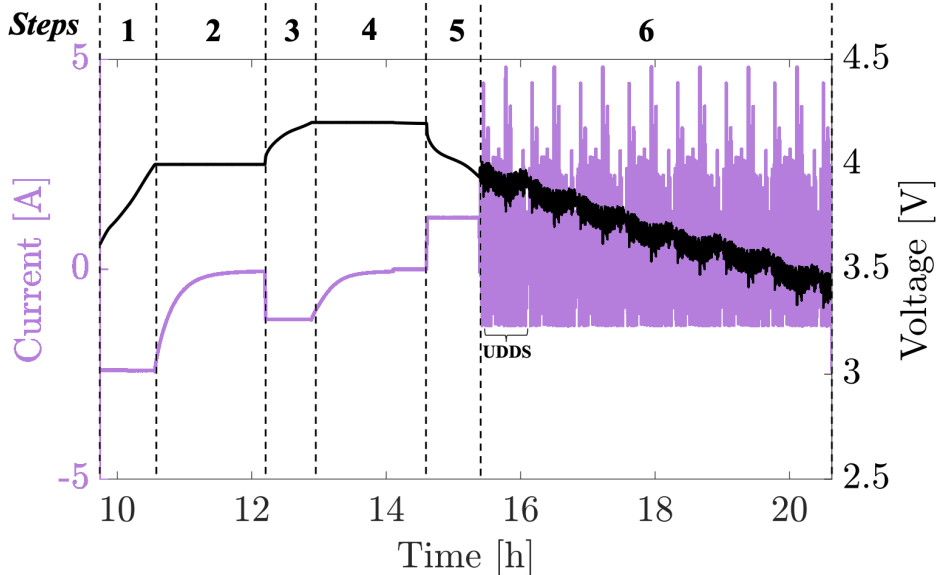


Figure 3.2: UDDS Cycling Protocol: CC and CV charging is alternated, then in Step 5 a CC discharge to 80% SOC is carried out. UDDS discharge begins in Step 6 [2].

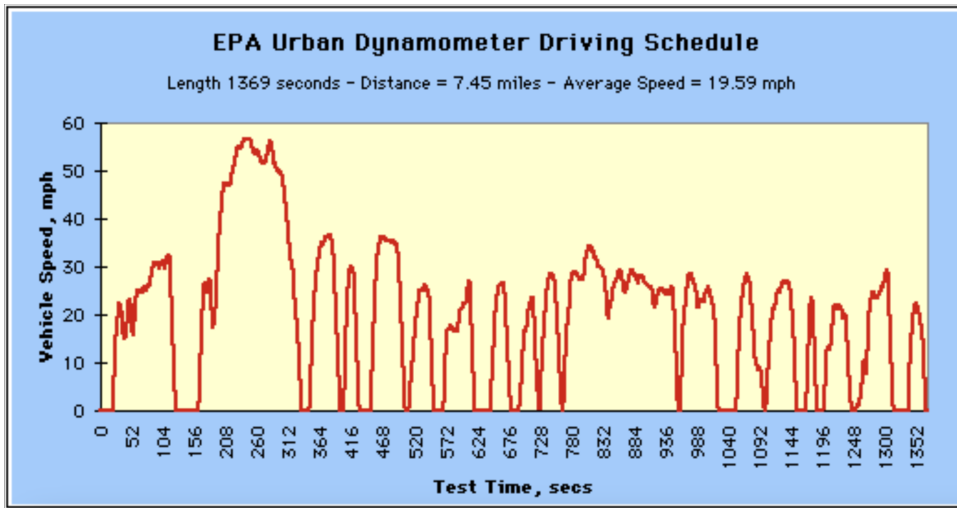


Figure 3.3: Step 6 of Cycling Protocol (UDDS), from the US Environmental Protection Agency [3]

The M50T cells were cycled repeatedly using this protocol over 23 months, and underwent periodic diagnostic tests or 'reference performance tests' (RPTs). A few cells have slightly fewer total diagnostic tests due to starting later or being retired early. See Table 3.2.

Each diagnostic test basically measured the evolution of a cell's capacity, internal resistance growth, and impedance spectrum changes as the cell was ageing (or undergoing more cycles).

Whenever a diagnostic test was scheduled, the normal cycling was paused and the cell

underwent a sequence of tests to characterise its state-of-health. See Figure 3.4. Of particular interest to us for the purpose of this study are the 'capacity tests', which will be discussed in the next section.

## Dataset Structure

Overall, 15 diagnostic tests were carried out. The diagnostic data are organised in the dataset by diagnostic cycle number (1-15). For example, files corresponding to "Diag 1" contain the results of the first diagnostic session (capacity test, HPPC, EIS for diagnostic #1), "Diag 2" for the second, and so on. At each successive diagnostic test, the cell has undergone more cycles. However, this number is different for each cell, see Table 3.2.

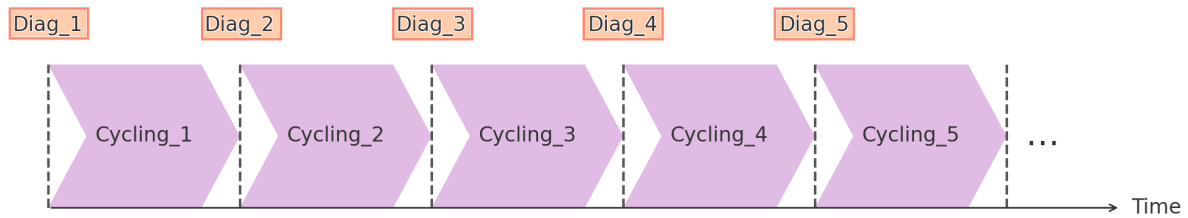


Figure 3.4: Timeline of the Cycling Protocol, Including Periodic Diagnostic Tests (RPTs) [2]

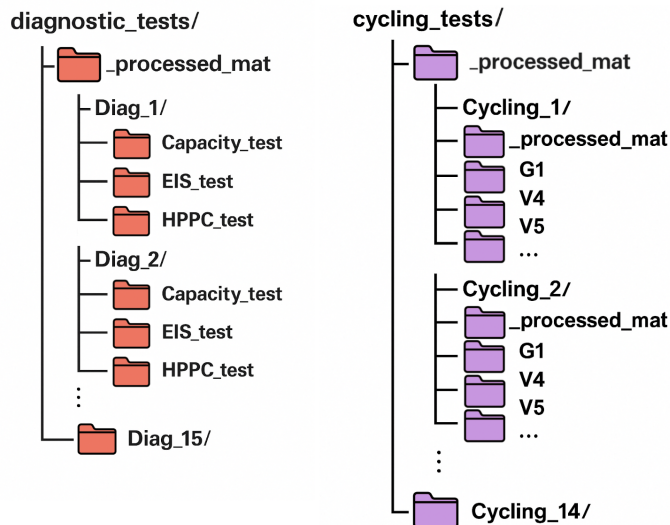


Figure 3.5: Experimental Dataset Structure for [2]

"Diag 1" captures the battery at its peak health (100%), while "Diag 15" captures it at its most degraded state (to varying degrees of degradation).

Each capacity test, as part of the diagnostic testing, includes a full discharge at a low constant current (C/20, or 0.24 A in this case, given the capacity of 4.85 Ah) from a 100%

state of charge (SOC) down to the cutoff voltage (2.5V). The parameters captured include voltage, current, charge capacity, discharge capacity, charge energy and discharge energy. See Figure 3.6 for an example of cell W9's voltage-time curves, collected as part of each capacity test, as it degrades over 341 cycles. The data points were recorded at high temporal resolution throughout the discharge (1 Hz) and generally it took about  $\sim$ 70k seconds or  $\sim$ 20 hours for a full C/20 discharge.

Table 3.2: Number of Cycles Undergone for Each Cell

	W3	W4	W5	W7	W8	W9	W10	G1	V4	V5
Diag_1	0	0	0	0	0	0	0	0	0	0
Diag_2	25	25	25	25	25	25	25	25	20	12
Diag_3	75	75	75	75	75	75	75	30	45	18
Diag_4		123	125	125	125	122	122	37	70	29
Diag_5		132	159	N	148	144	146	62	95	-
Diag_6		159	167		150	145	148	87	120	-
Diag_7		176	187		151	146	151	112	145	-
Diag_8		179	194		157	150	159	137	170	-
Diag_9		-	219		185	179	188	162	194	-
Diag_10		-	244		222	216	225	187	219	-
Diag_11		-	269		247	241	250	212	244	-
Diag_12		-	294		272	266	275	-	-	-
Diag_13		-	319		297	291	300	-	-	-
Diag_14		-	344		322	316	325	-	-	-
Diag_15		-	369		347	341	350	-	-	-

Additional information about the experimental data is contained in Appendices A1.2. The full raw data is 250 GB in size, downloadable from [87].

### Experimental Data in the Context of the Data Generation

As established, the PSO algorithm searches for a set of 8 electrochemical parameters that minimise the error between the P2D model's output voltage and some experimental voltage data, which we take from this dataset. Thus we have a reference for the real battery behaviour at different stages in the degradation, and the model aims to reproduce it by tuning the 8 unknown parameters. So overall, the P2D model's parameters are grounded in experimental observations from these 10 real cells.

The diagnostic capacity tests were used for the parametrisation of the P2D model, however the "real-driving" cycling data was not (i.e data from the 6-step cycling protocol). This is for a few reasons. Firstly, the capacity-test discharging was done at a very low, constant C-rate (C/20), and because of this the measured voltage curve closely represents the cell's equilibrium open-circuit voltage trajectory (with minimal distortion from internal polarisation) across the full SOC range. This makes it ideal for the P2D model fitting.

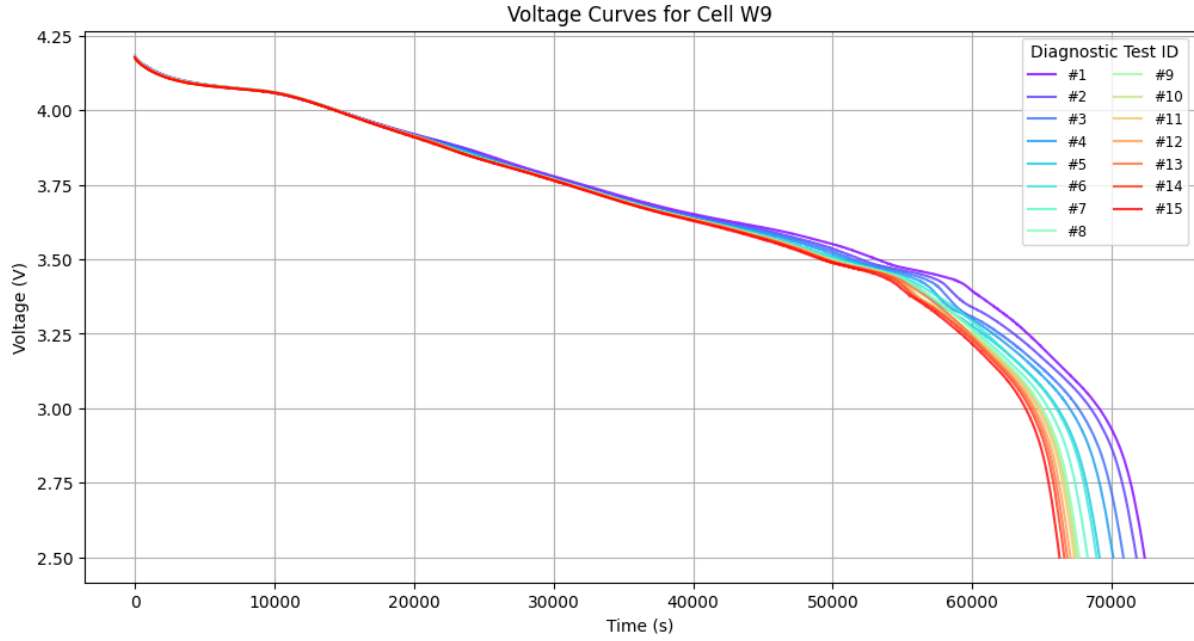


Figure 3.6: Cell W9's voltage-time curves as it degrades over 341 Cycles

Conversely, the cycling data is quite dynamic and covers a wide range of conditions in shorter periods of time, according to the dynamic load profile from UDDS which is meant to simulate real-driving. The cell undergoes varying current pulses (accelerations, decelerations, idle periods), and the high C rates combined with the dynamism (varying loads) can make the voltage response less 'clean', in that it's more like a complex convolution of many effects (i.e IR drops) rather than a direct indicator of the OCV or capacity. The computational cost for the P2D model to fit this data is also much higher because of its complexity.

In summary, the diagnostic data is cleaner and simpler compared to the cycling data. It gives a better measure of the true cell capacity and voltage response, which makes it much better suited to the parametrisation of the model, and also the subsequent synthetic-data generation. Figure 3.2 can provide a good visual example of this; the constant-current periods in Steps 1, 3 and 5 show simple, clean signals while the data in Step 6 (UDDS discharge) is much more complex.

For these reasons, using diagnostic test data is considered a standard approach to the P2D model parameterisation. For example, a paper using the same experimental dataset [88] used the diagnostic tests to parametrise the model, and then the parametrised model could predict the response to the complex profiles with reasonable accuracy. This paper [89] also uses this approach.

An additional point worth mentioning, with regards to the data generation, is that the experimental data does not span a large range of SoH values. The minimum value occurring in the dataset is  $\sim 91\%$ . Considering EV manufacturers generally define the End-of-Life

point for cells at about 75-80% SoH, this does serve as a limitation for the study.

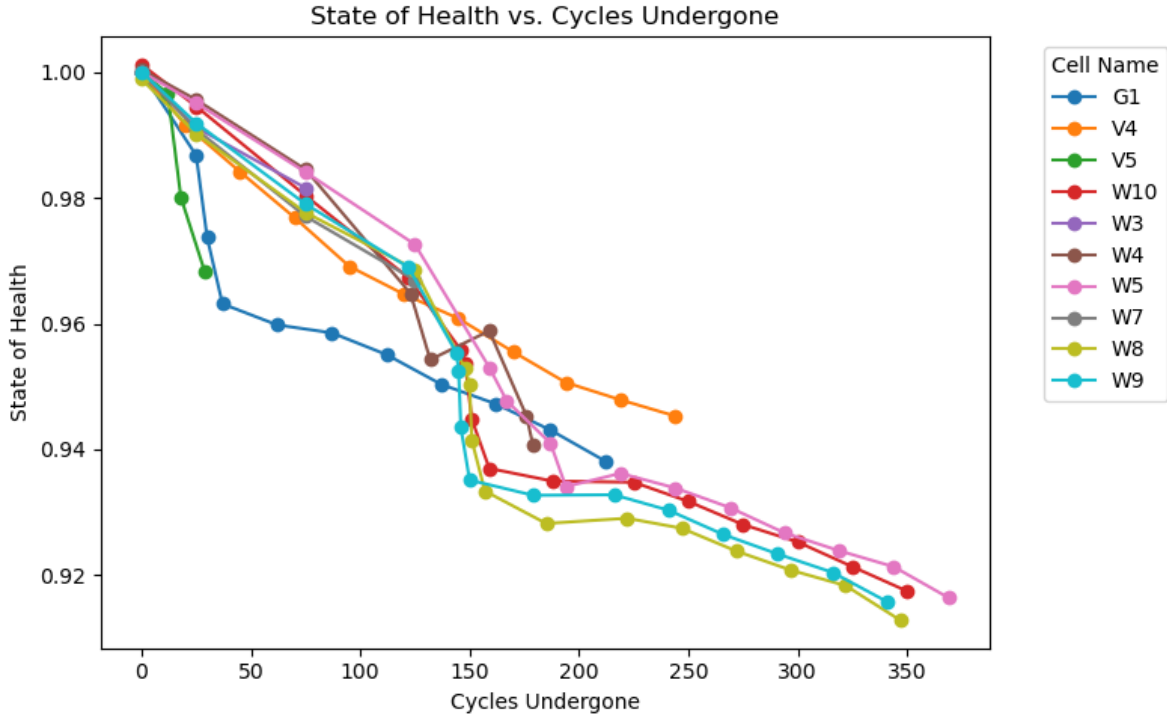


Figure 3.7: Relationship between Battery Cycling and Capacity Fade of Each Cell

### 3.1.3 Generating the Synthetic Dataset

This section will summarise the approach used to generate the synthetic data, and delve into how we adapt the P2D model to account for the degradation in the experimental dataset - this step requires a thorough feature analysis, with regards to established mathematical foundations (see Appendix A1.3). The model is calibrated for further experiments using the results of these experiments.

#### General Overview

To create a synthetic dataset representative of real battery behavior, the physics-based P2D model is calibrated against experimental discharge data. The experimental data consisted of diagnostic discharge curves spanning 0.91–1.00 state of health (SOH), which covers the battery's early degradation range. The P2D model's eight key electrochemical parameters (see Table 3.1) are selected for tuning due to their nature as part of the model; they strongly influence the cell voltage profile, and are also known to evolve as the battery ages.

The PSO algorithm iteratively adjusts the parameters' values so that the model's simulated voltage closely matches each experimental discharge curve. Through this calibration procedure, the P2D model produces 'synthetic' voltage profiles that closely mirror the experimental curves at each SOH point.

By demonstrating that the P2D model can reproduce the experimental discharge profiles with high accuracy, we can have confidence that it captures the underlying physics of degradation.

Creating the synthetic data for scenarios where no direct experimental reference exists would be the next step, but given time and resource constraints this falls outside of the scope of this project. However, this approach of using the calibrated electrochemical model to generate synthetic data across more ageing conditions is consistent with recent methodologies, as discussed in the previous Section 3.1.2. A deep understanding and investigation of the 8 key parameters, as well as the other fixed parameters, would be necessary to achieve a reliable extrapolation of the model into untested ageing regimes, i.e. to generate credible synthetic voltage profiles for SoH levels beyond those captured by this set of experimental data.

Due to time limitations of the project, an investigation into the 8 key parameters will be the sole focus in this project work, together with the subsequent validation of the synthetic data created via this approach of data-driven modelling.

## Mathematical Foundations

An important aspect of the parameter fitting was the use of bounded ranges for each parameter, i.e the bounds of the PSO search space.

The original model constrains each parameter to vary only within  $\pm 30\%$  of its initial guess value during the PSO optimisation. The initial guesses were based on literature values for a healthy cell, and the  $\pm 30\%$  possible deviation was chosen to make sure the identified parameters remained physically plausible. There is no specific justification provided by the author for the exact  $\pm 30\%$  possible deviation, i.e the specific value of  $\pm 30\%$ , but it can be viewed as a practical tolerance which accounts for variability between cells in terms of chemistry differences, measurement uncertainty, etc. while enforcing the physical feasibility of the values.

Part of the feature analysis involved examining these parameters and their relationships to degradation processes for the LG Chem cell, and considering whether this  $\pm 30\%$  bound is adequate for the data generation.

Both the LG Chem INR21700-M50 and M50T have an NMC 811 formulation for the cathode and a Graphite-SiO<sub>x</sub> anode [77]. The degradation mechanisms described in [78] are suitable for this type of cell.

In the Appendices A1.3 I have provided an in-depth analysis of the equations which underlie the degradation mechanisms, and how they relate to each of the 8 parameters. The aim of this analysis is to investigate the established relationships between the parameters and how

the cell degradation may affect these parameters. Thus, these established relationships can be referenced when analysing the evolution of the 8 parameter values as the cell degrades (or, how PSO tunes the parameters to approximate the degraded curves).

This is especially necessary as the experimental reference data captures a larger SOH range than just a 100% healthy state, for which the P2D model was originally calibrated. So, to account for this inherent diversity of the experimental data, and replicate it, experiments which involved both reducing and increasing the parameter bounds were carried out. The aim of these experiments was to find the best bounds for the data generation.

## Experimental Design

Varying the PSO bounds was tested, from as little as  $\pm 10\%$  up to  $\pm 1000\%$  deviation. To recall, these values reflect the possible deviation from the initial parameter estimates, i.e the limits of the PSO search space.

Two scenarios were ran: one in which a non-negative lower bound was enforced, i.e reflecting that the parameter values cannot be negative, and another in which the parameters were allowed to become negative, which would in reality not be physically feasible (none of the parameters can be negative-valued). This was to investigate the difference between how the PSO chooses the parameter values in each case; how much would the absence of sign constraints distort the fitted values, since PSO has no intrinsic sense of physical feasibility unless enforced by the bounds? PSO could choose negative values simply because it leads to a lower RMSE / fitting error. So, examining the optimised parameter sets in each scenario is one way of showing how the bounds affect the model's behaviour.

Then, within each scenario the bounds were varied from  $\pm 10\%$  to  $\pm 1000\%$  in increments of 10%, and then from  $\pm 1000\%$  to  $\pm 10000\%$  in increments of 50%. This was to investigate the effect of narrow bounds, medium-size bounds and very large bounds on the model's behaviour.

Additionally, another 2 experiments were carried out in which two parameters' initial values were changed, ( $D_{s,n}$  and  $D_{s,p}$ ). The P2D model was defined using initial values from [1], in which there are both 'experimental' values and 'simulated' values for the parameters. In [4] a combination of experimental and simulated values were chosen for the P2D model, not just one or the other. For example, the value for the 'positive electrode diffusion coefficient'  $D_{s,p}$  is set at  $4.10 \times 10^{-15}$ , the simulated value, while the 'positive electrode maximum concentration' or 'ctp' value chosen is the experimental value. It can be assumed that the model was tested using various configurations of these experimental and simulated values, and the best final configuration was chosen. My results agree with this, as the configuration using the values selected by [4] did have the lowest loss.

I only did a short experiment, as there would be many different configurations possible to try otherwise. I tested 4 configurations in total; A, in which the initial values remained the same, B in which the  $D_{s,p}$  value was changed to the experimental value, C in which the  $D_{s,n}$  value was changed to the experimental value, and D in which both the  $D_{s,p}$  and  $D_{s,n}$  values were initialised with the experimental values. The model could not even compute results for Configuration C, so this was omitted from the final results. Additionally, the results for D were poor, so they were omitted from the main body of the report, but can be seen in Appendices A1.3.2.

The simulated  $D_{s,n}$  value was actually 1800% larger than the experimental value, so perhaps it is somehow dramatically out of sync with the rest of the parameters, causing the computation error. Still, the model uses a combination of experimental and simulated values without issues. However, the experimental  $D_{s,p}$  value did work, although the results were poor; the simulated value is only 170% larger than the experimental value.

The point of these experiments is to test how the model performs when its bounds are changed to varying degrees, and also see how the parameters change. Testing different initial values provides some additional insight.

### Experiments to Determine Parameter Variability

In each experiment, the loss between the simulated output and the experimental reference is minimised by adjusting the 8 parameters. Thus we can investigate the set of values PSO came up with to see whether there are patterns in how the parameter values are chosen, and if they reflect the expected relationship between the parameter and degradation; or, if the parameter values are chosen randomly by PSO, in a way that minimises the loss but does not reflect the expected change in parameter value over degradation. It can be expected that very large bounds would lead to the latter, a high loss but struggling to capture the degradation trends, while very narrow bounds would have a high loss and also struggle to capture the degradation trends due to being over-constrained.

First of all, it is worth mentioning that only 4 cells underwent all 15 diagnostic tests (cells W5, W8, W9 and W10). So, there is actually more data available in the earlier stages of degradation (10 cells/test in Diag 1,2,3 as opposed to 4 cells/test in Diag 13,14,15). Thus, the amount of data in the later stages of degradation is less.

The amount of time to compute one simulation generally ranges from 5-20 minutes, as such only one sample was computed for each combination of pp-value and capacity test per cell. This was repeated for each scenario/condition (i.e lower bound set to zero or allowed to be non-zero). 'pp-value' refers to the bound width / deviation, i.e a pp-value of 0.3 is equivalent to a deviation of  $\pm 30\%$  from the initial values.

For the first experiment, bounds of  $\pm 250\%$  to  $\pm 500\%$  achieved the lowest loss in capturing all stages of degradation (i.e simulating the voltage output), see Figure 3.8.

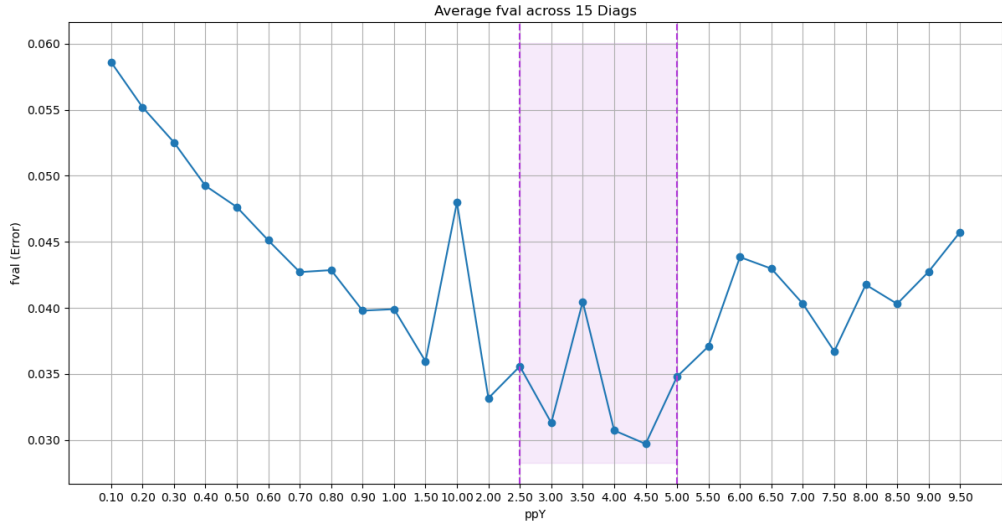


Figure 3.8: Average Loss Across All Cells During Degradation: X-axis represents bound width ( $0.10 = \pm 10\%$ ,  $5 = \pm 500\%$ ), Y-axis represents RMSE Loss Between Simulated and Experimental Data

In Appendices A1.3 it was established that each of the 8 parameters is expected to have a decreasing trend as the cell degrades. We can expect D1, the electrolyte diffusion coefficient, as an example, to decrease on average. See the following plots which investigate the trend of D1 values depending on the PSO bounds:

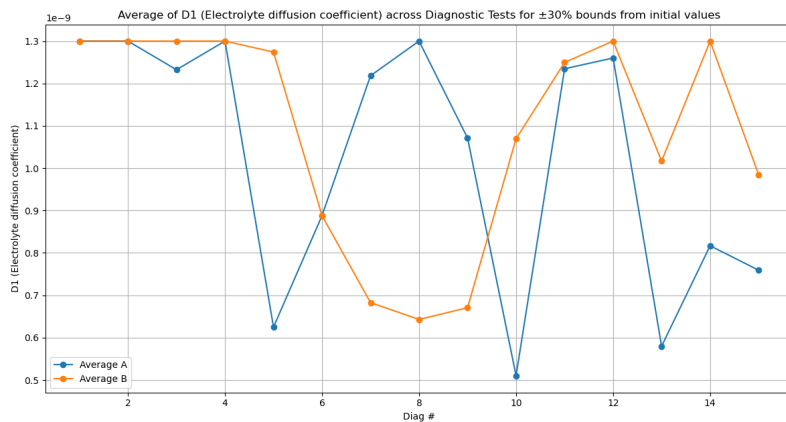


Figure 3.9: Average D1 Value For Bounds of  $\pm 30\%$  Initial Value - No Apparent Trend

Figure 3.8 would suggest that the bounds varying  $\pm 250\%$  to  $\pm 500\%$  result in the best results for the model, as they achieve the lowest RMSE. However, Figure 3.12 could suggest otherwise. The D1 value shows no clear trend for either configuration A or B. PSO is likely

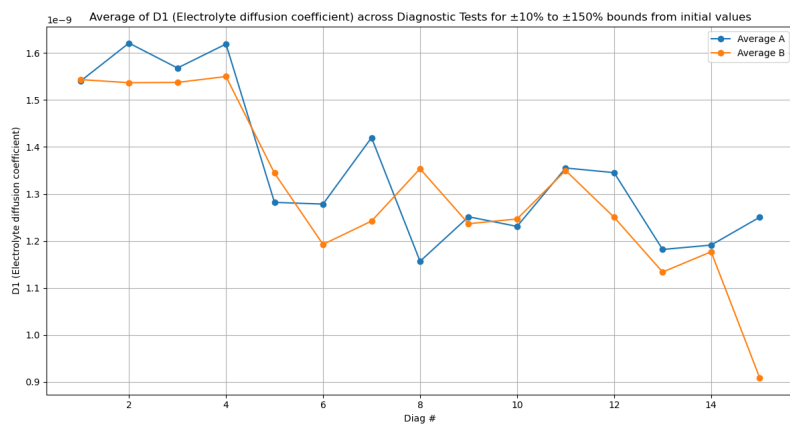


Figure 3.10: Average D1 Value Across Bounds of  $\pm 10\%$  to  $\pm 150\%$  - Shows Decreasing Trend

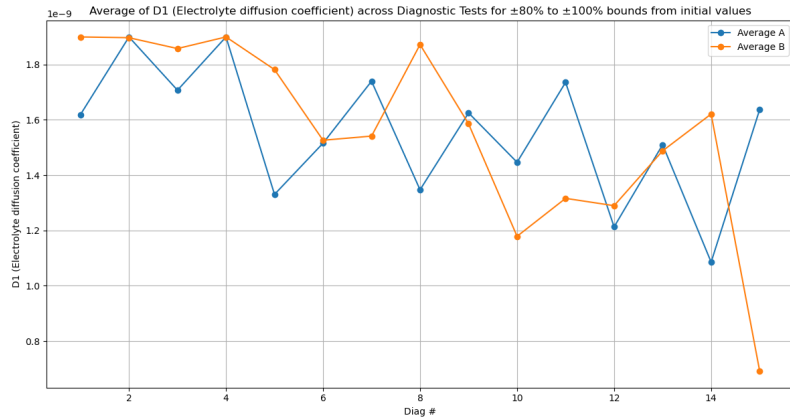


Figure 3.11: Average D1 Value Across Bounds of  $\pm 80\%$  to  $\pm 100\%$  - Shows Decreasing Trend

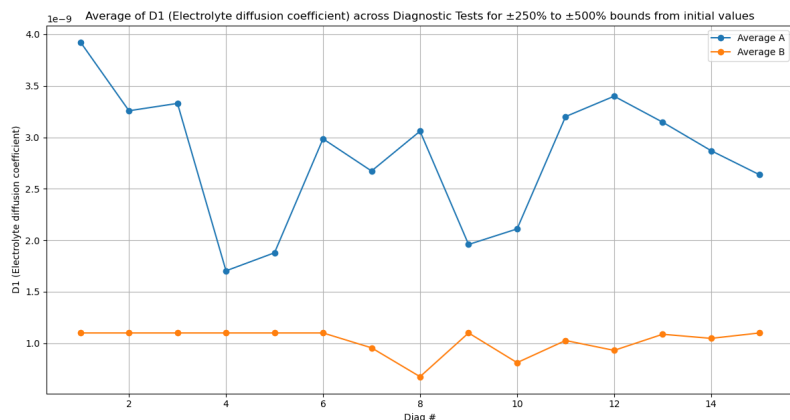


Figure 3.12: Average D1 Value Across Bounds of 250% to 500% - No Apparent Trend

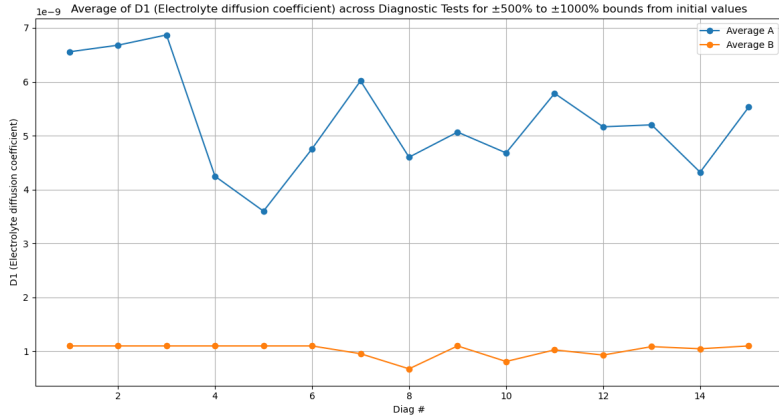


Figure 3.13: Average D1 Value Across Bounds of 500% to 1000% - No Apparent Trend

choosing values that result in the best solution to minimise the loss, but these bounds do not replicate physical conditions. Meanwhile, the baseline  $\pm 30\%$  value that was originally used in the model does not achieve any better; see Figure 3.9. The D1 values again seem to be random and there is no trend. This is expected, however, as the  $\pm 30\%$  value is likely too constrained to capture the degradation pattern.

Figure 3.10 shows that within the range of  $\pm 10\%$  to  $\pm 150\%$ , although the loss is not as low as values in the range of  $\pm 250\%$  to  $\pm 500\%$  for example, D1 has what appears to be a decreasing trend, in alignment with physical expectations that the electrolyte diffusion slows down as the cell degrades (e.g. due to SEI thickening and particle cracking) as discussed in Appendices A1.3. This is the aim for the synthetic data generation - to define bounds that enforce the physical limits of the parameters, but are not so constrained that the degradation behaviour cannot be captured. Figure 3.11 looks at the more narrow range of  $\pm 80\%$  to  $\pm 100\%$ , which achieves a similar trend.

Of course, the results must be taken with a 'grain of salt' so to speak, as the amount of data for this analysis is small (303 total generated samples), as well as the range of degradation over which the samples are generated. However, there does appear to be a decreasing trend in D1's value. Other parameters show similar results - see Appendices A1.3.2.

Overall, a value of  $\pm 100\%$  was chosen for the data generation, in order to balance capturing the degradation patterns with the enforcement of physical limits. This is also due to the fact that above  $\pm 100\%$  from the initial values, the parameter values could become negative. Although a zero-bound could be enforced, the bounds would then become asymmetrical, i.e. this would introduce an asymmetrical search space, and that disturb the PSO convergence process. For example, in Pypop documentation [90], for each decision variable (i.e one of the 8 parameters being optimised)  $x_i$ , the lower and upper bound  $[x_i^{\min}, x_i^{\max}]$  is specified.

These bounds are centred on the initial values  $x_i^0$  by setting

$$x_i^{\min} = x_i^0 - \Delta_i, \quad x_i^{\max} = x_i^0 + \Delta_i,$$

In this case, the bounds are specified as  $x_i^0 \pm \Delta_i$ , so that the exploration is unbiased in both directions. This is standard in PSO. Asymmetrical boundaries are possible, but bias is a side-effect. Imagine that the initial value is at 150. For bounds of  $\pm 200\%$  the initial value, with a lower limit of zero, that puts the bounds at [0, 450]. Particles would tend to accumulate near 0, the closer bound, due to how PSO works with its global/personal 'best' finding.

So, for subsequent experiments, the bounds are  $\pm 100\%$  from the initial values to provide a flexibility for the 8 parameters in response to the battery ageing.

## Generating the Data

To emphasise again, no extrapolation beyond the original experimental conditions was introduced when generating the synthetic dataset. The synthetic discharge profiles were created only for the same range of conditions that were empirically observed (SOH 0.91–1.00), with no additional or more degraded states simulated outside this range. In other words, each synthetic curve has a one-to-one correspondence with an actual measured experimental curve, differing only in that it is produced by the calibrated model instead of direct measurement. There are some inherent differences in terms of noise, there is the initialisation period of the P2D model, etc. The term "synthetic" here denotes that the data were obtained from simulation; it does not imply any invented behaviour or extrapolated scenario, which falls outside the scope of the project. The synthetic dataset stays within the bounds of observed data, as high fidelity to reality must be maintained before extrapolation or the introduction of parameter trends.

For each experimental curve, 10 synthetic samples were produced. As such, the final synthetic dataset has 1010 samples. Figure 3.14 illustrates the average error between each synthetic sample and the corresponding experimental reference sample at different points of degradation. It is quite noticeable that the error is much higher for the first 3 diagnostic tests, after which it reduces and stays constant at about  $\sim 0.025$  V. The final overall RMSE across all samples is 0.0363 V, however, the average across diagnostic tests 4–15 is only 0.0237 V.

Figure 3.15 shows how the RMSE values are distributed; in most cases the P2D model is fitting the experimental data quite closely, as can be seen in that the bulk of the distribution sits at the lower RMSE values. There are however some apparent 'poor' fits on the right-tail, likely the majority of these consist of diagnostic test samples from Diags 1,2,3. To investigate this, I plotted the distribution of RMSE across only Diags 4–15 in Figure 3.16 as well. There

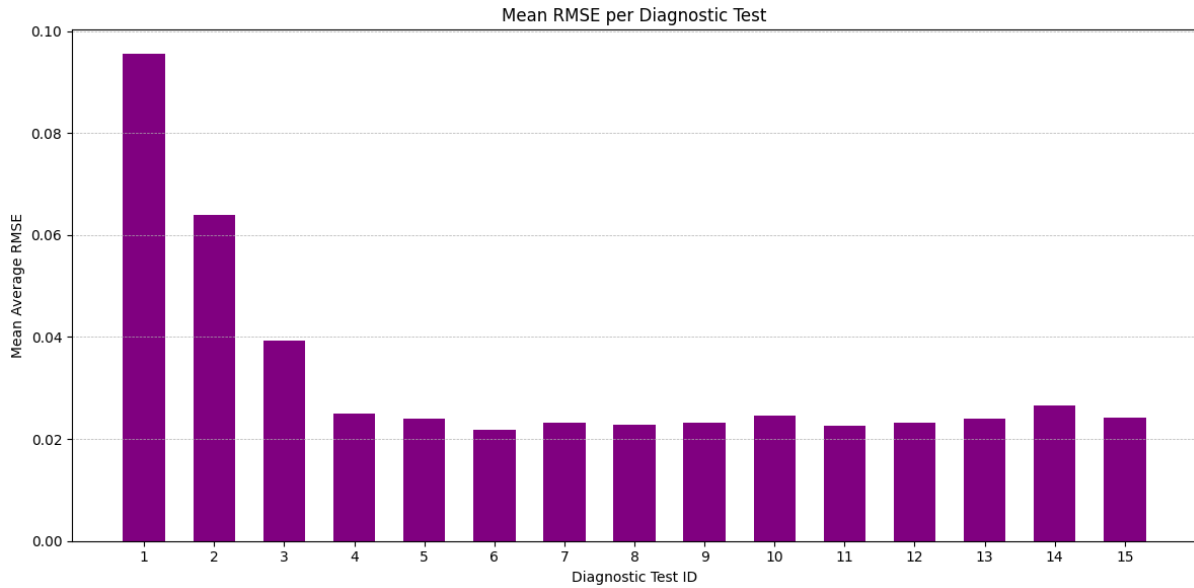


Figure 3.14: Mean RMSE (V) Across All Diagnostic Tests

are very few occurrences of samples above 0.03 V RMSE, and virtually none above 0.04 V RMSE (only 9 out of 1010 total samples). Comparing the RMSE distributions shows that the model struggles to capture the battery's behaviour at 'peak' health, or near-peak health, and it actually appears to capture it better after some initial degradation.

There is a differing amount of cycles undergone for each cell per diagnostic test; diagnostic test 2 was generally carried out after 25 cycles, and diagnostic test 3 after 75 cycles, though some cells underwent a few less. See Figure 3.2 from Section 3.1.2. See Figure 3.7 from Section 3.1.2 which shows the SoH vs Cycles undergone - I have also plotted the average SoH of the cells at each diagnostic test in Figure 3.17. Based on this summarisation of the data, it would appear the P2D model is more successful at replicating the data from a  $\sim 97$  SoH and below.

There could be a few reasons for this. In Appendix A1.2.1, differing initial capacities of the M50T cells is investigated. This could be one reason for discrepancy - there are cell-to-cell variations in terms of starting capacity, or SoH (since we are using the capacity-based definition of SoH). This will be discussed in Section 4.

See Figure 3.19 which shows the synthetic voltage curves over battery degradation, similar to Figure 3.6 in Section 3.1.2. As can be seen, the P2D model clearly struggles to capture the battery at its peak state of health, in diagnostic tests 1-3, but after that it somewhat accurately mimics the expected curves. Aside from unsuccessfully capturing the peak state of health, there are some differences which are most noticeable after the  $\sim 50$ k second mark; for example, Figure 3.6 shows some fan-out behaviour in the different curves before hitting the knee-point. There is also more variation in the knee-location and slope, although this is most apparent in the peak-health curves from diagnostic tests 1,2,3, after which the

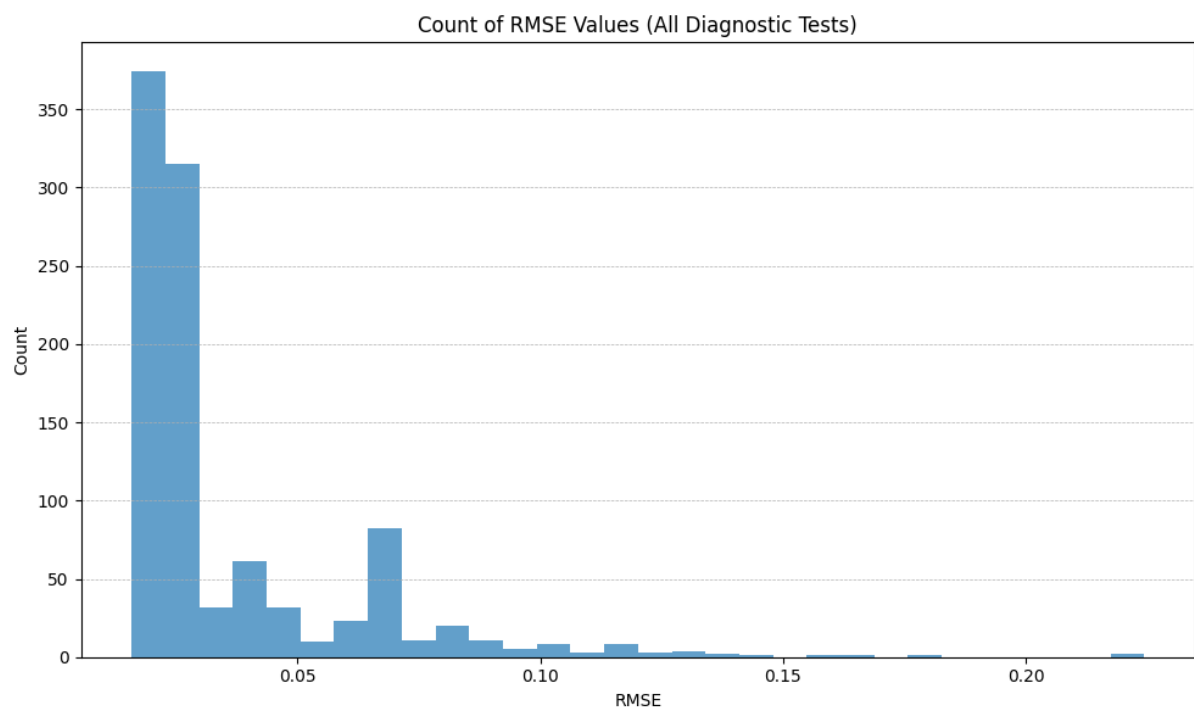


Figure 3.15: Occurrence of Different RMSE Values Across All Diagnostic Tests

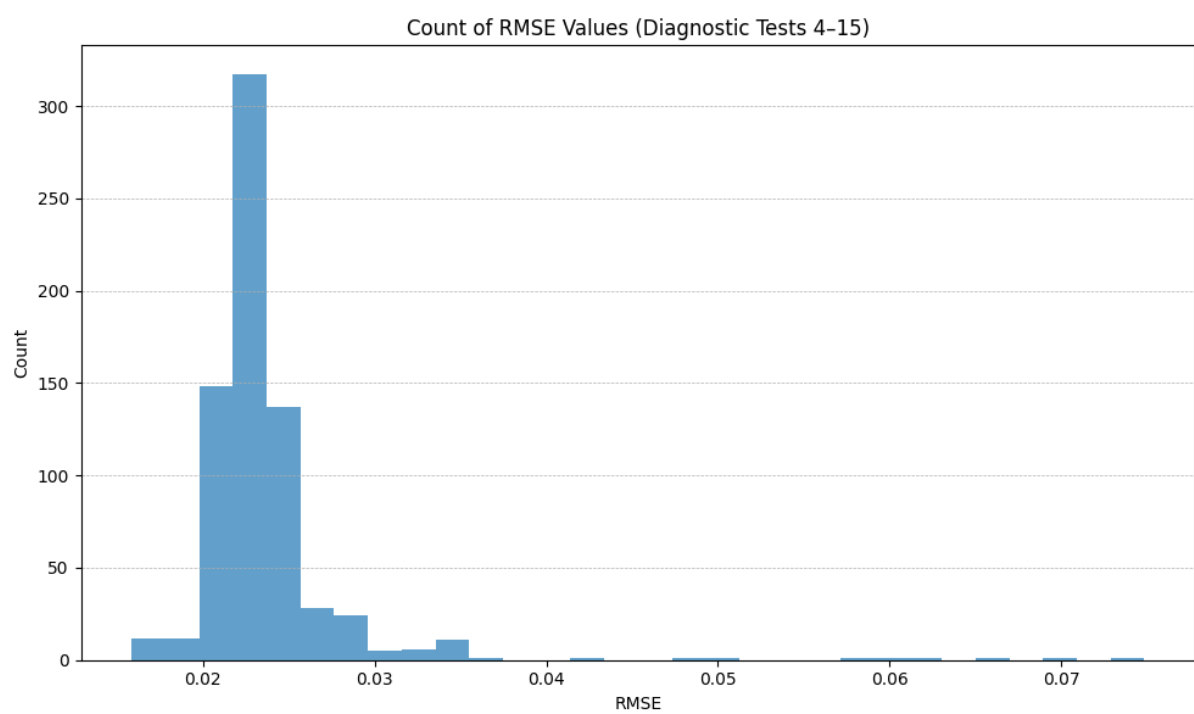


Figure 3.16: Occurrence of Different RMSE Values Across Diagnostic Tests 4-15

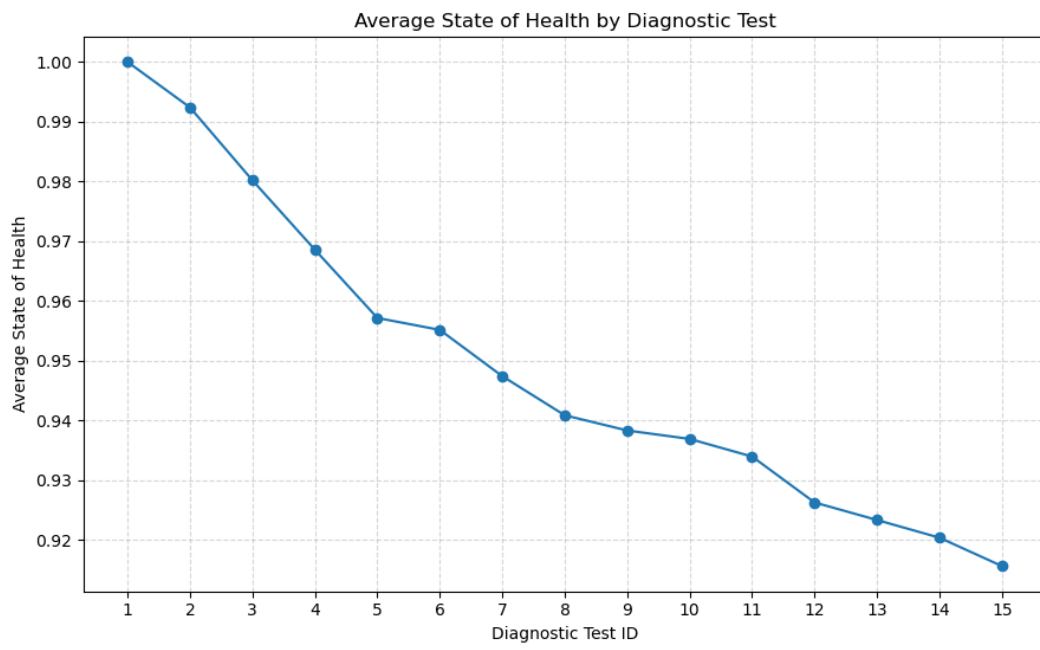


Figure 3.17: Average SoH per Diagnostic Test

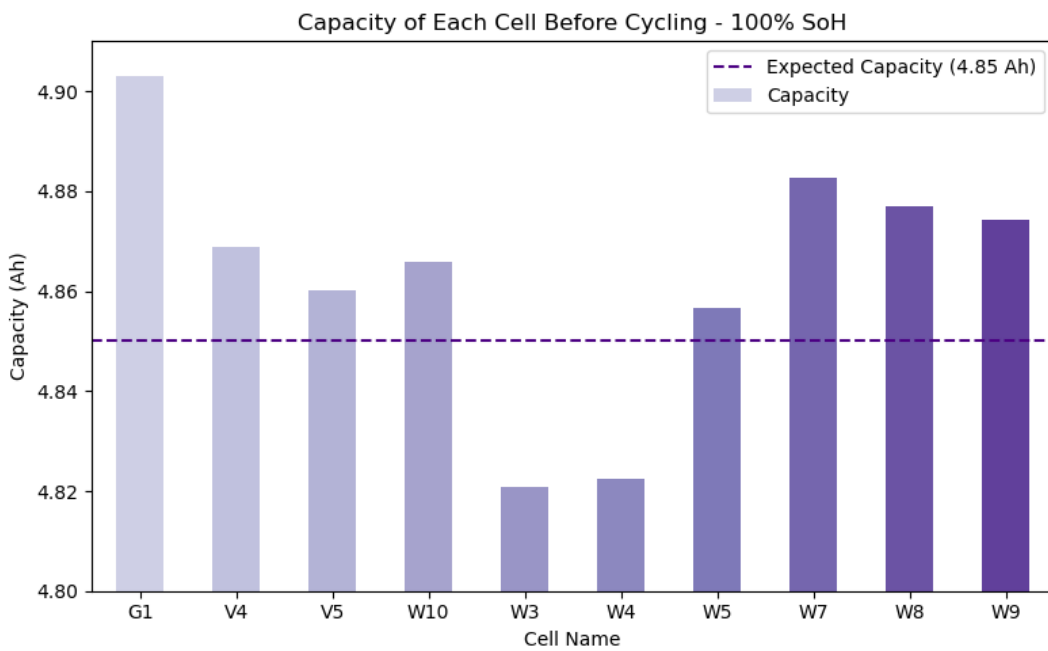


Figure 3.18: Differing Initial Capacities of the M50T Cells

variation is not as significant (see Figure 3.6).

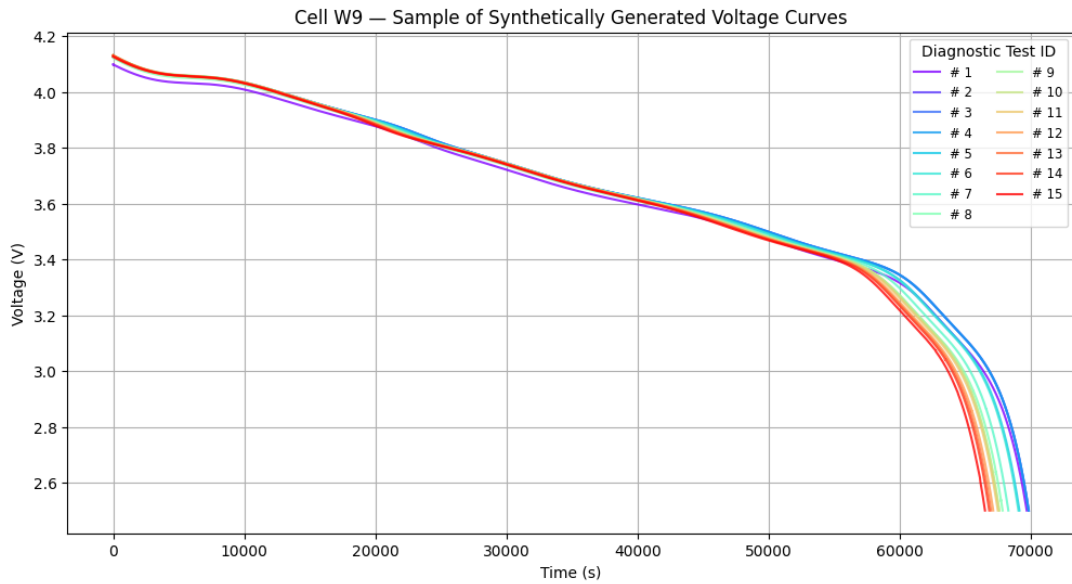


Figure 3.19: Synthetic Voltage-Time curves based on Cell W9's data, as it degrades over 341 Cycles

Figure 3.20 represents one of the curves with the highest RMSE in the dataset - the difference in timespan between the full discharge is significant. Figure 3.21 represents another curve from the first diagnostic test, with a slightly lower loss, however the discrepancy in discharge behaviour is especially noticeable after the knee of the curve, and again the final time for discharge varies from the experimental reference.

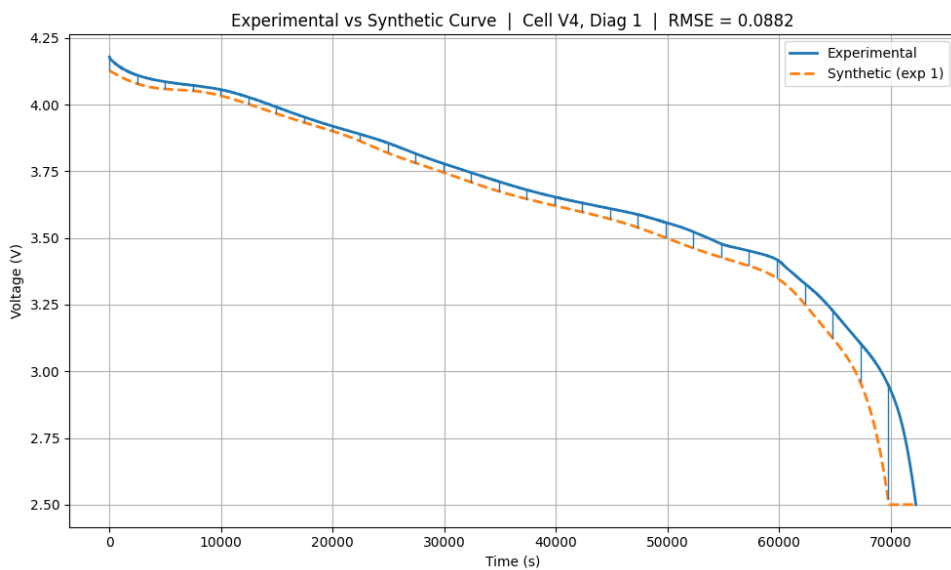


Figure 3.20: Very High RMSE Synthetic Sample for V4 Diagnostic #1

To see a more representative example of the data, see Figure 3.22 which has an average RMSE value (amongst the samples created for diagnostic tests 4-15). Even in this example

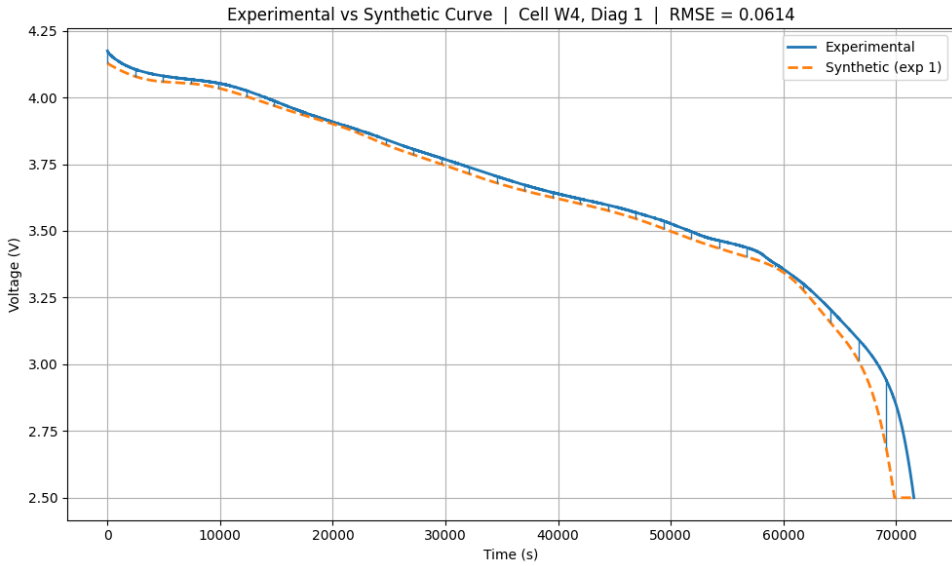


Figure 3.21: High RMSE Synthetic Sample for W4 Diagnostic #1

where the model is capturing the curve with a low RMSE, there are some apparent discrepancies; first of all, the simulated curve is noticeably smoother than the 'real' curve. Additionally, there is a noticeable dip at the knee of the curve in the experimental data, which does not appear in the synthetic data. This is a discrepancy present in the majority of the samples, even the ones with low RMSE - clearly the P2D model fails to capture this behaviour. For example, see Figure 3.22 which shows a sample with quite a low RMSE value. The experimental data is well-approximated, but still there are some minor discrepancies in the shape of the curve, most apparent at the knee-point.

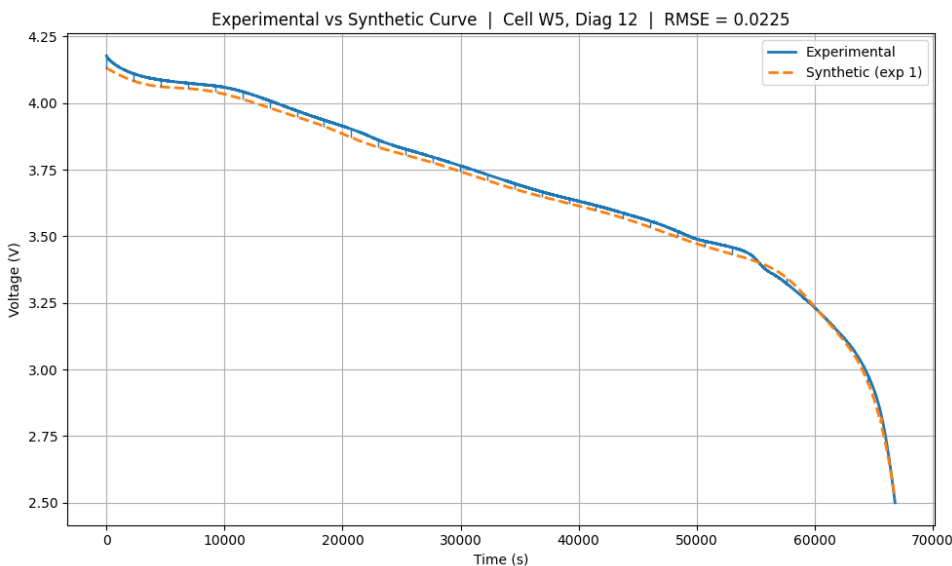


Figure 3.22: Average RMSE Synthetic Sample for W5 Diagnostic #12

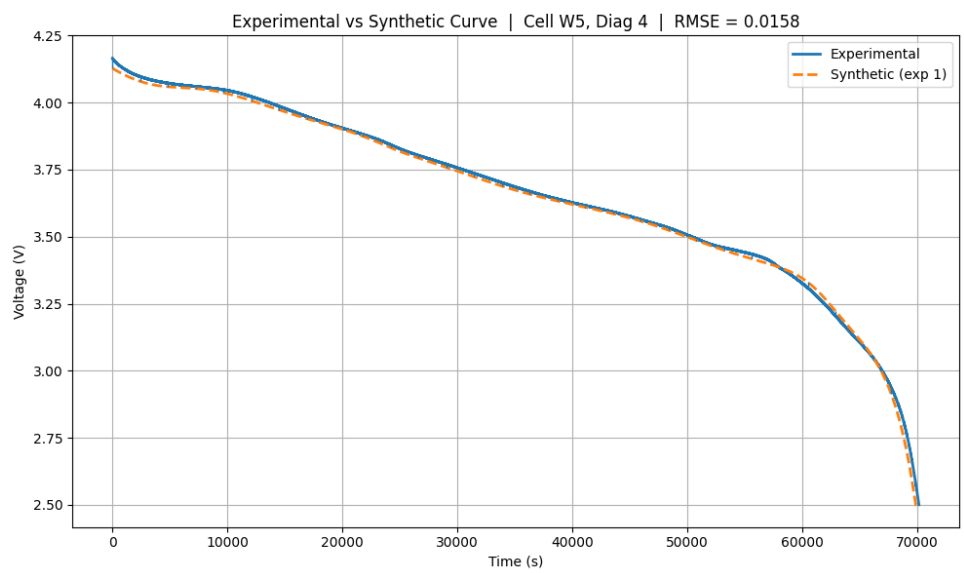


Figure 3.23: Very Low RMSE Synthetic Sample for W5 Diagnostic #4

## 3.2 Validation of the Generated Data

As established in Chapter 2, capturing 'real' battery degradation data is very time-consuming and expensive. Additionally, existing data is limited in the range of scenarios it covers (cycling conditions, range of degradation covered, etc.) as well as the amount of data (i.e number of samples) and types of batteries for which data is available.

The experimental dataset used in this study consists of only 101 discharge curves (from the diagnostic tests) across a SoH range of 0.91-1.00. This scarcity of reference curves makes it difficult to train or benchmark a system for the purpose of SoH estimation. This is typical of publicly available datasets. The results in Section 3.2.2 show that use of this dataset alone is not sufficient to train a SoH estimation model. In order to support LiB health prognostics, investigation into the augmentation of the existing dataset via synthesis of data is valuable. The results in Section 3.2.2 show that this method did support enabled the creation of an SVR-based SoH estimation model which when evaluated on experimental data, achieved a high accuracy and significantly improved the prediction fidelity compared to the model trained on the 'real' experimental data alone.

This section includes the data pre-processing pipeline, and the experimental method for validating the data via the SVR model. The final model accuracy is evaluated for when the model is trained on (a) only experimental data, and (b) only synthetic curves.

### 3.2.1 Data Pre-processing

The code and data can be found here: <https://github.com/maria15034/MAI-Project>.

Firstly, the raw data for both datasets must be prepared - see 'Data\_Preparation.ipynb'. The 'sorted\_labelled\_data.xlsx' file has the labels for both datasets.

The experimental data is quite straightforward to prepare. It is saved into 'experimental\_data\_all.csv' with the columns 'time', 'voltage', 'cell\_name', 'diagnostic\_test\_ID', 'state\_of\_health'.

The synthetic data is captured at 0.2 Hz instead of 1 Hz - i.e, one voltage data point every 5 seconds instead of every second, so to align the synthetic samples with the experimental ones it was necessary to upsample the data. This was done using a simple linear interpolation method, via numpy's 'interp' function. The synthetic data also includes an 'initialisation' period, i.e this is why the P2D MATLAB implementation involves an 'initime' variable of the value '200' in the solver; 200 seconds are given for the initialisation of the simulation model, i.e to establish some consistent initial states before the discharge begins. So, when preparing the synthetic data, any values for  $t < 0$  were simply discarded.

The prepared data is concatenated into these .csv files for ease of use in modelling the data.

The synthetic data csv 'experimental\_data\_all.csv' has an additional column, 'experiment' which refers to the experiment number (of which there are 10 per diag per cell).

## Noise analysis

Prior to modelling, some further analysis of the data samples is done. Figure 3.24 shows a statistical comparison between the voltage-time curves in the synthetic and experimental data. The values in Table 3.3 show that there is very little difference between the curves, at least statistically.

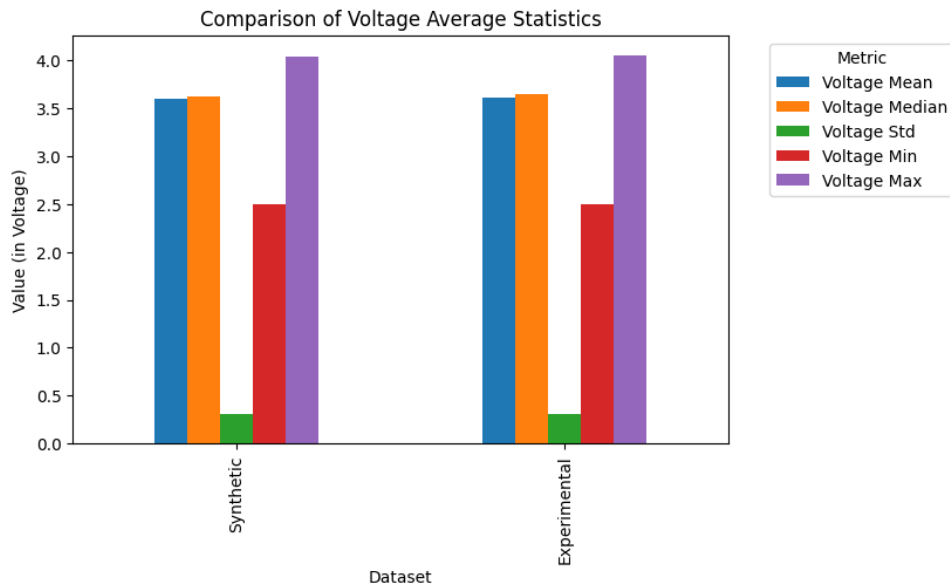


Figure 3.24: Statistical Comparison of Voltage-Time Curves

Table 3.3: Voltage Average Statistics

	Voltage Mean	Voltage Median	Voltage Std	Voltage Min	Voltage Max
Synthetic (clean)	$3.60 \times 10^0$	$3.63 \times 10^0$	$3.05 \times 10^{-1}$	$2.50 \times 10^0$	$4.04 \times 10^0$
Experimental	$3.61 \times 10^0$	$3.65 \times 10^0$	$3.12 \times 10^{-1}$	$2.50 \times 10^0$	$4.06 \times 10^0$

However, looking closely at the voltage data shows that there are small fluctuations, or noise, in the experimental data which do not appear in the synthetic data. See Figures 3.25, 3.26, and 3.27.

So, it is clear based on these figures that there is some very small fluctuations in the experimental data that does not appear in the synthetic data. This is likely some noise from the acquisition of the experimental data, i.e sensor noise. The synthetic data also has approximately 1/5 of the data points of the experimental data (0.2 Hz as opposed to the 1 Hz sampling of the experimental data), and the linear interpolation done in the data preparation to align the synthetic points with the experimental points further smooths the synthetic data. Some supplemental experiments that take this noise into account were done and are discussed in the Appendices3.2.2.

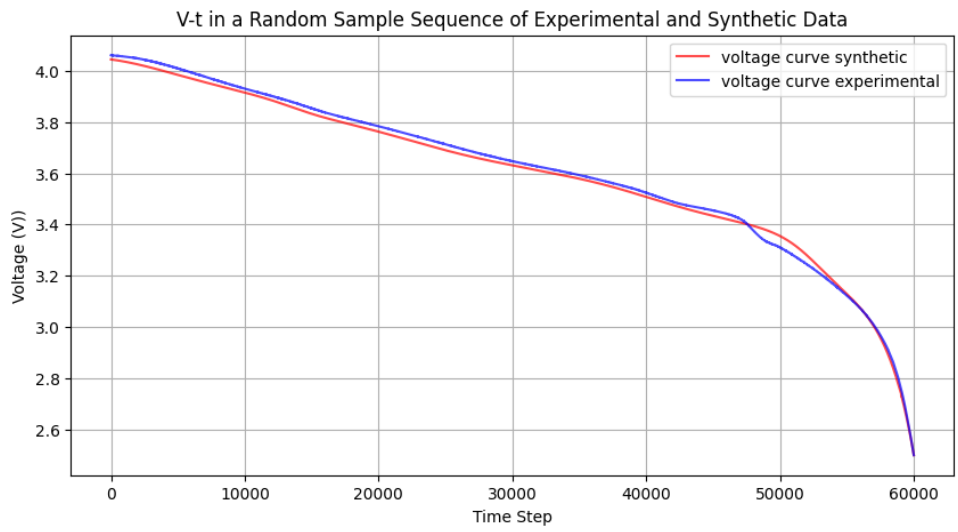


Figure 3.25: Random Data Sample

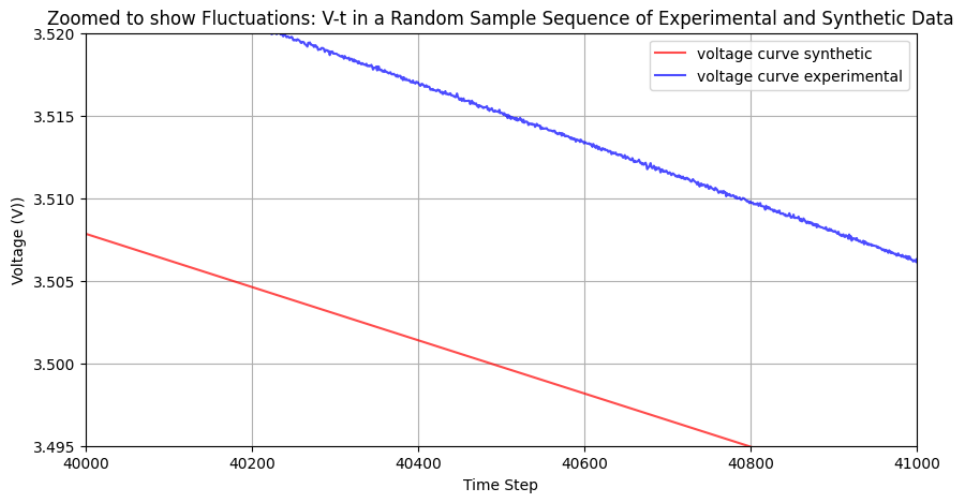


Figure 3.26: Random Data Sample - Zoomed

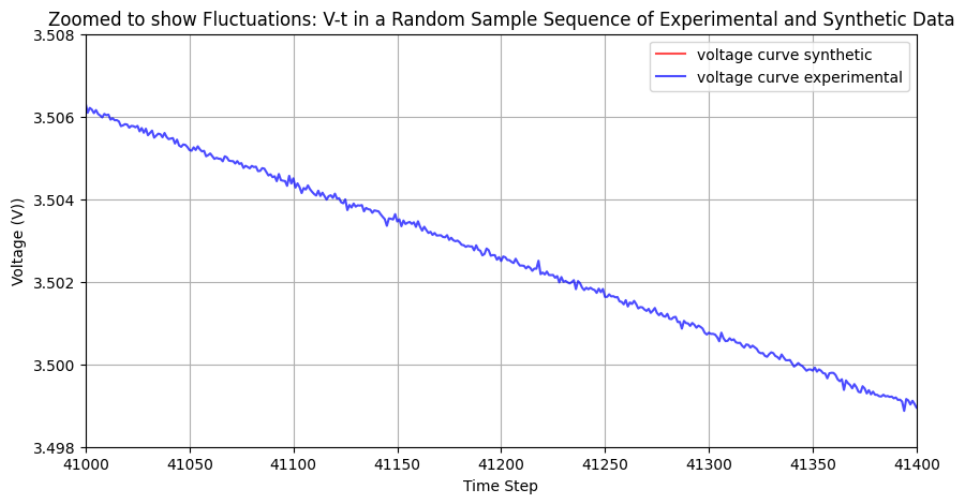


Figure 3.27: Random Data Sample - Further Zoomed on Experimental Curve to show noise

## Preparing Input for Modelling

The discharge curves are now prepared into organised .csv files, but they still have to be turned into fixed-length feature vectors to be provided as input to the models in Section 3.2.2.

Each voltage-time discharge curve is converted into a fixed-length sequence of two features (voltage and its instantaneous slope  $dV/dt$ ), and a single target label (the cell's SoH).

To do this, 2 methods of extracting sequences are tested.

The first method involves taking the full sequence and padding it to the maximum sequence length amongst all curves in both datasets (72774 data points). The padding is done with values of 2.5 V as this is the cutoff point for the curves.

The second method involves truncating the sequences to a fixed length. Using this method also explores the hypothesis that the most valuable data is stored in the end parts of the curves; For example, if you look at Figure 3.6 which shows the experimental voltage-time curves as the W9 cell degrades over time, or Figure 3.19 which shows the same but for the synthetic samples, the biggest visual difference between the discharge curves occurs in the last  $\sim 15k$  data points. This method is tested for 3 different sequence lengths; one for which only the last 20k points are taken, one for which the last 40k points are taken, and one for which the last 60k points are taken.

Each method is evaluated in Section 3.2.2 to see which achieves the best results for the model/experiment at hand.

Within each group, the following column is computed:

$$(\text{seq\_length}, 3) = [[V, \frac{dV}{dt}, \text{SoH}]]_{\text{seq\_length} \times 1}$$

Where  $dV/dt$  is computed as follows (the time step is discussed in Section 3.2.2):

$$\left. \frac{dV}{dt} \right|_i = \frac{V_{i+1} - V_i}{t_{i+1} - t_i}$$

Each of the input features is also scaled between 0 and 1, using the following formulae. SoH uses global scaling since the ranges are the same for both datasets. When denormalising the output of the model in 3.2.2, the relevant scaling values used to normalise voltage and  $dV/dt$  are used.

$$\text{SoH}_{\text{scaled}} = \frac{\text{SoH} - \min(\text{SoH})}{\max(\text{SoH}) - \min(\text{SoH})}.$$

$$v_{\text{exp, scaled}} = \frac{v_{\text{exp}} - \min(v_{\text{exp}})}{\max(v_{\text{exp}}) - \min(v_{\text{exp}})}, \quad v_{\text{syn, scaled}} = \frac{v_{\text{syn}} - \min(v_{\text{syn}})}{\max(v_{\text{syn}}) - \min(v_{\text{syn}})}.$$

To normalise  $dV/dt$ , the following equation is used, but the voltage min/max is not global, it's based on whether  $dV/dt$  is for the experimental or synthetic data (these labels would make the equations messy so they are omitted).

$$\frac{dV}{dt}_{i,\text{scaled}} = \frac{\frac{V_{i+1} - V_i}{t_{i+1} - t_i} - (dV/dt)_{\min}}{(dV/dt)_{\max} - (dV/dt)_{\min}} \quad (3.1)$$

$$\text{where } (dV/dt)_{\min} = \min_j \left\{ \frac{V_{j+1} - V_j}{t_{j+1} - t_j} \right\}, \quad (dV/dt)_{\max} = \max_j \left\{ \frac{V_{j+1} - V_j}{t_{j+1} - t_j} \right\}.$$

### 3.2.2 Modelling the Data

Preliminary experiments included trying out different models, i.e deep models like LSTM, TCN, and shallower models like SVR, GPR. It was found that the deep models were not able to capture the data, and the shallow models performed well. This is likely due to the nature of the data; shallow models are better suited to constrained data. Additionally, we are only using simple voltage-curves as input data, or in later experiments  $dV/dt$  curves as well, but not additional metadata.

These models are quite commonly used in these battery health studies, as seen in Chapter 2. Even in the case where deep models are used, it is generally in combination with a shallow model which performs initial feature extraction.

The following experiments are based on the SVR model. It is implemented using CVXOPT to solve the quadratic programming (QP) problem. The steps are as follows:

1. Derive the mathematical formulation of  $\epsilon$ -SVR.
2. Incorporate sample weights.
3. Use a train/test split to evaluate performance.
4. Calculate and display error metrics (MSE and MAE).

The CVXOPT package is used to solve the Quadratic Programming (QP) problem in the dual formulation of SVR.

#### Mathematical Formulation of $\epsilon$ -SVR

##### 1a. Primal Problem

For a given training dataset  $\{(x_i, y_i)\}_{i=1}^N$  where  $x_i \in R^d$  and  $y_i \in R$ , the  $\epsilon$ -SVR primal formulation is typically expressed as:

$$\min_{w, b, \xi, \xi^*} \frac{1}{2} \|w\|^2 + C \sum_{i=1}^N (\xi_i + \xi_i^*)$$

subject to

$$\begin{aligned} y_i - w^\top x_i - b &\leq \epsilon + \xi_i, \\ w^\top x_i + b - y_i &\leq \epsilon + \xi_i^*, \\ \xi_i, \xi_i^* &\geq 0, \quad i = 1, \dots, N. \end{aligned}$$

## 1b. Dual Problem

Introducing Lagrange multipliers  $\alpha_i, \alpha_i^*$ , we obtain the dual problem:

$$\max_{\alpha, \alpha^*} -\frac{1}{2} \sum_{i=1}^N \sum_{j=1}^N (\alpha_i - \alpha_i^*)(\alpha_j - \alpha_j^*) K(x_i, x_j) - \epsilon \sum_{i=1}^N (\alpha_i + \alpha_i^*) + \sum_{i=1}^N y_i (\alpha_i - \alpha_i^*)$$

subject to

$$\sum_{i=1}^N (\alpha_i - \alpha_i^*) = 0, \quad 0 \leq \alpha_i, \alpha_i^* \leq C, \quad i = 1, \dots, N.$$

For a **linear** kernel,  $K(x_i, x_j) = x_i^\top x_j$ .

For an **RBF** kernel,  $K(x_i, x_j) = \exp(-\gamma \|x_i - x_j\|^2)$ .

## 2. Incorporating Sample Weights

To give certain samples more importance, scale the effective  $C$  for each sample by a weight  $w_i$ . That is, let

$$C_i = w_i \cdot C,$$

which modifies the box constraints to

$$0 \leq \alpha_i, \alpha_i^* \leq C_i = w_i C.$$

## Final Prediction

Once we have solved for  $\alpha_i$  and  $\alpha_i^*$ , the prediction for a new point  $x$  is

$$f(x) = \sum_{i=1}^N (\alpha_i - \alpha_i^*) K(x_i, x) + b,$$

where  $b$  is recovered from the support vectors via the Karush–Kuhn–Tucker (KKT)

conditions.

## Experimental Design for Validation of Synthetic Data

The main experimental design was based on findings from preliminary experiments, which will be included in the Appendices.

RBF kernel is used for all of the experiments - preliminary experiments showed it captured the data much better than the linear kernel. Additionally, the incorporation of sample weights in step 2 made very little impact on the model predictions in the case of experiments that combined the synthetic and experimental data into a unified dataset. So, this step was discarded in the final baseline experiments.

Additionally, the final experiments did not incorporate a 'unified' dataset experiment. This is because in preliminary experiments, it was not possible to come to a clear conclusion based on mixing the training data.

For example, incorporating synthetic data into the experimental data improved prediction on the experimental test-set; However, this could be for a few reasons.

As the experimental samples are so few, i.e with a train-test split of 80-20% this leaves only 80 samples for the model to learn from. Incorporating some synthetic data (which has been shown to model the degradation to a reasonable degree of accuracy) could thus improve the model accuracy when predicting on experimental data due to a lack of existing data.

Perhaps in the 80 samples no samples modelling a SoH value of 91% were included, thus if a synthetic sample that models this is included it will improve the model performance. Or, more likely than not, it is due to the converse situation, i.e. the discrepancy seen between the P2D-generated data and the experimental data at a high SoH, as was discussed in Section 3.1.3.

Thus, despite the fact the synthetic data improved the predictive performance of the model, if there were many more experimental samples, the incorporation of synthetic data could possibly make the model accuracy worse. So, it is not possible to make a completely clear conclusion about the validity of the synthetic data based on this 'unified-dataset' scenario. As another example, in the case where the model was trained on synthetic data, and experimental data was incorporated into the dataset, the predictive results on synthetic data got worse. This makes sense as the experimental data does vary from the synthetic data to a degree that it could skew results. There are enough examples in the synthetic dataset to make this conclusion, as opposed to the first example. This is the justification for the experimental design of a), b) as follows.

The first baseline experiment involved training the model on purely experimental data and seeing whether it was capable of predicting on experimental and synthetic data. In both

cases, the results were poor. This can be explained by the lack of data (101 samples).

The second experiment involved training the model on purely synthetic data and seeing whether it is capable of predicting on experimental data. This is the most important experiment of the baseline experiments, and the one that concludes the validity of the generated synthetic data when it comes to modelling the data. This experiment answers the following question - if a SoH prediction model has only seen these simulated discharge curves, would it be able to make an accurate prediction about the SoH for real, experimental data?

In both experiments, a hyperparameter tuning process was carried out for the SVR. Many combinations of the  $C$ ,  $\gamma$  and  $\epsilon$  hyperparameters were evaluated, using cross-validation, until an optimal hyperparameter combination was found to model the data.

The hyperparameter tuning experiment results are presented in Table A1.5.

Experiment	I/P Features	I/P Sequence Prep. Method	$C$	$\epsilon$	$\gamma$	Avg MSE
1	Voltage	1, 20k	4400	0.0001	$1 \times 10^{-6}$	0.0516
		1, 40k	4400	0.001	$1 \times 10^{-6}$	0.0321
		1, 60k	1600	0.0001	$1 \times 10^{-6}$	0.0289
		2	100	0.0001	$1 \times 10^{-6}$	0.0357
1	Voltage, dV/dt	1, 20k	400	$1 \times 10^{-6}$	$1 \times 10^{-6}$	0.0524
		1, 40k	400	$1 \times 10^{-6}$	$1 \times 10^{-6}$	0.0406
		1, 60k	400	0.001	$1 \times 10^{-6}$	0.0470
		2	2000	$1 \times 10^{-6}$	$1 \times 10^{-6}$	0.0754
2	Voltage	1, 20k	1500	0.001	$1 \times 10^{-5}$	0.0486
		1, 40k	1500	0.001	$1 \times 10^{-6}$	0.0061
		1, 60k	200	0.001	$1 \times 10^{-6}$	0.0040
		2	100	$1 \times 10^{-6}$	$1 \times 10^{-6}$	0.0394
2	Voltage, dV/dt	1, 20k	100	$1 \times 10^{-7}$	$1 \times 10^{-4}$	0.0451
		1, 40k	2000	$1 \times 10^{-7}$	$1 \times 10^{-6}$	0.0058
		1, 60k	200	0.001	$1 \times 10^{-6}$	0.0041
		2	100	$1 \times 10^{-6}$	$1 \times 10^{-6}$	0.0398

Table 3.4: Optimal SVR hyperparameters for each experiment and input-preparation method.

## Experiment 1 Results

To recall, experiment 1 involves training the model on solely experimental data. In this section its predictions on both experimental and synthetic data are shown in Figure 3.28.

The results of the hyperparameter tuning, for each method of data preparation (see Section 3.2.1) are shown:

The results were best when only voltage was used as an input feature, and Method 1 of input sequence preparation was used, with a 60k sequence length. The average MSE of this approach was 0.0289, and the average RMSE was 0.17.

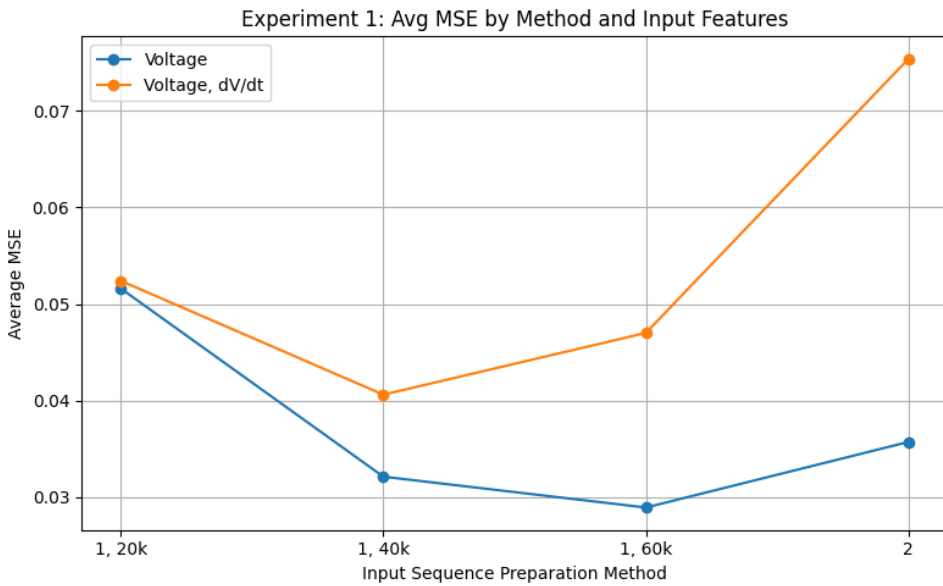


Figure 3.28: Hyperparameter Tuning Results for Different I/P Features and Sequence Prep. Methods

In Figures 3.29 and 3.30 see some results of the model predicting SoH on synthetic data. The MSE was 0.028, or the RMSE 0.167 for both examples.

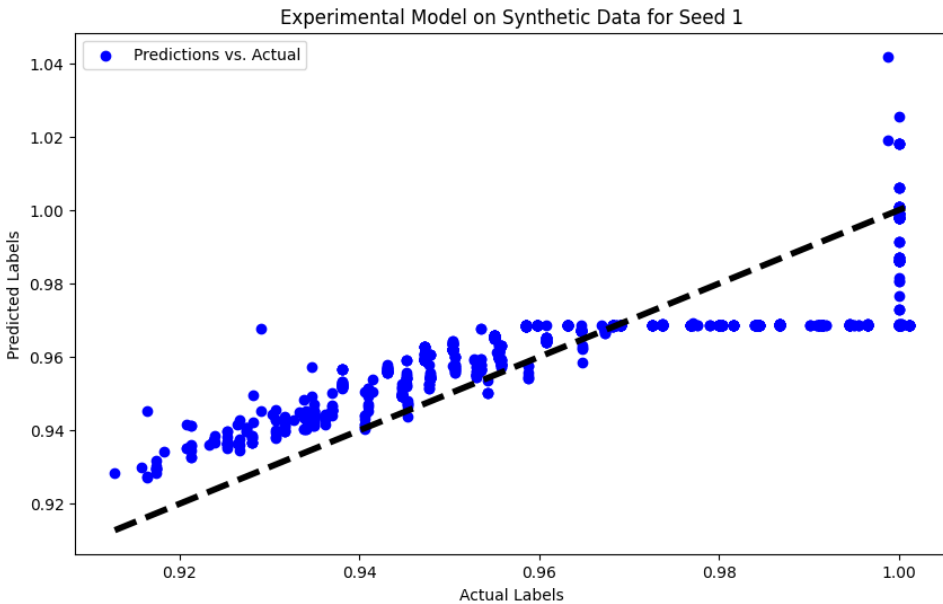


Figure 3.29: Example of Experiment 1 Best Model Predicting on Synthetic Data

As expected, the predictive capability of the model which was trained solely on experimental data, is poor on synthetic data. This can be explained by the lack of available data, only 101 samples, for training the model. There is a plateau after SoH  $\sim 0.96$ - $0.97$ , which could be explained by the discrepancy between the synthetic data and the experimental data at a high SoH (See Section 3.1.3). Further investigation into the reason for this discrepancy, and accounting for it in the data-generation, could improve this model's results.

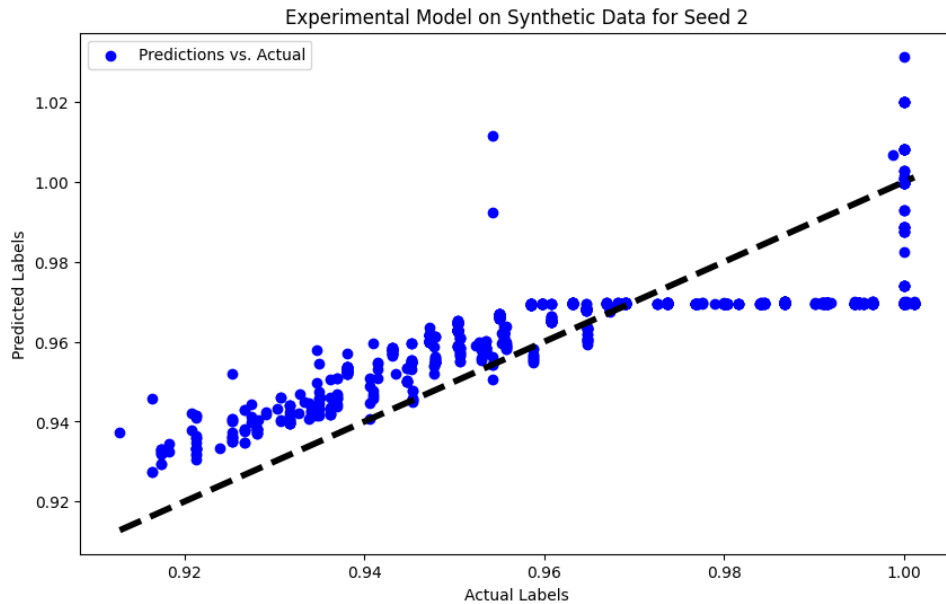


Figure 3.30: Example of Experiment 1 Best Model Predicting on Synthetic Data

## Experiment 2 Results

To recall, experiment 2 involves training the model on solely synthetic data. In this section its predictions on both experimental and synthetic data are shown.

The results of hyperparameter tuning, for each method of data preparation (see Section 3.2.1) are shown in Figure 3.31.

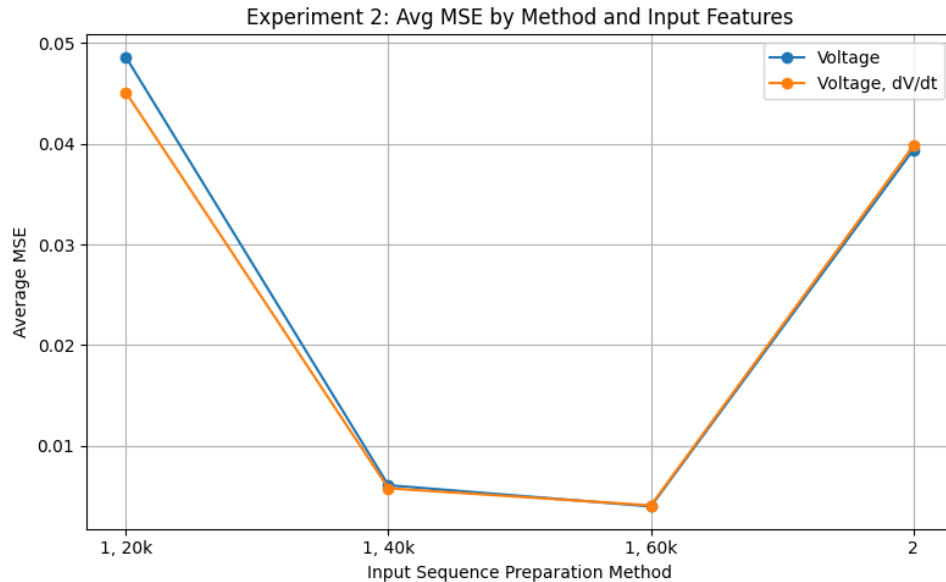


Figure 3.31: Hyperparameter Tuning Results for Different I/P Features and Sequence Prep. Methods

The results were again best when only voltage was used as an input feature, and Method 1 of input sequence preparation was used, with a 60k sequence length. It seems that the

model does not extract much value using the  $dV/dt$  input, and also from the first  $\sim 10\text{-}30k$  points of the discharge curves (given that using only the last 40-60k points achieves the best results). The average MSE of this approach was 0.004, and the average RMSE was 0.02.

In Figures 3.32 and 3.33 see some results of the model predicting on experimental data. These results represent the average results of this model, they achieve MSEs of 0.0041 and 0.0044 respectively, or RMSEs of 0.0638 and 0.0664 respectively.

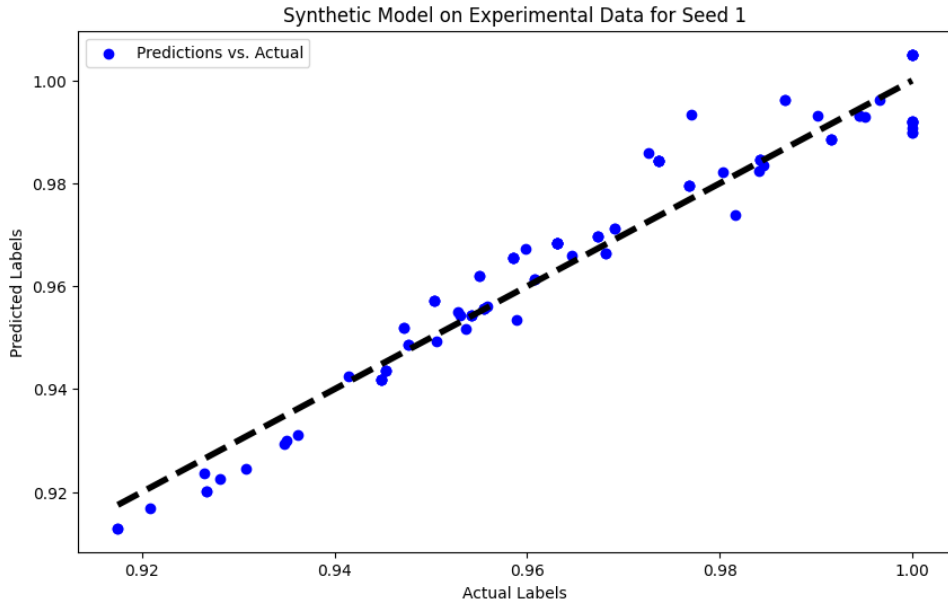


Figure 3.32: Example of Experiment 2 Best Model Predicting on All Experimental Data

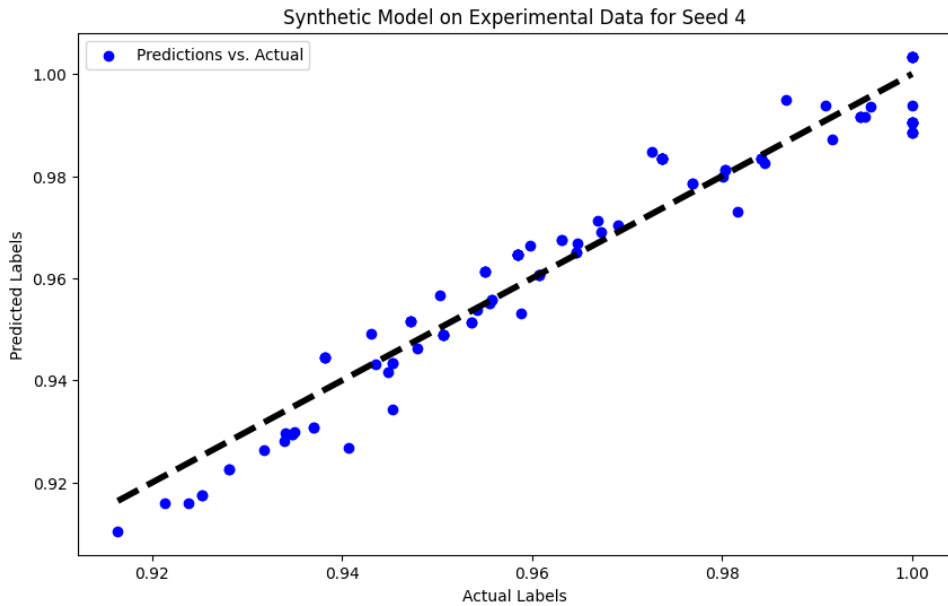


Figure 3.33: Example of Experiment 2 Best Model Predicting on All Experimental Data

The results shown in Figures 3.32 and 3.33 show that the model trained on purely synthetic

data has what appears to be quite a good predictive capability on the experimental data. In Section 3.2.2, the accuracy of the model will be determined. Overall, this result shows that the synthetic discharge curves capture the degradation behaviour of the real cells with such a fidelity that the SoH estimator trained exclusively on this synthetic data can still generalise and predict the SoH of entirely unseen experimental curves, with little error. The data is not perfect, for example an investigation for the outliers at higher SoH values would have to be carried out to improve the data further; but, it is capturing the degradation well.

More results are contained in the Appendices, i.e the experimental-data trained model predicting on experimental data. Some information about supplemental experiments involving noise addition are included as well.

### Predictive Accuracy of Model Trained on Solely Synthetic Data

See Figures ?? to 3.37 for examples of how the accuracy was computed. The points on the boundary lines were considered as being correctly predicted for the computation of the accuracy. The correctly predicted samples are signified by a green colour, while the incorrectly predicted samples are signified by a red colour. Table 3.5 summarises the results for bounds down to  $\pm 0.1\%$ .

Error bound	In bounds	Accuracy (%)
$\pm 2.0\%$	101/101	100.0
$\pm 1.5\%$	101/101	100.0
$\pm 1.0\%$	95/101	94.1
$\pm 0.9\%$	84/101	83.2
$\pm 0.8\%$	82/101	81.2
$\pm 0.7\%$	79/101	78.2
$\pm 0.6\%$	62/101	61.4
$\pm 0.5\%$	53/101	52.5
$\pm 0.4\%$	44/101	43.6
$\pm 0.3\%$	37/101	36.6
$\pm 0.2\%$	29/101	28.7
$\pm 0.1\%$	17/101	16.8

Table 3.5: Prediction accuracies within various absolute error bounds.

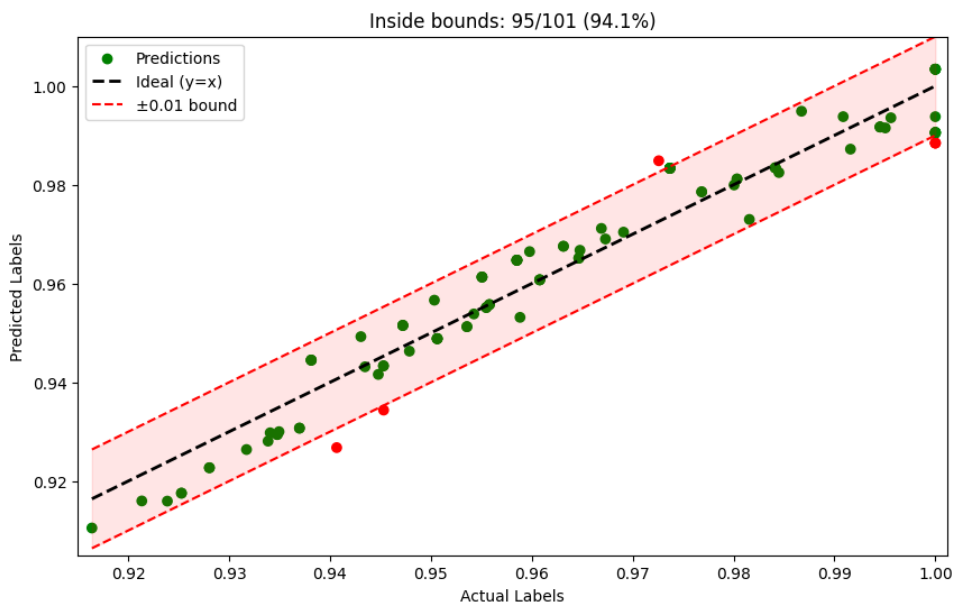


Figure 3.34: Scatter of predicted vs. actual labels with  $\pm 1\%$  error bounds; 95 of 101 predictions (94.1%) lie within tolerance.

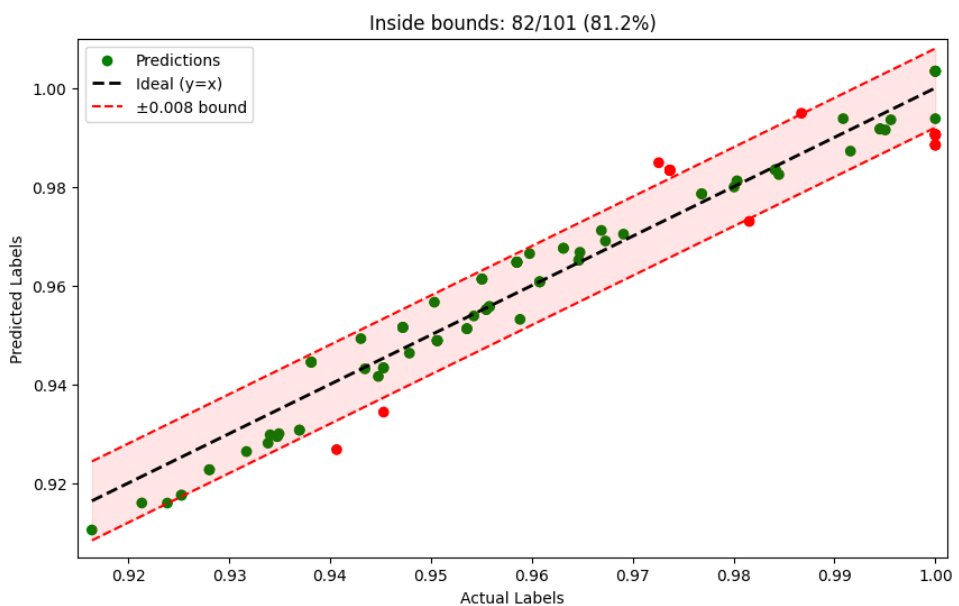


Figure 3.35: Scatter of predicted vs. actual labels with  $\pm 0.8\%$  error bounds; 82 of 101 predictions (81.2%) lie within tolerance.

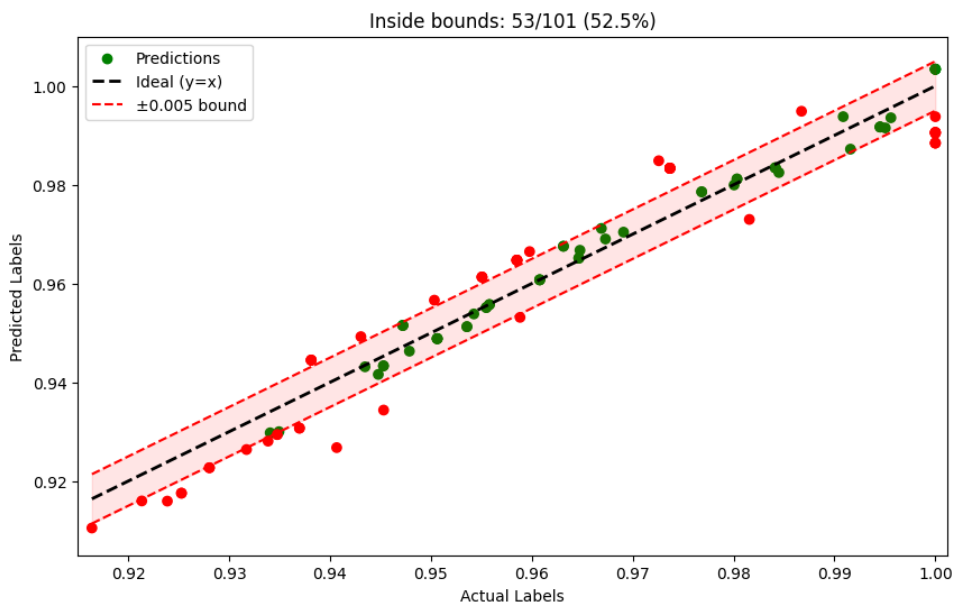


Figure 3.36: Scatter of predicted vs. actual labels with  $\pm 0.5\%$  error bounds; 82 of 101 predictions (52.5%) lie within tolerance.

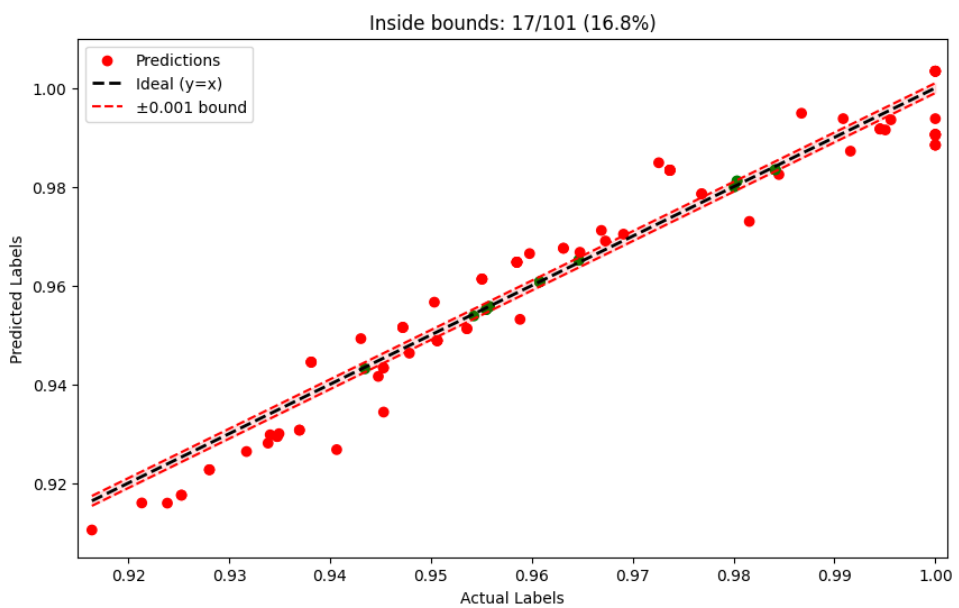


Figure 3.37: Scatter of predicted vs. actual labels with  $\pm 0.1\%$  error bounds; 17 of 101 predictions (16.8%) lie within tolerance.

## 4 Results and Evaluation

### Achievements/Contributions:

- (i) Detailed review of battery model literature.
- (ii) Explored and evaluated a range of battery datasets to identify an appropriate experimental dataset to explore the main hypothesis.
- (iii) Explored and evaluated a number of advanced battery models identifying a suitable model to explore enhancement (synthesis/augmentation) of the experimental dataset.
- (iv) Adapted the battery model to allow for synthetic data generation; explored a range of methods to allow more model variations.
- (v) Developed and explored a number of data-driven models to test the ability of the synthetic data to improve the predictive capability of a data-driven model.
- (vi) Devised experiments to test the selected data-driven model(s) to predict experimental performance of unseen test battery characteristics when trained exclusively on experimental data and then exclusively on synthetic data.
- (vii) Analysis and reflection on the outcomes of these experiments.

In the final Conclusions chapter the main conclusions from this detailed study on Battery SoH are summarised, as well as the potential to employ P2D models to augment experimental data, or the extrapolation of the model to create more diverse data, and also for the purpose of improving the predictive capabilities of data-driven models without a need for expensive and time consuming additional studies on LiO<sub>2</sub> batteries.

## 5 Conclusions and Future Work

This project demonstrated a methodology for generating and validating synthetic LIB degradation data using a calibrated P2D model, coupled with machine learning. Experiments were carried out progressively to adapt the model to better capture the degradation behaviour. The P2D model parameters were fit to the degrading experimental discharge curves, via PSO, and the model was able to closely replicate key degradation behaviours. The generated voltage discharge curves were generated for SoH levels ranging from 1.00 to 0.91, i.e that of the real data, and these simulated profiles closely matched the experimental ones; the average RMSE between synthetic and measured voltages was  $\sim 0.024$  V across diagnostic cycles 4–15. However, the model did struggle with capturing battery behaviour at higher SoH, contrary to expectations; diagnostic tests 1-3 had an average RMSE of X, % higher than the average of the succeeding tests. Additionally, a cursory visual analysis shows that the simulated curves are smoother and fail to capture some of the effects that occur in the real voltage curves, especially at the knee-point of the curves where the  $dV/dt$  decreases rapidly. In future work, investigation of these aspects would be very valuable.

The synthetic samples were additionally validated by training an SVR model on them and subsequently evaluating its predictive capability on experimental data. It achieved a very high accuracy – 94.1% of the test predictions fell within a  $\pm 1\%$  error margin of the actual SoH. This result showed that a high-accuracy SoH estimation model could be developed, having been trained solely on synthetic data; this validates that a well-calibrated simulation model can substitute for real degradation data in training ML models.

This result also supports the hypothesis that the P2D-model can sufficiently encode realistic degradation behaviour through optimisation of the 8 key electrochemical parameters; and, in future work, an even more in-depth experimentation could be done to extrapolate the model to provide data for entirely 'unseen' situations. For example, the data generation could expand the data to cover degradation levels beyond 0.91 SoH. This approach could be used to overcome the scarcity of experimental data available for battery health prognostics.

It would also be valuable to try a set of experiments using more input features. For example, parameter metadata was collected when generating the synthetic data, which could have been used as input to the ML model. Other parameters were included in the experimental

data too, i.e charge energy, discharge energy, or the EIS and HPPC data.

Additionally, introducing 'realistic' noise into the synthetic voltage data could be carried out to mimic the noise present in the experimental data; this was attempted in some additional experiments, though the simplistic method of doing so made no improvements to the model. Further experiments on this point could improve model results. Additionally, it was observed that the experimental data has what appears to be low amplitude, high frequency noise, probably due to the way the data was acquired (i.e sensor noise). Denoising the experimental data could possibly improve either the PSO-based optimisation of the model parameters, or alternatively the SVR-based SoH estimation, as the curves would more closely resemble each other (the synthetic data is very smooth). Initial experiments could include basic filtering, followed by more complex methods. It could be interesting to decompose the signal and try to characterise the source of the noise, i.e 50 Hz may indicate powerline noise.

Proprietary cycle life data from industry is often inaccessible to researchers, and long-term ageing experiments are time-consuming and costly to make. Overall, this work demonstrates a methodology for using P2D simulation models to generate LiB degradation data, thus enabling the development of data-driven BMS for real-time deployment, on-system.

# Bibliography

- [1] C.-H. Chen, F. B. Planella, K. O'regan, D. Gastol, W. D. Widanage, and E. Kendrick, "Development of experimental techniques for parameterization of multi-scale lithium-ion battery models," *Journal of The Electrochemical Society*, vol. 167, no. 8, p. 080534, 2020.
- [2] G. Pozzato, A. Allam, and S. Onori, "Lithium-ion battery aging dataset based on electric vehicle real-driving profiles," *Data in brief*, vol. 41, p. 107995, 2022.
- [3] [Online]. Available:  
<https://www.epa.gov/vehicle-and-fuel-emissions-testing/dynamometer-drive-schedules>
- [4] S. B. Lee and S. Onori, "A robust and sleek electrochemical battery model implementation: a matlab(R) framework," *Journal of The Electrochemical Society*, vol. 168, no. 9, p. 090527, 2021.
- [5] McKinsey & Company, "Battery 2030: Resilient, sustainable, and circular,"  
<https://www.mckinsey.com/industries/automotive-and-assembly/our-insights/battery-2030-resilient-sustainable-and-circular>, 2023, accessed: 2024-12-10.
- [6] IDTechEx, "Advanced li-ion battery technologies 2024-2034: Technologies, players, forecasts," <https://www.idtechex.com/en/research-report/advanced-li-ion-battery-technologies-2024-2034-technologies-players-forecasts/1002>, 2023, accessed: 2024-12-10.
- [7] S&P Global Market Intelligence, "Lithium-ion battery capacity to grow steadily to 2030," <https://www.spglobal.com/market-intelligence/en/news-insights/research/lithium-ion-battery-capacity-to-grow-steadily-to-2030>, 2023, accessed: 2024-12-10.
- [8] European Automobile Manufacturers' Association (ACEA), "Electric cars: Tax benefits and incentives 2024,"  
<https://www.acea.auto/fact/electric-cars-tax-benefits-and-incentives-2024/>, 2024, accessed: 2024-12-10.

- [9] European Commission, "Fit for 55: Eu reaches new milestone to make all new cars and vans zero-emission by 2035," [https://climate.ec.europa.eu/news-your-voice/news/fit-55-eu-reaches-new-milestone-make-all-new-cars-and-vans-zero-emission-2035-2023-03-28\\_en](https://climate.ec.europa.eu/news-your-voice/news/fit-55-eu-reaches-new-milestone-make-all-new-cars-and-vans-zero-emission-2035-2023-03-28_en), 2023, accessed: 2024-12-10.
- [10] EVBoosters, "Electric vehicle sales forecast to hit 30 million by 2027 as global adoption accelerates," <https://evboosters.com/ev-charging-news/electric-vehicle-sales-forecast-to-hit-30-million-by-2027-as-global-adoption-accelerates/#:~:text=Europe%20is%20also%20setting%20a,seeing%20a%20surge%20in%20interest>, 2023, accessed: 2024-12-10.
- [11] Recurrent Auto, "Ev adoption in the us: Current trends and insights," <https://www.recurrentauto.com/research/ev-adoption-us>, 2023, accessed: 2023-12-10.
- [12] R. Xiong, Y. Zhang, J. Wang, H. He, S. Peng, and M. Pecht, "Lithium-ion battery health prognosis based on a real battery management system used in electric vehicles," *IEEE Transactions on Vehicular Technology*, vol. 68, no. 5, pp. 4110–4121, 2018.
- [13] M. T. Lawder, P. W. Northrop, and V. R. Subramanian, "Model-based sei layer growth and capacity fade analysis for ev and phev batteries and drive cycles," *Journal of The Electrochemical Society*, vol. 161, no. 14, p. A2099, 2014.
- [14] B. Yang, Y. Qian, Q. Li, Q. Chen, J. Wu, E. Luo, R. Xie, R. Zheng, Y. Yan, S. Su *et al.*, "Critical summary and perspectives on state-of-health of lithium-ion battery," *Renewable and Sustainable Energy Reviews*, vol. 190, p. 114077, 2024.
- [15] T. Yamanaka, H. Nakagawa, S. Tsubouchi, Y. Domi, T. Doi, T. Abe, and Z. Ogumi, "Correlations of concentration changes of electrolyte salt with resistance and capacitance at the surface of a graphite electrode in a lithium ion battery studied by in situ microprobe raman spectroscopy," *Electrochimica Acta*, vol. 251, pp. 301–306, 2017.
- [16] X.-B. Han, K. Kannari, and S. Ye, "In situ surface-enhanced raman spectroscopy in li-o<sub>2</sub> battery research," *Current Opinion in Electrochemistry*, vol. 17, pp. 174–183, 2019.
- [17] W. Choi, H.-C. Shin, J. M. Kim, J.-Y. Choi, and W.-S. Yoon, "Modeling and applications of electrochemical impedance spectroscopy (eis) for lithium-ion batteries," *Journal of Electrochemical Science and Technology*, vol. 11, no. 1, pp. 1–13, 2020.
- [18] D. Dees, E. Gunen, D. Abraham, A. Jansen, and J. Prakash, "Electrochemical modeling of lithium-ion positive electrodes during hybrid pulse power characterization tests," *Journal of the Electrochemical Society*, vol. 155, no. 8, p. A603, 2008.

- [19] C. Lin, Q. Yu, R. Xiong *et al.*, "A study on the impact of open circuit voltage tests on state of charge estimation for lithium-ion batteries," *Applied Energy*, vol. 205, pp. 892–902, 2017.
- [20] M. Spielbauer, P. Berg, M. Ringat, O. Bohlen, and A. Jossen, "Experimental study of the impedance behavior of 18650 lithium-ion battery cells under deforming mechanical abuse," *Journal of Energy Storage*, vol. 26, p. 101039, 2019.
- [21] G. Davies, K. W. Knehr, B. Van Tassell, T. Hodson, S. Biswas, A. G. Hsieh, and D. A. Steingart, "State of charge and state of health estimation using electrochemical acoustic time of flight analysis," *Journal of The Electrochemical Society*, vol. 164, no. 12, p. A2746, 2017.
- [22] D. Seals, P. Ramesh, M. D'Arpino, and M. Canova, "Physics-based equivalent circuit model for lithium-ion cells via reduction and approximation of electrochemical model," *SAE International Journal of Advances and Current Practices in Mobility*, vol. 4, no. 2022-01-0701, pp. 1154–1165, 2022.
- [23] S. Onori, P. Spagnol, V. Marano, Y. Guezennec, and G. Rizzoni, "A new life estimation method for lithium-ion batteries in plug-in hybrid electric vehicles applications," *International Journal of Power Electronics*, vol. 4, no. 3, pp. 302–319, 2012.
- [24] D. D. Frey, S. Fukuda, and G. Rock, *Improving complex systems today*. Springer, 2011.
- [25] A. Eddahech, O. Briat, and J.-M. Vinassa, "Determination of lithium-ion battery state-of-health based on constant-voltage charge phase," *Journal of Power Sources*, vol. 258, pp. 218–227, 2014.
- [26] X. Feng, J. Li, M. Ouyang, L. Lu, J. Li, and X. He, "Using probability density function to evaluate the state of health of lithium-ion batteries," *Journal of Power Sources*, vol. 232, pp. 209–218, 2013.
- [27] B. Saha, S. Poll, K. Goebel, and J. Christophersen, "An integrated approach to battery health monitoring using bayesian regression and state estimation," in *2007 IEEE autotestcon*. Ieee, 2007, pp. 646–653.
- [28] P. Hashemzadeh, M. Désilets, M. Lacroix, and A. Jokar, "Investigation of the p2d and of the modified single-particle models for predicting the nonlinear behavior of li-ion batteries," *Journal of Energy Storage*, vol. 52, p. 104909, 2022.
- [29] A. Jokar, B. Rajabloo, M. Désilets, and M. Lacroix, "Review of simplified pseudo-two-dimensional models of lithium-ion batteries," *Journal of Power Sources*, vol. 327, pp. 44–55, 2016.

- [30] B. Yang, J. Wang, P. Cao, T. Zhu, H. Shu, J. Chen, J. Zhang, and J. Zhu, "Classification, summarization and perspectives on state-of-charge estimation of lithium-ion batteries used in electric vehicles: A critical comprehensive survey," *Journal of Energy Storage*, vol. 39, p. 102572, 2021.
- [31] M. Shen and Q. Gao, "A review on battery management system from the modeling efforts to its multiapplication and integration," *International Journal of Energy Research*, vol. 43, no. 10, pp. 5042–5075, 2019.
- [32] M.-K. Tran, A. DaCosta, A. Mevawalla, S. Panchal, and M. Fowler, "Comparative study of equivalent circuit models performance in four common lithium-ion batteries: Lfp, nmc, lmo, nca," *Batteries*, vol. 7, no. 3, p. 51, 2021.
- [33] X. Hu, S. Li, and H. Peng, "A comparative study of equivalent circuit models for li-ion batteries," *Journal of Power Sources*, vol. 198, pp. 359–367, 2012.
- [34] Q. Zhang, Y. Shang, Y. Li, N. Cui, B. Duan, and C. Zhang, "A novel fractional variable-order equivalent circuit model and parameter identification of electric vehicle li-ion batteries," *ISA transactions*, vol. 97, pp. 448–457, 2020.
- [35] G. L. Plett, "Extended kalman filtering for battery management systems of lipb-based hev battery packs: Part 1. background," *Journal of Power sources*, vol. 134, no. 2, pp. 252–261, 2004.
- [36] J. Remmlinger, M. Buchholz, T. Soczka-Guth, and K. Dietmayer, "On-board state-of-health monitoring of lithium-ion batteries using linear parameter-varying models," *Journal of Power Sources*, vol. 239, pp. 689–695, 2013.
- [37] S. Sepasi, R. Ghorbani, and B. Y. Liaw, "Inline state of health estimation of lithium-ion batteries using state of charge calculation," *Journal of Power Sources*, vol. 299, pp. 246–254, 2015.
- [38] G. L. Plett, "Extended kalman filtering for battery management systems of lipb-based hev battery packs: Part 3. state and parameter estimation," *Journal of Power sources*, vol. 134, no. 2, pp. 277–292, 2004.
- [39] S. Santhanagopalan and R. E. White, "Online estimation of the state of charge of a lithium ion cell," *Journal of power sources*, vol. 161, no. 2, pp. 1346–1355, 2006.
- [40] L. Lu, X. Han, J. Li, J. Hua, and M. Ouyang, "A review on the key issues for lithium-ion battery management in electric vehicles," *Journal of power sources*, vol. 226, pp. 272–288, 2013.
- [41] A. Eddahech, O. Briat, N. Bertrand, J.-Y. Delétage, and J.-M. Vinassa, "Behavior and state-of-health monitoring of li-ion batteries using impedance spectroscopy and

- recurrent neural networks," *International Journal of Electrical Power & Energy Systems*, vol. 42, no. 1, pp. 487–494, 2012.
- [42] J. Qu, F. Liu, Y. Ma, and J. Fan, "A neural-network-based method for rul prediction and soh monitoring of lithium-ion battery," *IEEE access*, vol. 7, pp. 87178–87191, 2019.
- [43] S. J. Kim, S. H. Kim, H. M. Lee, S. H. Lim, G.-Y. Kwon, and Y.-J. Shin, "State of health estimation of li-ion batteries using multi-input lstm with optimal sequence length," in *2020 IEEE 29th International Symposium on Industrial Electronics (ISIE)*. IEEE, 2020, pp. 1336–1341.
- [44] M. Data. (2024) Battery degradation datasets (two types of lithium-ion batteries). Accessed: 2024-12-13. [Online]. Available: <https://data.mendeley.com/datasets/v8k6bsr6tf/1>
- [45] G. Ma, S. Xu, B. Jiang, C. Cheng, X. Yang, Y. Shen, T. Yang, Y. Huang, H. Ding, and Y. Yuan, "Real-time personalized health status prediction of lithium-ion batteries using deep transfer learning," *Energy & Environmental Science*, vol. 15, no. 10, pp. 4083–4094, 2022.
- [46] Y. Yuan, G. Ma, and S. Xu, "The Dataset for: Real-time personalized health status prediction of lithium-ion batteries using deep transfer learning," Mendeley Data, 2022, accessed: 2024-12-13. [Online]. Available: <https://data.mendeley.com/datasets/nsc7hnsg4s/2>
- [47] "Lithium-ion battery aging dataset based on electric vehicle real-driving profiles," Open Science Framework, 2022, accessed: 2024-12-13. [Online]. Available: [https://osf.io/qsabn/?view\\_only=2a03b6c78ef14922a3e244f3d549de78](https://osf.io/qsabn/?view_only=2a03b6c78ef14922a3e244f3d549de78)
- [48] Y. Wang, C. Liu, R. Pan, and Z. Chen, "Experimental data of lithium-ion battery and ultracapacitor under dst and udss profiles at room temperature," *Data in brief*, vol. 12, pp. 161–163, 2017.
- [49] K. A. Severson, P. M. Attia, N. Jin, N. Perkins, B. Jiang, Z. Yang, M. H. Chen, M. Aykol, P. K. Herring, D. Fraggedakis *et al.*, "Data-driven prediction of battery cycle life before capacity degradation," *Nature Energy*, vol. 4, no. 5, pp. 383–391, 2019.
- [50] K. Severson *et al.*, "Data-driven prediction of battery cycle life before capacity degradation," Available at Matr.io, 2019, accessed: 2024-12-13. [Online]. Available: <https://data.matr.io/1/projects/5c48dd2bc625d700019f3204>
- [51] C.-H. Chen, F. Brosa Planella, K. O'Regan, D. Gastol, W. D. Widanage, and E. Kendrick, "Experimental data for "development of experimental techniques for parameterization of multi-scale lithium-ion battery models"," Zenodo, 2020, accessed: 2024-12-13. [Online]. Available: <https://doi.org/10.5281/zenodo.4032561>

- [52] C. Birkl and D. Howey, "Oxford battery degradation dataset 1: Long term battery ageing tests of 8 kokam (slpb533459h4) 740 mah lithium-ion pouch cells," University of Oxford, 2017, accessed: 2024-12-13. [Online]. Available: <https://ora.ox.ac.uk/objects/uuid:03ba4b01-cfed-46d3-9b1a-7d4a7bdf6fac>
- [53] T. Raj, A. A. Wang, C. W. Monroe, and D. A. Howey, "Investigation of path-dependent degradation in lithium-ion batteries," *Batteries & Supercaps*, vol. 3, no. 12, pp. 1377–1385, 2020.
- [54] T. Raj and D. A. Howey, "Path Dependent Battery Degradation Dataset Part 1: Investigation of Path Dependent Degradation in Lithium-Ion Batteries," Oxford Research Archive, 2020, accessed: 2024-12-13. [Online]. Available: <https://ora.ox.ac.uk/objects/uuid:de62b5d2-6154-426d-bcbb-30253ddb7d1e>
- [55] J. M. Reniers, G. Mulder, and D. A. Howey, "Unlocking extra value from grid batteries using advanced models," *Journal of power sources*, vol. 487, p. 229355, 2021.
- [56] ——, "Oxford energy trading battery degradation dataset: Data associated with paper "Unlocking Extra Value from Grid Batteries Using Advanced Models"," Oxford Research Archive, 2020, accessed: 2024-12-13. [Online]. Available: <https://ora.ox.ac.uk/objects/uuid:9aae61af-2949-49f1-8ad5-6aea448979e5>
- [57] N. DASHlink, "Prognostics data repository," 2020, accessed: 2024-12-13. [Online]. Available: <https://c3.ndc.nasa.gov/dashlink/resources/133/>
- [58] NASA Intelligent Systems Division, "Pcoe data set repository," 2020, accessed: 2024-12-13. [Online]. Available: <https://www.nasa.gov/intelligent-systems-division/discovery-and-systems-health/pcoe/pcoe-data-set-repository/>
- [59] B. Bole, C. S. Kulkarni, and M. Daigle, "Adaptation of an electrochemistry-based li-ion battery model to account for deterioration observed under randomized use," in *Annual conference of the PHM society*, vol. 6, no. 1, 2014.
- [60] Center for Advanced Life Cycle Engineering (CALCE), "Battery data," 2020, accessed: 2024-12-13. [Online]. Available: <https://calce.umd.edu/battery-data>
- [61] Y. Preger, H. M. Barkholtz, A. Fresquez, D. L. Campbell, B. W. Juba, J. Romàn-Kustas, S. R. Ferreira, and B. Chalamala, "Degradation of commercial lithium-ion cells as a function of chemistry and cycling conditions," *Journal of The Electrochemical Society*, vol. 167, no. 12, p. 120532, 2020.
- [62] Battery Archive, "Cycle list data," 2020, accessed: 2024-12-13. [Online]. Available: [https://batteryarchive.org/cycle\\_list.html?time=0001](https://batteryarchive.org/cycle_list.html?time=0001)

- [63] P. Kollmeyer, "Panasonic 18650pf li-ion battery data," 2018. [Online]. Available: <https://data.mendeley.com/datasets/wykht8y7tg/1>
- [64] C. Vidal, P. Kollmeyer, M. Naguib, P. Malysz, O. Gross, and A. Emadi, "Robust xev battery state-of-charge estimator design using a feedforward deep neural network," *SAE International Journal of Advances and Current Practices in Mobility*, vol. 2, no. 2020-01-1181, pp. 2872–2880, 2020.
- [65] P. Kollmeyer, C. Vidal, M. Naguib, and M. Skells, "Lg 18650hg2 li-ion battery data and example deep neural network xev soc estimator script," *Mendeley Data*, vol. 3, p. 2020, 2020.
- [66] K. De Craemer and K. Trad, "Cyclic ageing with driving profile of a lithium ion battery module," *ResearchData*, Feb, 2021.
- [67] EVERLASTING Consortium, "Deliverable d2.3: Battery management system requirements and specifications," EVERLASTING Project, Tech. Rep., 2020, accessed: 2024-12-13. [Online]. Available: [https://everlasting-project.eu/wp-content/uploads/2020/03/EVERLASTING\\_D2.3\\_final\\_20200228.pdf](https://everlasting-project.eu/wp-content/uploads/2020/03/EVERLASTING_D2.3_final_20200228.pdf)
- [68] K. Trad, "Lifecycle ageing tests on commercial 18650 Li ion cell @ 25°C and 45°C," Data stored at 4TU.ResearchData, 2021, funding: Electric Vehicle Enhanced Range, Lifetime And Safety Through INGenious battery management (grant code 713771). [Online]. Available: [https://data.4tu.nl/articles/\\_/13739296](https://data.4tu.nl/articles/_/13739296)
- [69] A. Devie, G. Baure, and M. Dubarry, "Intrinsic variability in the degradation of a batch of commercial 18650 lithium-ion cells," *Energies*, vol. 11, no. 5, p. 1031, 2018.
- [70] Battery Archive, "Battery cycle list data," 2024, accessed: 2024-12-13. [Online]. Available: [https://batteryarchive.org/cycle\\_list.html?time=0001](https://batteryarchive.org/cycle_list.html?time=0001)
- [71] "Arbin lbt22023 battery chargers," <https://www.machinetools.com/en/for-sale/585774-arbin-lbt22023-battery-chargers>, 2023, accessed: 2024-12-10.
- [72] "Arbin lbt22023 480 v 24-channel battery tester, 60 v, 15 amp, 2022," <https://surplusrecord.com/listing/arin-lbt22023-480-v-24-channel-battery-tester-60-v-15-amp-2022-457750/?srsltid=AfmBOoqNUjnAC7-ohgmQaZADTCF5-Xah0O9148W2nSyAcHn0BpKoFEpz>, 2022, accessed: 2024-12-10.
- [73] "Incumax ic500 incubator with forced air circulation, 19.4 cu," <https://www.labx.com/item/incumax-ic500-incubator-with-forced-air-circulation-19-4-cu/DIS-41276-IC-500>, 2023, accessed: 2024-12-10.

- [74] “Interface 1010e,”  
<https://www.fishersci.com/shop/products/interface-1010e/NC2303947>, 2023,  
accessed: 2024-12-10.
- [75] T. Hofmann, J. Hamar, M. Rogge, C. Zoerr, S. Erhard, and J. P. Schmidt,  
“Physics-informed neural networks for state of health estimation in lithium-ion  
batteries,” *Journal of the Electrochemical Society*, vol. 170, no. 9, p. 090524, 2023.
- [76] P. J. Weddle, S. Kim, B.-R. Chen, Z. Yi, P. Gasper, A. M. Colclasure, K. Smith, K. L.  
Gering, T. R. Tanim, and E. J. Dufek, “Battery state-of-health diagnostics during fast  
cycling using physics-informed deep-learning,” *Journal of Power Sources*, vol. 585, p.  
233582, 2023.
- [77] Battery Design, “LG 21700 M50 Battery Specification,” 2024, accessed: 2024-12-10.  
[Online]. Available: <https://www.batterydesign.net/lg-21700-m50/>
- [78] S. E. O’Kane, W. Ai, G. Madabattula, D. Alonso-Alvarez, R. Timms, V. Sulzer, J. S.  
Edge, B. Wu, G. J. Offer, and M. Marinescu, “Lithium-ion battery degradation: how to  
model it,” *Physical Chemistry Chemical Physics*, vol. 24, no. 13, pp. 7909–7922, 2022.
- [79] S. Xia, X. Wu, Z. Zhang, Y. Cui, and W. Liu, “Practical challenges and future  
perspectives of all-solid-state lithium-metal batteries,” *Chem*, vol. 5, no. 4, pp.  
753–785, 2019.
- [80] S. Carelli and W. G. Bessler, “Prediction of reversible lithium plating with a pseudo-3d  
lithium-ion battery model,” *Journal of The Electrochemical Society*, vol. 167, no. 10, p.  
100515, 2020.
- [81] W. Ai, L. Kraft, J. Sturm, A. Jossen, and B. Wu, “Electrochemical thermal-mechanical  
modelling of stress inhomogeneity in lithium-ion pouch cells,” *Journal of The  
Electrochemical Society*, vol. 167, no. 1, p. 013512, 2020.
- [82] J. Kim, H. Chun, M. Kim, S. Han, J.-W. Lee, and T.-K. Lee, “Effective and practical  
parameters of electrochemical li-ion battery models for degradation diagnosis,” *Journal  
of Energy Storage*, vol. 42, p. 103077, 2021.
- [83] T. Li, X.-Z. Yuan, L. Zhang, D. Song, K. Shi, and C. Bock, “Degradation mechanisms  
and mitigation strategies of nickel-rich nmc-based lithium-ion batteries,”  
*Electrochemical Energy Reviews*, vol. 3, pp. 43–80, 2020.
- [84] X. Han, L. Lu, Y. Zheng, X. Feng, Z. Li, J. Li, and M. Ouyang, “A review on the key  
issues of the lithium ion battery degradation among the whole life cycle,”  
*ETransportation*, vol. 1, p. 100005, 2019.

- [85] J. Kennedy and R. Eberhart, "Particle swarm optimization," in *Proceedings of ICNN'95-international conference on neural networks*, vol. 4. ieee, 1995, pp. 1942–1948.
- [86] "Tolerances and stopping criteria." [Online]. Available: <https://www.mathworks.com/help/optim/ug/tolerances-and-stopping-criteria.html>
- [87] [Online]. Available: [https://osf.io/qsabn/files/f33e7c73-f978-40e7-9150-8fb0cedcb2e4?view\\_only=2a03b6c78ef14922a3e244f3d549de78](https://osf.io/qsabn/files/f33e7c73-f978-40e7-9150-8fb0cedcb2e4?view_only=2a03b6c78ef14922a3e244f3d549de78)
- [88] S. Ha, G. Pozzato, and S. Onori, "Electrochemical characterization tools for lithium-ion batteries," *Journal of Solid State Electrochemistry*, vol. 28, no. 3, pp. 1131–1157, 2024.
- [89] E. Namor, D. Torregrossa, R. Cherkaoui, and M. Paolone, "Parameter identification of a lithium-ion cell single-particle model through non-invasive testing," *Journal of Energy Storage*, vol. 12, pp. 138–148, 2017.
- [90] "Standard particle swarm optimizer with a global topology (sps0)." [Online]. Available: <https://pypop.readthedocs.io/en/latest/ps0/sps0.html>
- [91] "Lg chem m50 buy online." [Online]. Available: <https://www.nkon.nl/en/lg-inr21700-m50-4850mah-7-3a-clear.html>
- [92] [Online]. Available: <https://www.dnkpower.com/wp-content/uploads/2019/02/LG-INR21700-M50-Datasheet.pdf>
- [93] [Online]. Available: <https://www.batteryspace.com/prod-specs/11514.pdf>
- [94] "Lg m50t grade a high capacity 5000mah 21700 cell's test." [Online]. Available: <https://www.thunderheartreviews.com/2019/08/lg-m50t-grade-a-test.html>
- [95] "Flashlight forum post on 21700 m50." [Online]. Available: <https://budgetlightforum.com/t/test-review-of-lg-21700-m50-5000mah-grey/56763>

multirow

# A1 Appendix

The code I reference in this section can be found in the following Github repository, unless otherwise mentioned: <https://github.com/maria15034/MAI-Project>.

## A1.1 P2D Model MATLAB Implementation

This section provides a detailed overview of the MATLAB code used for the P2D model implementation from [4]. The code can be found at the DEARLIBS Github repository: <https://github.com/DEARLIBS>. There may be some repetition from the main body of the report, which is necessary to explain the code and thus explain the process used to create controlled degradation data within the P2D simulation framework.

One of the main steps involves defining the baseline parameters. These include the subset of 8 key transport / kinetic parameters to be identified via PSO (diffusion coefficients, conductivities, reaction rate constants). Notice how these 8 parameters are defined in terms of the values in the 'kk' vector, instead of fixed values. The kk vector will be passed to the optimiser for solving. See Figure A1.1

The initial guesses for the 8 parameters must also be defined, along with the bounds for these values via the 'pp' variable. For example,  $pp = 0.3$  indicates a search space constrained to  $\pm 30\%$  from the initial guesses. See Figure A1.2

The objective function implementation can be seen in Figure A1.3. In essence, this function is necessary to give the PSO guidance. It is used to evaluate each 'candidate' parameter set passed by PSO; when called, 'kk' or the candidate parameters are passed as input, and the P2D model parameter set is updated to be used by the simulator (i.e the baseline values are replaced with the new candidate values from PSO). Then using the same initial conditions and time span previously defined, the P2D model ODEs are integrated with the new candidate parameter set. After this integration, the modelled voltage vector is extracted and compared to the experimental voltage vector using RMSE as the error metric.

So, the objective function is used as part of an iterative process where PSO uses the RMSE value to adjust its particle positions, and eventually converge to the optimal parameter

```

%% Design Parameters
ep=0.335; % Porosity at positive % 0.335**
es=0.47; % Porosity at membrane % 0.47**
en=0.25; % Porosity at negative % 0.25**
brugp=2.43; % Bruggeman coefficient at positive
brugs=2.57; % Bruggeman coefficient at separator
brugn=2.91; % Bruggeman coefficient at negative
lp=75.6e-6; % Thickness at positive (unit:m)
ls=12e-6; % Thickness at membrane (unit:m)
ln1=85.2e-6; % Thickness at negative (unit:m)
Rpp=5.22e-6; % Radius of solid particle at positive (unit:m)
Rpn=5.86e-6; % Radius of solid particle at negative (unit:m)
F=96487; % Faraday constant (unit: C/mol)
R=8.3143; % Ideal gas constant (unit: J/(mol K))
t1=0.363; % Transference coefficient
ap=(3/Rpp)*(1-ep); % Particle surface area to volume at positive (unit: m^2/m^3)
an=(3/Rpn)*(1-en); % Particle surface area to volume at negative (unit: m^2/m^3)
T=298.15; % Temperature (K)
Acell=0.11; % Electrode area (m^2)
Capa=5; % Nominal capacity (Ah)
iapp = Capa*Crate/Acell;

%% Transport parameters
c0=1000; % Electrolyte concentration (unit: mol/m^3) %csol
D1=kk(1)*10^(-9); % Electrolyte diffusion coefficient (unit: m^2/s)
Kappa=kk(2); % Conductivity (unit: S/m)
ctp=51765; % Maximum solid phase concentration at positive (unit: mol/m^3)
ctn=29583; % Maximum solid phase concentration at negative (unit: mol/m^3)
Dbulk=D1; % Electrolyte diffusivity (unit: m^2/s)
sigmap=kk(3); % Solid phase conductivity at positive (unit: S/m)
sigman=kk(4); % Solid phase conductivity at negative (unit: S/m)
Dsp=kk(5)*10^(-15); % Solid particle diffusivity at positive (unit: m^2/s)
Dsn=kk(6)*10^(-14); % Solid particle diffusivity at negative (unit: m^2/s)

Keffp=Kappa*(ep^brugp); % Liquid phase conductivity at positive (unit: S/m)
Keffs=Kappa*(es^brugs); % Liquid phase conductivity at membrane (unit: S/m)
Keffn=Kappa*(en^brugn); % Liquid phase conductivity at negative (unit: S/m)
D2pos=(ep^brugp)*Dbulk; % Electrolyte diffusivity at positive (unit: m^2/s)
D2sep=(es^brugs)*Dbulk; % Electrolyte diffusivity at membrane (unit: m^2/s)
D2neg=(en^brugn)*Dbulk; % Electrolyte diffusivity at negative (unit: m^2/s)

%% Kinetic parameters
kp=kk(7)*10^(-11); % Reaction rate constant at positive (unit: m^2.5/(mol^0.5 s))
kn=kk(8)*10^(-12); % Reaction rate constant at negative (unit: m^2.5/(mol^0.5 s))

```

Figure A1.1: Define Baseline Parameters

```

%% PSO identification (Input upper & lower bounds for parameters to be identified. Input your options for PSO)
pp=0.3; % Deviation for upper and lower bounds (percentage)
D10=1; % Electrolyte diffusion coefficient
Kappa0=1.17; % Conductivity
sigmap0=0.18; % Solid phase conductivity at positive
sigman0=215; % Solid phase conductivity at negative
Dsp0=4; % Solid particle diffusivity at positive
Dsn0=3.3; % Solid particle diffusivity at negative
kp0=0.7; % Reaction rate constant at positive
kn0=0.7; % Reaction rate constant at negative

```

Figure A1.2: Define Initial Guesses and Bounds for PSO

combination that minimises the RMSE value.

The P2D model is represented by a system of ODEs, which are solved using MATLAB's ode15s solver; See Figure A1.4. This solver was chosen as it is good for 'stiff' and nonlinear equations. A 'stiff' system is one in which the parameters may change at vastly different rates. The solver uses the C-rate and the updated parameters to compute the cell voltage at each time step.

```
%>>> %% Objective function
function obj=P2Dobj(kk)

global y0 f MM N M NM initime Totexp Numexp loss_values

try

% adapt solver functions for better conditioning
M0 = MM(initime,y0(:,kk));
vw = 1./max(abs(M0),[],2);
mw = diag(vw);

F = @(t,y) vw.*f(t,y(:,kk));
M1 = @(t,y) mw*MM(t,y(:,kk));

time=linspace(0,Totexp+200,Numexp+3);
opt = odeset('Mass', M1,'MStateDependence','weak','RelTol',1e-5,'AbsTol',1e-5,'InitialStep',1e-3,'MaxStep',5);
warning('off','all');
[T,Y] = ode15s(F,time, y0, opt);

x=importdata('voltage/Diag10_V4.txt'); % this is the loaded experimental data
obj=rms(x(:,1)-(Y(4:Numexp+3,1+N+1+M+1+NM+1+N+NM+1)-Y(4:Numexp+3,1+N+1+M+1+NM+1+N+NM+1+N+NM+2+NM+2)));
loss_values = [loss_values; obj];

catch
    obj=1000;
    loss_values = [loss_values; obj];
end
end
```

Figure A1.3: Objective Function Definition

In Figure A1.5, the PSO is configured with a swarm of 10 particles ('SwarmSize', 10), in which each particle is a candidate set of the eight parameters. First, these particles are each initialised with a random set of parameter values within the specified bounds - this randomness helps in exploring various regions of the solution space initially. The objective function is used to evaluate the position of each particle until after several iterations, some convergence criteria are met.

The convergence criteria can be changed depending on what is required. For example, in the original implementation of DEARLIBs the stopping criterion is defined using the 'MaxIterations', which is basically a bound on the number of solver iterations [86]. This was changed to use the 'FunctionTolerance' criterion instead, which sets "a lower bound on the change in the value of the objective function during a step". This change meant the algorithm would terminate only when the objective function was no longer improving, generally meaning that the optimal solution was found (with the exception of getting stuck in local minima, though PSO is good at avoiding this with its global 'best' solution strategy, with the exception of using a low SwarmSize). The results were much more consistent and

```

%% Solver

% Adapt solver functions for better conditioning
M0 = MM(initime,y(:,kk));
vw = 1./max(abs(M0),[],2);
mw = diag(vw);

F = @(t,y) vw.*f(t,y(:,kk));
M1 = @(t,y) mw*MM(t,y(:,kk));

tsp=100000; % simulation end time
opt = odeset('Mass', M1,'MStateDependence','weak','RelTol',1e-5,'AbsTol',1e-5,'InitialStep',1e-3,'MaxStep',5,'Events',@stopcondition);
warning('off','all');
tic
[T,Y] = ode15s(F,[0 tsp], y0, opt);
toc

% Plot output
figure(1)
p1=plot(T-initime,(Y(:,1+N+1+M+1+NM+1+N+NM+N+NM+1)-Y(:,1+N+1+M+1+NM+1+N+NM+N+NM+N+2+NM+2)), 'LineWidth',2);
hold on;

time1=linspace(0,Totexp,Numexp);
p2=plot(time1,x(:,1),'o','MarkerSize',3,'color','red');
ylim([2.5 4.5]);
set(gca,'FontSize',15);
xlabel('Time(seconds)', 'FontSize',15);
ylabel('Voltage(V)', 'FontSize',15);
legend('P2D Model','Experiment');
legend('boxoff');
hold off;

```

Figure A1.4: Solver

meaningful using 'FunctionTolerance' compared to simply stopping the computation when the specified number of iterations was reached via 'MaxIterations'. The value of 0.01 balanced the computation time with achieving a low final RMSE.

```

%% PSO identification (Input upper & lower bounds for parameters to be identified. Input your options for PSO)
pp=0.3; % Deviation for upper and lower bounds (percentage)
D10=1; % Electrolyte diffusion coefficient
Kappa0=1.17; % Conductivity
sigmap0=0.18; % Solid phase conductivity at positive
sigman0=215; % Solid phase conductivity at negative
Dsp0=4; % Solid particle diffusivity at positive
Dsn0=3.3; % Solid particle diffusivity at negative
kp0=0.7; % Reaction rate constant at positive
kn0=0.7; % Reaction rate constant at negative

Lower_bound = [D10-pp*D10 Kappa0-pp*Kappa0 sigmap0-pp*sigmap0 sigman0-pp*sigman0 Dsp0-pp*Dsp0 Dsn0-pp*Dsn0 kp0-pp*kp0 kn0-pp*kn0];
Upper_bound = [D10+pp*D10 Kappa0+pp*Kappa0 sigmap0+pp*sigmap0 sigman0+pp*sigman0 Dsp0+pp*Dsp0 Dsn0+pp*Dsn0 kp0+pp*kp0 kn0+pp*kn0];

options = optimoptions('particleswarm', 'SwarmSize', 10, 'Display', 'iter', 'FunctionTolerance', 0.01);

tic
[kk,fval] = particleswarm(@(kk)P2Dobj(kk), n_vars, Lower_bound, Upper_bound, options);
toc

D1=kk(1)*10^(-9); % Electrolyte diffusion coefficient (unit:m2/s)
Kappa=kk(2); % Conductivity (unit:S/m)
sigmap=kk(3); % Solid phase conductivity at positive (unit:S/m)
sigman=kk(4); % Solid phase conductivity at negative (unit:S/m)
Dsp=kk(5)*10^(-15); % Solid particle diffusivity at positive (unit:m^2/s)
Dsn=kk(6)*10^(-14); % Solid particle diffusivity at negative (unit:m^2/s)
kp=kk(7)*10^(-11); % Reaction rate constant at positive (unit:m^2.5/(mol^0.5 s))
kn=kk(8)*10^(-12); % Reaction rate constant at negative (unit:m^2.5/(mol^0.5 s))

save('identified_params_kinetic','fval','D1','Kappa','sigmap','sigman','Dsp','Dsn','kp','kn');

```

Figure A1.5: Particle Swarm Optimisation

Initial conditions are also set up for the 'differential states', i.e the variables in the model that are defined by differential equations (see lines 102-376 of DEARLIBS code). In my project I am focusing solely on simulating the discharge behaviour of the battery, so only the initial conditions given for a battery at 100% SOC are used. The initial conditions are highly important for the ODE solver as it must start from physically meaningful conditions to provide an accurate simulation of the battery's behaviour.

```

%% Initial condition guess (Put your initial guess)
U(1:1+N+1+M+1+NM+1)=1;
U(1+1+N+1+M+1+NM+1:N+1+N+1+M+1+NM+1)=.27;
U(1+1+N+1+M+1+NM+1:N+N+1+N+1+M+1+NM+1+N)=0.9014;
U(1+1+N+1+M+1+NM+1:N+N+1+N+1+M+1+NM+1+N+NM)=.27;
U(1+1+N+1+M+1+NM+1+N+NM+N:NM+1+N+1+M+1+NM+1+N+NM+N)=0.9014;
U(1+1+N+1+M+1+NM+1+N+NM+N:NM+2+1+N+1+M+1+NM+1+N+NM+N+NM)=4.30430037;
U(1+1+N+1+M+1+NM+1+N+NM+N:NM+2+1+N+1+M+1+NM+1+N+NM+N+NM+N+2)=.9202000152e-1;
U(1+1+N+1+M+1+NM+1+N+NM+N:NM+N+2+NM+2:1+N+1+M+1+NM+1+N+NM+N+NM+N+2+NM+2)=0;

y0 = (U(1:1+N+1+M+1+NM+1:N+1+M+1+NM+1+N+NM+N+NM+N+2+NM+2));

x=importdata('voltage/Diag10_V4.txt'); % change this
DiagX_Y = 'Diag10_V4'; % set this dynamically

```

Figure A1.6: Establishment of Initial Conditions

It is additionally noted by [69] that the P2D model can be less accurate at a lower SOC, i.e simulating the charging behaviour may be less consistent than simulating the discharging behaviour of the battery.

In summary, the code generates synthetic data based off of some reference experimental data which represents a degraded battery's voltage response. This experimental voltage profile serves as the target that the PSO will try to match by tuning parameters.

Degradation often causes lower diffusion coefficients (due to loss of active material or particle cracking), lower reaction rate constants (due to surface film buildup like SEI increasing resistance), or reduced electrolyte conductivity (due to solvent decomposition or Li inventory loss). It might thus be expected that the values of  $D_{s,n}$ ,  $D_{s,p}$ ,  $k_n$ ,  $k_p$ , etc. will be reduced by some percentage based on the amount of degradation present in the experimental data. This is examined in Section 4.

## A1.2 Experimental Data

This section contains some additional information about the experimental data used from [87].

### A1.2.1 Cell Capacity

The M50 and M50T's nominal capacities are listed as 5 Ah in the datasheets though their 'minimum guaranteed capacity' is 4.85 Ah. The P2D model was originally calibrated with the nominal value of 5 Ah in mind.

The experimental data measures the capacity of each cell in its maximum State-of-Health (i.e when the battery is completely new), which you can see fluctuates around 4.85 Ah;

Online the cell is also listed for sale with a 'typical capacity' of 4.85 Ah [91].

This is an important point to mention as the actual or 'real' measured capacity values tend to fall around 4.85 Ah for these cells, but the 'nominal' value published by LG Chem is 5 Ah. This could be a source of discrepancy between the P2D model simulation results and

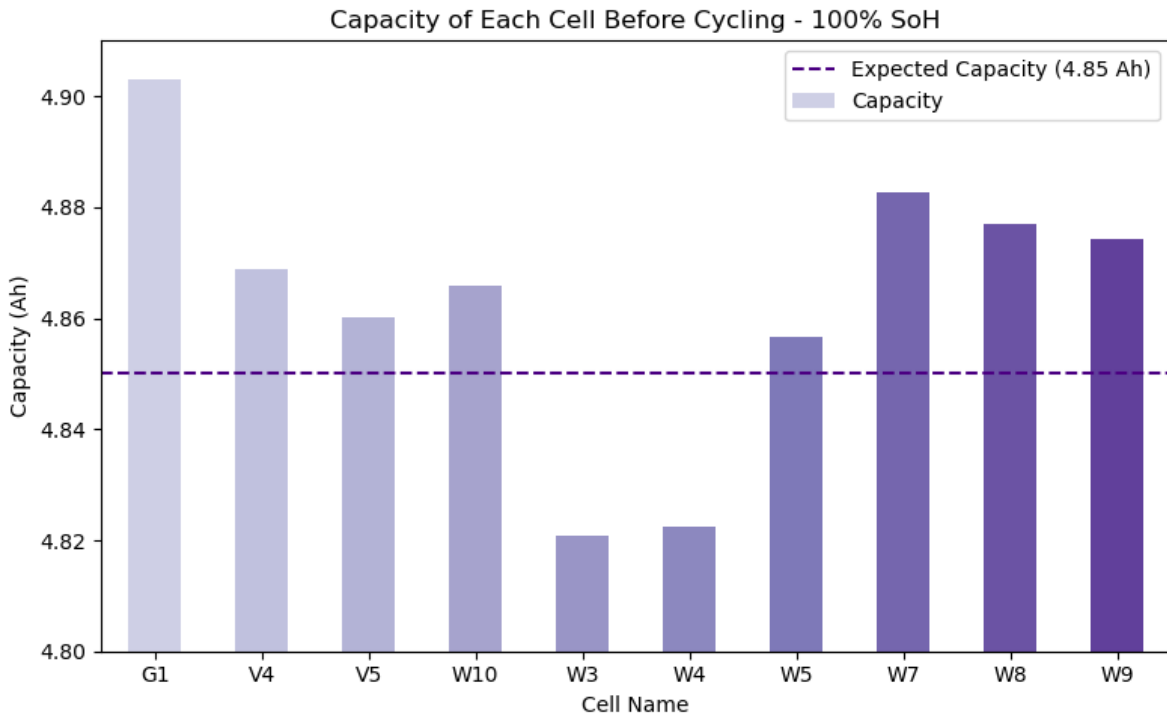


Figure A1.7: Differing Initial Capacities of the M50T Cells

experimental data.

### A1.2.2 Comparative Analysis of the M50 vs. M50T

This section investigates discrepancies between the LG Chem INR21700-M50T and the LG Chem INR21700-M50.

See their datasheets here [92] [93]. I have included all of the relevant information from these datasheets in Table A1.1. I removed the tests/conditions/benchmarks which weren't in common between them.

Based on their datasheets, it appears the batteries are more or less of the same design, but possibly intended for different purposes. It is worth mentioning that information about the difference between these cells are scarce, so blogs/forums were referenced in this section.

The M50T has a very slightly lower operational temperature range. The dimensions are also very slightly larger (by 0.3 mm in diameter and 0.6 mm in height, though this is labelled as 'tentative'). The main apparent difference lies in the 'Max Discharge Current', which likely corresponds to the reduction in cycle life for the M50T compared to the M50 (300 versus 500, respectively).

Given the difference in Max Discharge Current between the cells, the batteries are possibly

intended for different purposes. M50T has a shorter life cycle, but a higher discharge rate / power output at 10-25 °C. (3C as opposed to 1.5C)

In [1] it is mentioned that "The LGM50 was manufactured for high energy applications (rather than high power)". The M50 could be designed to handle moderate power demands without compromising too much on cycle life or other characteristics, meanwhile the M50T supports a similar discharge rate except for 10-25 °C, at this temperature it could be used for higher power application, i.e, in electric scooters.

In practice, testers have found that pushing 15 A (Max Discharge Current) through the M50T causes significant voltage sag and heating, so effectively about 10 A is the realistic safe continuous load for either cell despite the M50T's higher allowed discharge current on paper [94]. It is noted that many sellers of the M50T "list it as a 10A cell, not a 15A one".

The reduction in max cycles for the M50T could simply be because a much higher discharge rate would lead to faster degradation. The M50 could meanwhile be aimed at lower-power devices. Actually, the M50 is popular in the flashlight community, for its large capacity amongst other reasons [95].

The key difference between the two is that the M50T has more allowable discharge current. The reduction in cycle life could possibly be explained by this, and mitigated if the cell is used conservatively (e.g. not pushing it at 15A at high temperature continuously).

Ultimately, the differences between these cells do not seem significant, they have the same chemistry and near identical manufacturer specifications. Any adjustments LG have made are not public information. Validation of the P2D model with regards to the experimental data is carried out in Section 4, and the low RMSE supports this conclusion.

### A1.2.3 Additional Diagnostic Data

This section contains some additional information about the experimental data captured.

In addition to capacity tests, each diagnostic session also includes HPPC tests and EIS measurements. These kind of tests and measurements were discussed in Section 2.1.1. The HPPC tests consisted of controlled current pulses at various SOC levels to measure the internal resistance (voltage drop) and power capability of the cell as it ages, while the EIS tests were conducted at selected SOC points (20%, 50%, and 80% SOC) and over a broad frequency range (10 kHz down to 0.01 Hz) to characterise the cell's impedance spectrum.

For the purpose of this study, only the capacity tests were used as they match the output of

the P2D model. Although it's outside the scope of this project, with further investigation into the P2D model it could be possible to use this additional data for either investigation, validation or improvement of the P2D model, or possibly for further synthetic data generation.

#### A1.2.4 UDDS Cycling Protocol

This section provides some more information as to how the experimental data was collected. See Table A1.2 and Table A1.3. Note that W3 and W7 were withdrawn from testing earlier because their impedance results were abnormal.

A full UDDS charge-discharge cycle consists of six steps as follows. The first step involves charging at constant current (CC) at the specified C-rate, until the cell voltage reaches 4.0 V. This step is meant to simulate different charging speeds (from slow to fast charge) across the tested cells, as listed in the dataset (as each cell was assigned one of the four C-rate conditions). The next steps are, constant voltage (CV) hold at 4.0 V, then resume the CC charging until the cell reaches 4.2 V, to bring the cell to 100% SOC. The next step involves CV hold at 4.2 V and letting the cell rest for 30 minutes. This is to make sure the cell is truly at full charge (saturation of the electrodes) and allows the voltage to relax, i.e by standardising the starting point for discharge.

The final steps are the discharge phase. First the cell is discharging at C/4 to 80% SOC - then the final step, the UDDS discharge begins. I will not get into the specifics of this, but the cell experiences varying current pulses to simulate accelerating, decelerating, and idling. At the end of this step the cell is at 20% SOC, which was the lower limit of discharge for the cycling.

These 6 steps repeat over the ageing of each cell. Each completion of these 6 steps constitutes a full cycle.

### A1.3 Establishing Mathematical Relationships Between the 8 Key Electrochemical Parameters and Common Degradation Mechanisms

Various studies have explored the degradation mechanisms which occur in LIB ageing. One study explored the model parameters that change most significantly with ageing, for NMC cells used in EVs. The parameters most indicative of ageing were the particle surface area of the cathode, the stoichiometry limits, and the porosities [82]. In this section the NMC-battery degradation mechanisms from [78] have been analysed to find out what the expected trend for each parameter could be(increase, decrease, or no change) as the battery

ages.

The 4 main mechanisms of degradation discussed in the paper include lithium plating, SEI formation, particle cracking and the loss of active material [78]. To note, another review [84] determined the graphite-silica anode (as in the M50/M50T) to be most prone to loss of lithium inventory due to the formation and thickening of the SEI, and the cathode to be most prone to loss of active material resulting from structural changes and stress from lithium intercalation/deintercalation.

In Table A1.4 they determined the bounds for the 8 unknown parameters for when the model was fit to experimental discharge data at 5 °C, 25 °C, and 35 °C, for ±30% bounds, using PSO. See [1]. In one set of experiments I investigated changed the initial values to the experimental ones used in [1], instead of the simulated ones.

### A1.3.1 Equations of Degradation Mechanisms

In this section the impact of the battery degradation mechanisms are examined, to see how each one of them ( i.e SEI growth, lithium plating, particle fracture, loss of active material) affects the governing equations and thus the 8 key parameters. The relevant equations are taken from [78]. Excessive detail is avoided, since there are a lot of different factors involved in each of these processes, please refer to the paper for more information.

#### SEI Layer Growth

'Solvent reduction' produces an increasingly resistive SEI, i.e ion transfer slows down:

$$\frac{\partial L_{\text{SEI}}}{\partial t} = \frac{c_{\text{sol},0} D_{\text{sol}}(T) \bar{V}_{\text{SEI}}}{2 L_{\text{SEI}}} \quad (\text{A1.1})$$

So as  $L_{\text{SEI}}$  (SEI layer thickness) grows,  $k_n$  or the reaction rate at negative/anode falls and electrolyte transport coefficients drop via pore clogging:

$$k_n(t) \propto \frac{1}{L_{\text{SEI}}} \quad (\text{A1.2})$$

Thus,  $D$  (electrolyte diffusion coefficient),  $k_n$  and  $\kappa$  (conductivity) all decrease with SEI growth.

#### Lithium Plating

Li metal is deposited and reduces the available active area -> lower  $k_n$ , (reaction rate const. at negative) and porosity (-> lower  $D$ ,  $\kappa$ ) exactly as SEI does, and causes loss of lithium inventory (LLI).

## Particle Fracture

Stress causes cracks,  $\sigma_n$ ,  $\sigma_p$  drop. Increases SEI growth so  $D$ ,  $\kappa$  and  $k_n$  are further reduced.

## Loss of Active Material (LAM)

Any loss of electrochemically active mass scales down reaction rates and electronic pathways. Bulk solid diffusivities  $D_{s,p}$ ,  $D_{s,n}$  remain essentially constant (SEI and plating occur outside the particles), so  $D_{s,n}$  is usually held fixed. (This aligns with results in the next Section).

### A1.3.2 Feature Analysis - More Plots

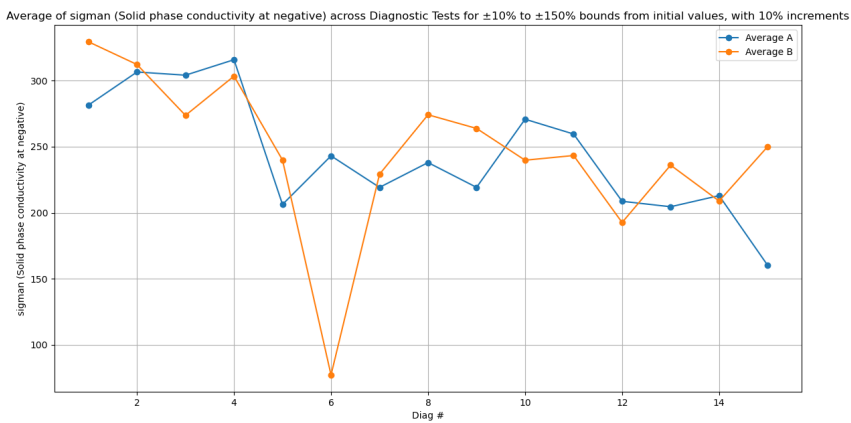


Figure A1.8: Average  $\sigma_n$  Value Across Bounds of 10% to 150% - Slightly Decreasing Trend

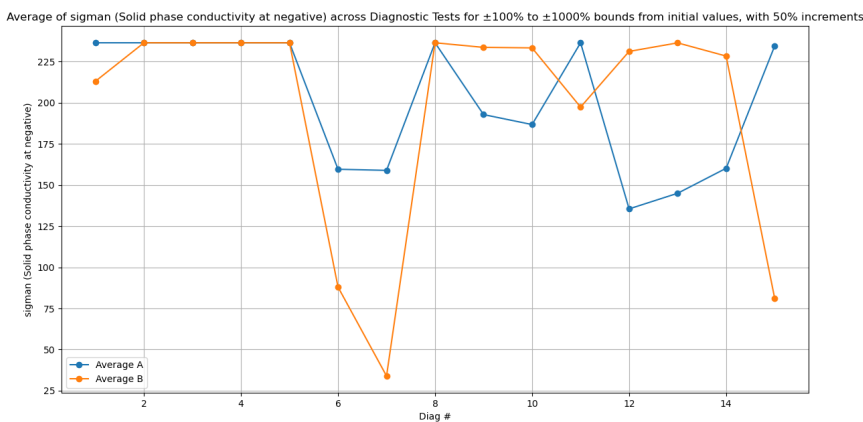


Figure A1.9: Average  $\sigma_n$  Value Across Bounds of 100% to 1000% - No Apparent Trend

More samples would have to be generated, ideally over a wider range of experimental data to examine these parameters and their relationships to the degradation.

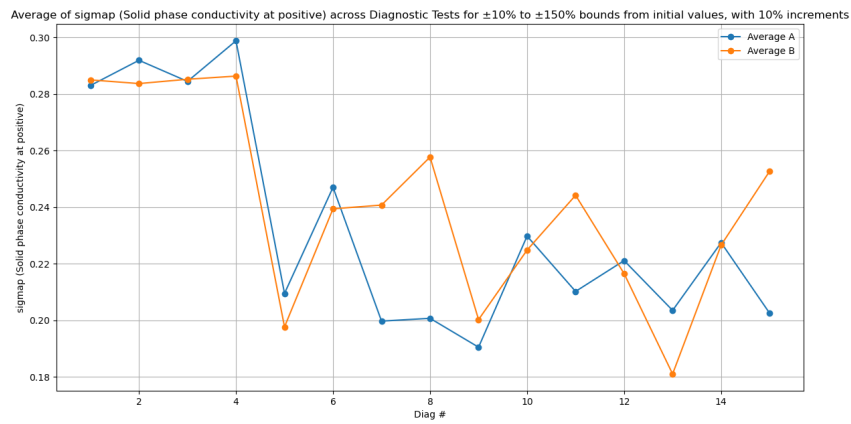


Figure A1.10: Average  $\sigma_p$  Value Across Bounds of 10% to 150% - Slightly Decreasing Trend

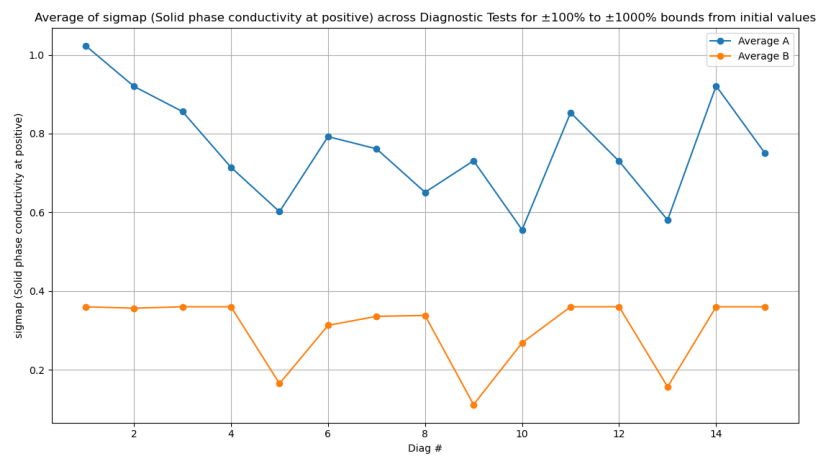


Figure A1.11: Average  $\sigma_p$  Value Across Bounds of 100% to 1000% - No Apparent Trend

Some plots including Config D, averaged across ALL bounds are shown in Figures A1.12, A1.13, A1.14, A1.15, A1.16, A1.17, A1.18, A1.19.

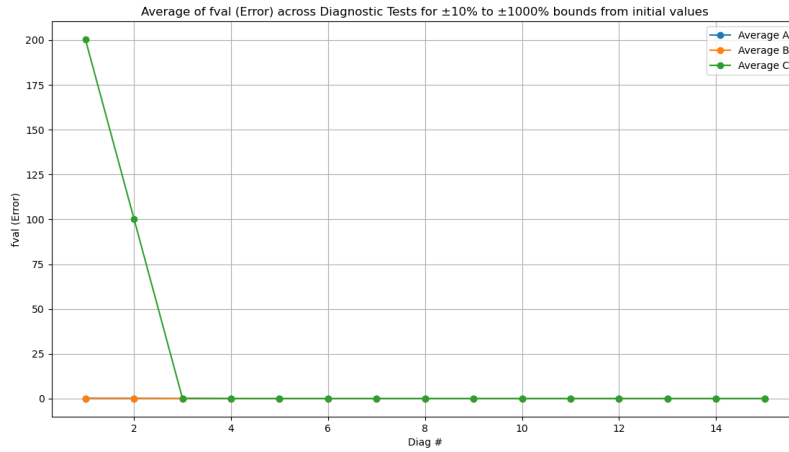


Figure A1.12: Average RMSE Error Value Across Bounds of 10% to 1000%

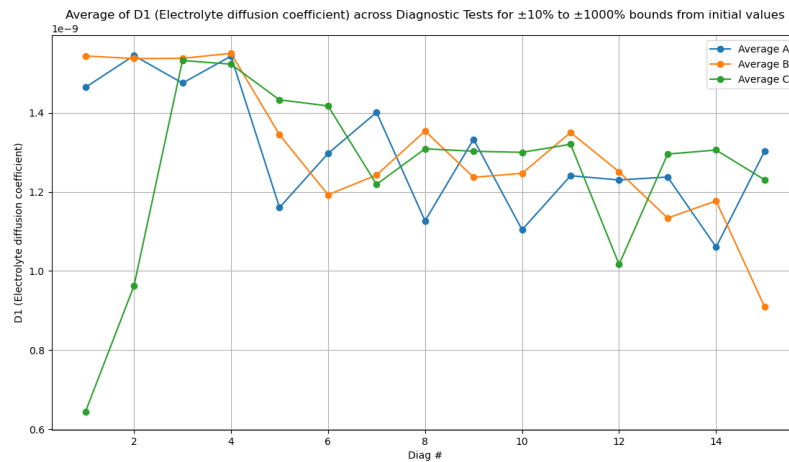


Figure A1.13: Average  $D$  Value Across Bounds of 10% to 1000%

### A1.3.3 Baseline Experiment Results

===== Experiment\_1\_voltage =====

— Method\_1\_20k —

1.  $C=4400, =0.0001, =1e-06 \rightarrow \text{Avg MSE}=0.0516$

— Method\_1\_40k —

1.  $C=4400, =0.001, =1e-06 \rightarrow \text{Avg MSE}=0.0321$

— Method\_1\_60k —

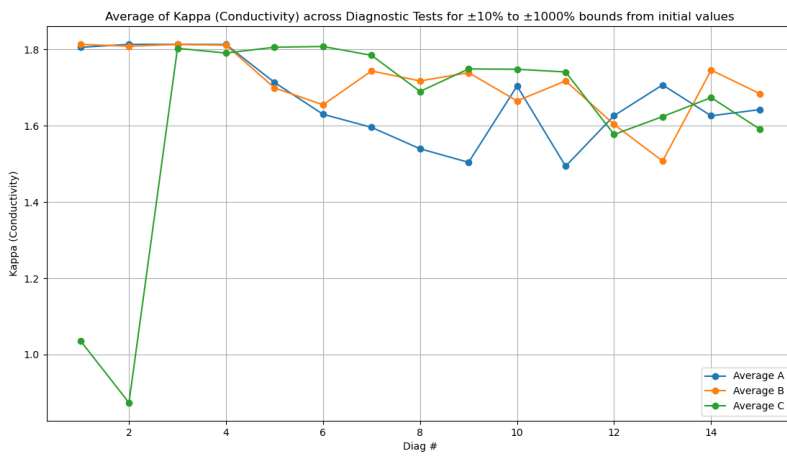


Figure A1.14: Average  $\kappa$  Value Across Bounds of 10% to 1000%

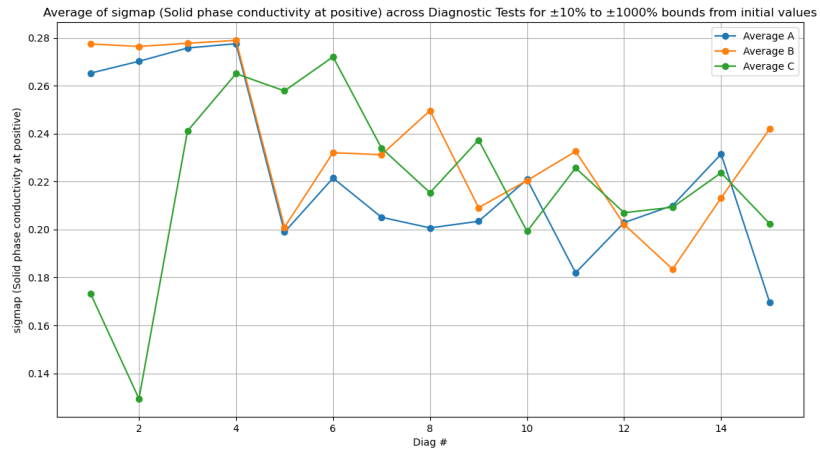


Figure A1.15: Average  $\sigma_p$  Value Across Bounds of 10% to 1000%

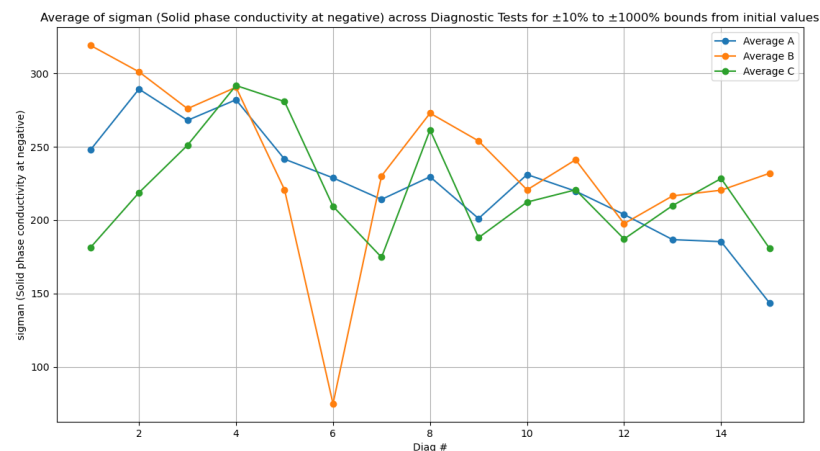


Figure A1.16: Average  $\sigma_n$  Value Across Bounds of 10% to 1000%

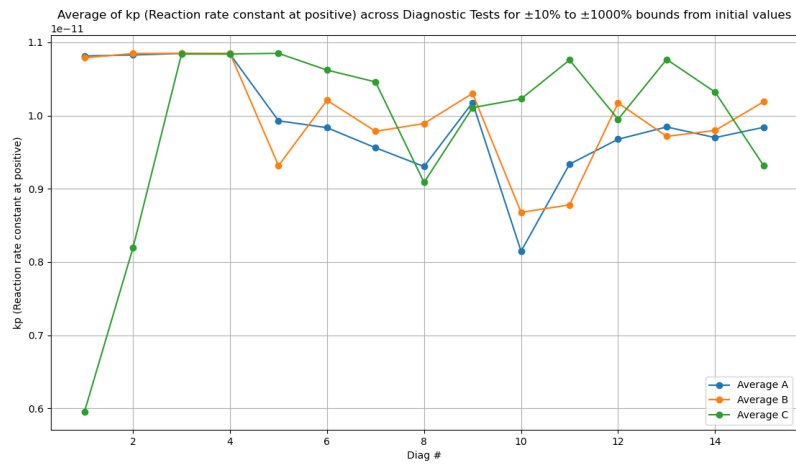


Figure A1.17: Average  $k_p$  Value Across Bounds of 10% to 1000%

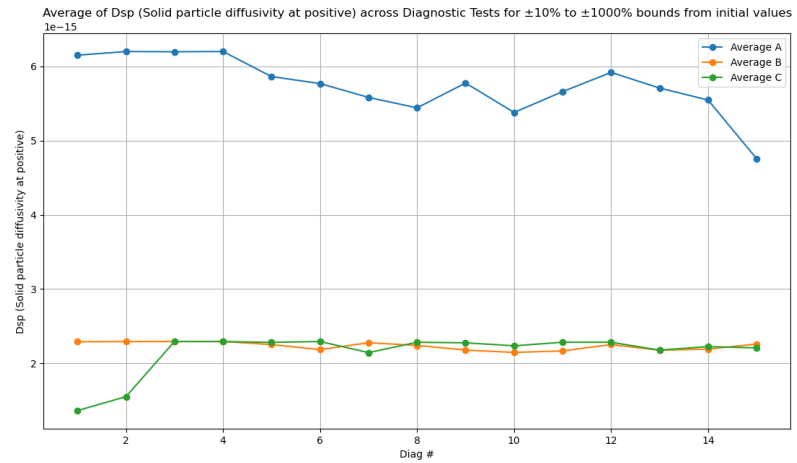


Figure A1.18: Average  $D_{s,p}$  Value Across Bounds of 10% to 1000%

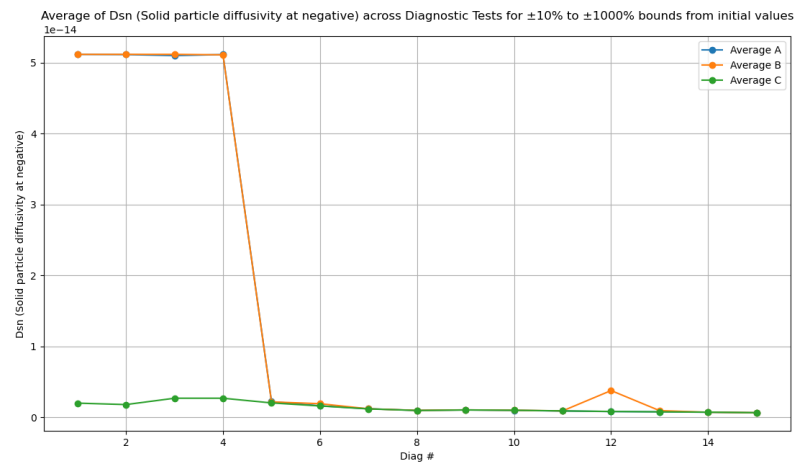


Figure A1.19: Average  $D_{s,n}$  Value Across Bounds of 10% to 1000%

1.  $C=1600, \alpha=0.0001, \beta=1e-06 \rightarrow \text{Avg MSE}=0.0289$

— Method\_2 —

1.  $C=100, \alpha=0.0001, \beta=1e-06 \rightarrow \text{Avg MSE}=0.0357$

===== Experiment\_1\_voltage\_dvdt =====

— Method\_1\_20k —

1.  $C=400, \alpha=1e-06, \beta=1e-06 \rightarrow \text{Avg MSE}=0.0524$

— Method\_1\_40k —

1.  $C=400, \alpha=1e-06, \beta=1e-06 \rightarrow \text{Avg MSE}=0.0406$

— Method\_1\_60k —

1.  $C=400, \alpha=0.001, \beta=1e-06 \rightarrow \text{Avg MSE}=0.0470$

— Method\_2 —

1.  $C=2000, \alpha=1e-06, \beta=1e-06 \rightarrow \text{Avg MSE}=0.0754$

===== Experiment\_2\_voltage =====

— Method\_1\_20k —

1.  $C=1500, \alpha=0.001, \beta=1e-05 \rightarrow \text{Avg MSE}=0.0486$

— Method\_1\_40k —

1.  $C=1500, \alpha=0.001, \beta=1e-06 \rightarrow \text{Avg MSE}=0.0061$

— Method\_1\_60k —

1.  $C=200, \alpha=0.001, \beta=1e-06 \rightarrow \text{Avg MSE}=0.0040$

— Method\_2 —

1.  $C=100, \alpha=1e-06, \beta=1e-06 \rightarrow \text{Avg MSE}=0.0394$

===== Experiment\_2\_voltage\_dvdt =====

— Method\_1\_20k — 1.  $C=100, \alpha=1e-07, \beta=0.0001 \rightarrow \text{Avg MSE}=0.0451$

— Method\_1\_40k — 1.  $C=2000, \alpha=1e-07, \beta=1e-06 \rightarrow \text{Avg MSE}=0.0058$

— Method\_1\_60k — 1.  $C=200, \alpha=0.001, \beta=1e-06 \rightarrow \text{Avg MSE}=0.0041$

— Method\_2 — 1.  $C=100, \alpha=1e-06, \beta=1e-06 \rightarrow \text{Avg MSE}=0.0398$

Extra Results: Despite the small training set of 80 samples, the model is able to predict on a testset of experimental data reasonably well(80-20 split). It achieves MSE 0.002 and 0.003, or RMSE 0.044 and 0.055 respectively for Figures A1.20 and A1.21.

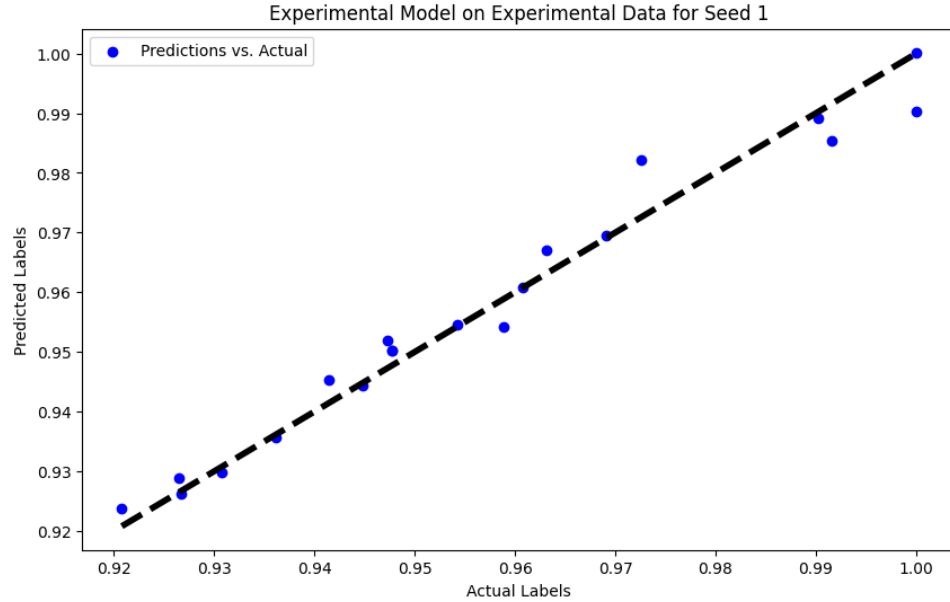


Figure A1.20: Experiment 1 Best Model Predicting on Experimental Data

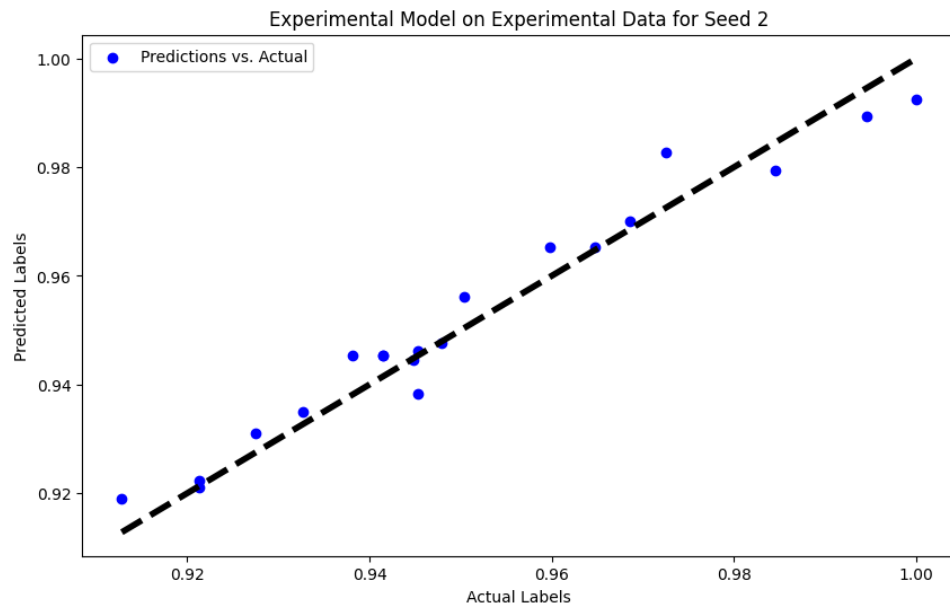


Figure A1.21: Experiment 1 Best Model Predicting on Synthetic Data

Synthetic model ends up struggling with this same SoH range.

Additional experimentals and results about adding noise to the data, LSTM, TCN are included in the Github.

Item	Condition / Note	Specification for M50	Specification for M50T
Energy	By Std. Charge / Discharge	Nominal 18.2 Wh Minimum 17.6 Wh	Nominal 18.2 Wh Minimum 17.6 Wh
Nominal Voltage	Average by Std. Charge / Discharge	3.63 V	3.63 V
Nominal Shipping SOC		Below 30%	Below 30%
Standard Charge	Constant Current	0.3C (1455 mA)	0.3C (1455 mA)
	Constant Voltage	4.2 V	4.2 V
	End Current (Cut-off)	50 mA	50 mA
Max Charge Voltage		4.20 ± 0.05 V	4.20 V (4.25 V limit)
Max Charge Current	0 – 25 °C	0.3C (1455 mA)	0.3C (1455 mA)
	25 – 45 °C	—	0.7C (3395 mA)
	25 – 50 °C	0.7C (3395 mA)	—
Standard Discharge	Constant Current	0.2C (970 mA)	0.2C (970 mA)
	End Voltage (Cut-off)	2.5 V	2.5 V
Max Discharge Current	-30 – -20 °C	0.2C (970 mA)	—
	-20 – 5 °C	0.3C (1455 mA)	—
	5 – 60 °C	1.5C (7275 mA)	—
	-20 – 10 °C	—	0.5C (2425 mA)
	10 – 25 °C	—	3.0C (14550 mA)
	25 – 55 °C	—	1.5C (7275 mA)
Minimum Discharge Voltage		2.5 V	2.5 V
Weight	Without washer	68 ± 1 g	Max 70 g (tentative)
Diameter		≤ 21.1 mm	≤ 21.44 mm (tentative)
Height		≤ 70.15 mm	≤ 70.80 mm (tentative)
Storage Temperature	1 day	-40 °C	N/A
	1 month	-20 – 60 °C	-20 – 55 °C
	3 months	-20 – 45 °C	-20 – 45 °C
	1 year	-20 – 20 °C	-20 – 25 °C
Initial AC Impedance	"Cell shall be measured at 1kHz after charge per 1.1"	≤ 25 mΩ	≤ 25 mΩ
Cycle Life	After 500 cycles	≥ 80% of Wh <sub>min</sub>	—
	After 300 cycles	—	≥ 80% of initial energy
Max Charge Current (Continuous)	0 – 25 °C	0.3C (1455 mA)	0.3C (1455 mA)
	25 – 45 °C	—	0.7C (3395 mA)
	25 – 50 °C	0.7C (3395 mA)	—
Max Discharge Current (Continuous)	-30 – -20 °C	0.2C (970 mA)	—
	-20 – 5 °C	0.3C (1455 mA)	—
	5 – 45 °C	1.5C (7275 mA)	—
	45 – 60 °C	1.5C (7275 mA)	—
	-20 – 10 °C	—	0.5C (2425 mA)
	10 – 25 °C	—	3.0C (14550 mA)
	25 – 55 °C	—	1.5C (7275 mA)
Storage Characteristics	"Cells shall be charged per 1.1 and stored in a temperature-controlled environment at 25°C ± 2°C for 30 days. After storage, cells shall be discharged per 1.2 to obtain the remaining energy"	≥ 90% of Wh <sub>min</sub>	—
	"Cells shall be charged per 1.1 and stored in a temperature-controlled environment at 24°C ± 2°C for 30 days. After storage, cells shall be discharged per 1.2 to obtain the remaining energy."	—	≥ 90% of Wh <sub>min</sub>
High-Temp. Storage Test	1 week at 60 °C	No leakage, ≥ 80% energy recovery	—
	1 week at 55 °C	—	No leakage, ≥ 80% of Wh <sub>min</sub>
Temperature Dependency of Capacity	"Cells shall be charged per 1.1 at 25 °C ± 2 °C and discharged per 1.2 at the following temperatures:"	Discharge at -10, 0, 25, 60 °C, ≥ 70%, ≥ 80%, ≥ 100%, ≥ 95% of Wh <sub>min</sub> respectively	Discharge at -10, 0, 25, 55 °C, ≥ 70%, ≥ 80%, ≥ 100%, ≥ 95% of Wh <sub>min</sub> respectively

Table A1.1: Cell specifications for M50 vs. M50T

Table A1.2: UDDS Cycling Protocol Steps and Exit Conditions

Step	Action	Exit condition
1	CC charge at C-rate specified in Table A1.3	Cell voltage reaches 4.0 V
2	CV charge	Charge current below 50 mA
3	CC charge at C/4	Cell voltage reaches 4.2 V
4	CV charge + 30 min rest	Charge current below 50 mA
5	CC discharge at C/4	20% of capacity discharged (80% SOC)
6	UDDS discharge	Additional 60% discharged (20% SOC)

Table A1.3: UDDS Protocol Charge C-rates Defined at 23 °C for Each Cell, with Corresponding Number of RPT cycles

Label	Charge C-rate	Temp. [°C]	Diagnostic test [cycle]														
			#1	#2	#3	#4	#5	#6	#7	#8	#9	#10	#11	#12	#13	#14	#15
W3	3C	23	0	25	75*	—	—	—	—	—	—	—	—	—	—	—	—
W4	C/4	23	0	25	75	123	132	159	176	179	—	—	—	—	—	—	—
W5	C/2	23	0	25	75	125	159	167	187	194	219	244	269	294	319	344	369
W7	C/4	23	0	25	75	125	141*	—	—	—	—	—	—	—	—	—	—
W8	C/2	23	0	25	75	125	148	150	151	157	185	—	—	—	—	—	—
W9	1C	23	0	25	75	122	144	145	146	150	179	216	241	266	291	316	341
W10	3C	23	0	25	75	122	146	148	151	159	188	225	250	275	300	325	350
G1	3C	23	0	25	30	37	62	—	—	—	—	—	—	—	—	—	—
V4	C/4	23	0	20	45	70	95	—	—	—	—	—	—	—	—	—	—
V5	1C	23	0	12	18	29	—	—	—	—	—	—	—	—	—	—	—

\*Cell was dismissed and the ageing campaign terminated.

<b>Parameter (Units)</b>	<b>Temp.</b>	<b>Lower Bound</b>	<b>Upper Bound</b>
$D$ (electrolyte diff. coeff, $\text{m}^2/\text{s}$ )	5 °C	$0.42 \times 10^{-9}$	$0.78 \times 10^{-9}$
	25 °C	$0.70 \times 10^{-9}$	$1.30 \times 10^{-9}$
	35 °C	$0.84 \times 10^{-9}$	$1.56 \times 10^{-9}$
$\kappa$ (electrolyte conductivity, $\text{S}/\text{m}$ )	5 °C	0.82	1.52
	25 °C	0.82	1.52
	35 °C	0.82	1.52
$\sigma_p$ (solid cond. – positive, $\text{S}/\text{m}$ )	5 °C	0.13	0.23
	25 °C	0.13	0.23
	35 °C	0.13	0.23
$\sigma_n$ (solid cond. – negative, $\text{S}/\text{m}$ )	5 °C	150.5	279.5
	25 °C	150.5	279.5
	35 °C	150.5	279.5
$D_{s,p}$ (solid diffusivity – pos., $\text{m}^2/\text{s}$ )	5 °C	$2.8 \times 10^{-15}$	$5.2 \times 10^{-15}$
	25 °C	$2.8 \times 10^{-15}$	$5.2 \times 10^{-15}$
	35 °C	$4.55 \times 10^{-15}$	$8.45 \times 10^{-15}$
$D_{s,n}$ (solid diffusivity – neg., $\text{m}^2/\text{s}$ )	5 °C	$0.56 \times 10^{-14}$	$1.04 \times 10^{-14}$
	25 °C	$2.31 \times 10^{-14}$	$5.94 \times 10^{-14}$
	35 °C	$4.2 \times 10^{-14}$	$10.8 \times 10^{-14}$
$k_p$ (reaction rate const. – pos., $\text{mol}/(\text{m}^2\text{s})$ )	5 °C	$0.14 \times 10^{-11}$	$0.26 \times 10^{-11}$
	25 °C	$0.49 \times 10^{-11}$	$0.91 \times 10^{-11}$
	35 °C	$0.91 \times 10^{-11}$	$1.69 \times 10^{-11}$
$k_n$ (reaction rate const. – neg., $\text{mol}/(\text{m}^2\text{s})$ )	5 °C	$0.63 \times 10^{-12}$	$1.17 \times 10^{-12}$
	25 °C	$0.49 \times 10^{-12}$	$0.91 \times 10^{-12}$
	35 °C	$0.91 \times 10^{-12}$	$1.69 \times 10^{-12}$

Table A1.4: Upper and lower bounds used for the eight identified parameters in the P2D model [4]. Bounds were set to  $\pm 30\%$  of the initial guess values for each parameter at each temperature.

Experiment	Method	$C$	$\epsilon$	$\gamma$	Avg MSE
Experiment_1_voltage	Method_1_20k	4400	0.0001	$1 \times 10^{-6}$	0.0516
	Method_1_40k	4400	0.001	$1 \times 10^{-6}$	0.0321
	Method_1_60k	1600	0.0001	$1 \times 10^{-6}$	0.0289
	Method_2	100	0.0001	$1 \times 10^{-6}$	0.0357
Experiment_1_voltage_dvdt	Method_1_20k	400	$1 \times 10^{-6}$	$1 \times 10^{-6}$	0.0524
	Method_1_40k	400	$1 \times 10^{-6}$	$1 \times 10^{-6}$	0.0406
	Method_1_60k	400	0.001	$1 \times 10^{-6}$	0.0470
	Method_2	2000	$1 \times 10^{-6}$	$1 \times 10^{-6}$	0.0754
Experiment_2_voltage	Method_1_20k	1500	0.001	$1 \times 10^{-5}$	0.0486
	Method_1_40k	1500	0.001	$1 \times 10^{-6}$	0.0061
	Method_1_60k	200	0.001	$1 \times 10^{-6}$	0.0040
	Method_2	100	$1 \times 10^{-6}$	$1 \times 10^{-6}$	0.0394
Experiment_2_voltage_dvdt	Method_1_20k	100	$1 \times 10^{-7}$	$1 \times 10^{-4}$	0.0451
	Method_1_40k	2000	$1 \times 10^{-7}$	$1 \times 10^{-6}$	0.0058
	Method_1_60k	200	0.001	$1 \times 10^{-6}$	0.0041
	Method_2	100	$1 \times 10^{-6}$	$1 \times 10^{-6}$	0.0398

Table A1.5: Top-ranked SVR hyperparameters ( $C$ ,  $\epsilon$ ,  $\gamma$ ) and corresponding average MSE for each experiment and method.